Viscous–Inviscid Interaction & Upstream Influence in Hypersonic Flow

A thesis submitted to the University of Manchester for the degree of Doctor of Philosophy in the Faculty of Science

Cesare Guardino

Department of Mathematics

January 1999

ProQuest Number: 10648393

All rights reserved

INFORMATION TO ALL USERS
The quality of this reproduction is dependent upon the quality of the copy submitted.

In the unlikely event that the author did not send a complete manuscript
and there are missing pages, these will be noted. Also, if material had to be removed,
a note will indicate the deletion.

ProQuest 10648393

Published by ProQuest LLC (2017). Copyright of the Dissertation is held by the Author.

All rights reserved.
This work is protected against unauthorized copying under Title 17, United States Code
Microform Edition © ProQuest LLC.

ProQuest LLC.
789 East Eisenhower Parkway
P.O. Box 1346
Ann Arbor, MI 48106 – 1346

(DWW 5Y)

Th 21157

JOHN RYLANDS
UNIVERSITY
LIBRARY OF
MANCHESTER

Contents

List of Figures

Abstract

This thesis is devoted to the study of viscous-inviscid interactions and upstream influence effects occurring in the hypersonic flow over slender two-dimensional or axially-symmetric bodies at zero angle-of-attack, under the assumption of the perfect gas law.

In Part I, self-similar solutions were obtained for the hypersonic flow near the leading-edge of three-quarter power-law bodies. The tangent wedge/cone approximation was used to relate the pressure distribution to the displacement thickness. Furthermore, the nature of the upstream influence effect was considered numerically, and it was discovered that upstream influence exists for axially-symmetric cases provided that the body slenderness ratio and surface temperature exceed certain critical values. The numerical results for two-dimensional flat plates were found to be in good agreement with solutions obtained by previous authors. Asymptotic results have also been obtained for very hot bodies, and the effects of varying the Prandtl number and ratio of specific heats have been considered. New analytical results have also been obtained for cases in which the boundary layer thickness is negligible in comparison to the body thickness, particularly for power-law bodies. It was discovered that the upstream influence effect decays exponentially as the leading edge is approached, and an analytic expression has been obtained for the upstream influence eigenvalue.

In Part II, the equations describing the interaction between the boundary

layer and inviscid flow were solved numerically for the hypersonic flow over compression or expansion corners with strong wall cooling. It was observed that the flow separates for compression ramps if the ramp angle is greater than a certain critical value. For axially-symmetric flows, it was observed that the pressure gradient becomes favourable at a certain distance downstream of the ramp corner, and that the minimum in the skin friction distribution increases with decreasing radius for fixed ramp angle. It was also discovered that the flow over expansion corners separates if the radius is smaller than a certain critical value. New self-similar solutions were also determined far downstream of the corner point for cases not involving separation, and also for flows exhibiting incipient separation. An asymptotic theory was used to describe the separation and reattachment process occurring in subcritical flows in order to remove the Goldstein singularity at the separation point. The resulting nonlinear inner interaction problem was successfully solved using a new unsteady algorithm, and it was observed that the separated region lies entirely upstream of the ramp corner. In addition, asymptotic solutions far upstream and downstream of the interaction region were derived, and the numerical solutions were found to be in very good agreement with both of these analytical results. Finally, it was shown that the asymptotic theory considered here, as well as marginal separation theory, can both be used to describe the separation process occurring in axially-symmetric flows.

Copyright & Declaration

No portion of the work referred to in this thesis has been submitted in support of an application for another degree or qualification of this or any other university or other institute of learning.

1. Copyright in text of this thesis rests with the Author. Copies (by any process) either in full, or of extracts, may be made **only** in accordance with instructions given by the Author and lodged in the John Rylands University Library of Manchester. Details may be obtained from the Librarian. This page must form part of any such copies made. Further copies (by any process) of copies made in accordance with such instructions may not be made without the permission (in writing) of the Author.

2. The ownership of any intellectual property rights which may be described in this thesis is vested in the University of Manchester, subject to any prior agreement to the contrary, and may not be made available for use by third parties without the written permission of the University, which will prescribe the terms and conditions of any such agreement.

Further information on the conditions under which disclosures and exploitation may take place is available from the Head of the Department of Mathematics.

Dedication & Acknowledgments

To my parents and grandparents

I wish to express my deepest gratitude to my supervisor Prof. A. I. Ruban for his unfailing support throughout the research and writing of this thesis. I would also like to thank Mr. S. H. Bos for many useful discussions and Mr. N. Battam for proof-reading this thesis.

"The dream of yesterday is the hope of today and the reality of tomorrow."

– Robert H. Goddard

Preface

Cesare Guardino graduated in 1994 with a First Class B.Sc. Honours degree in Mathematics from the University of Manchester. His final year dissertation was on "The structure and formation of the stars". The following year he obtained a M.Sc. in Fluid Mechanics and Applied Mathematics, from which he gained valuable experience in computational as well as experimental techniques including the use of wind tunnels and shock-tubes. He also published a thesis on the "Computation of hypersonic blunt body flows using flux-vector splitting techniques", which involved the direct numerical simulation of inviscid hypersonic flows over generic re-entry vehicles (see Guardino 1995).

The author has had a strong interest in spaceflight, aeronautics and astronomy from an early age, and is a student member of the American Institute of Aeronautics and Astronautics (AIAA). He also attended the "European Space School 1990", a one week course at Brunel University devoted to all areas of space research. He is also particularly interested in the application of hypersonic flow research to spaceflight.

Chapter 1

Introduction

1.1 Characteristics of Hypersonic Flows

The analysis and computation of hypersonic flows is of crucial importance in the design of vehicles capable of high speed flight, such as the space shuttle and the next generation of reusable launch vehicles. The present work addresses the hypersonic flow over two-dimensional or axially-symmetric slender bodies and compression ramps at zero angle-of-attack, as shown in Fig. 1.1. Notwithstanding the existence of powerful Euler/Navier-Stokes computer codes for the simulation of such flows, it is still desirable to supplement these tools with basic analytical concepts that explain and correlate the purely numerical results, and that may also reveal new ideas about improving the aerodynamic design and performance. Moreover, direct numerical solutions of the Navier-Stokes equations tend to struggle for accuracy in the range of Mach and Reynolds numbers which are encountered in hypersonic flight, such as during the atmospheric re-entry from orbit.

The theory of viscous hypersonic flows is described in detail in numerous books and journals (see, for example, Anderson 1989, Cheng 1993, Cox & Crabtree 1965 and Mikhailov *et al.* 1971), and only the most important features will be discussed

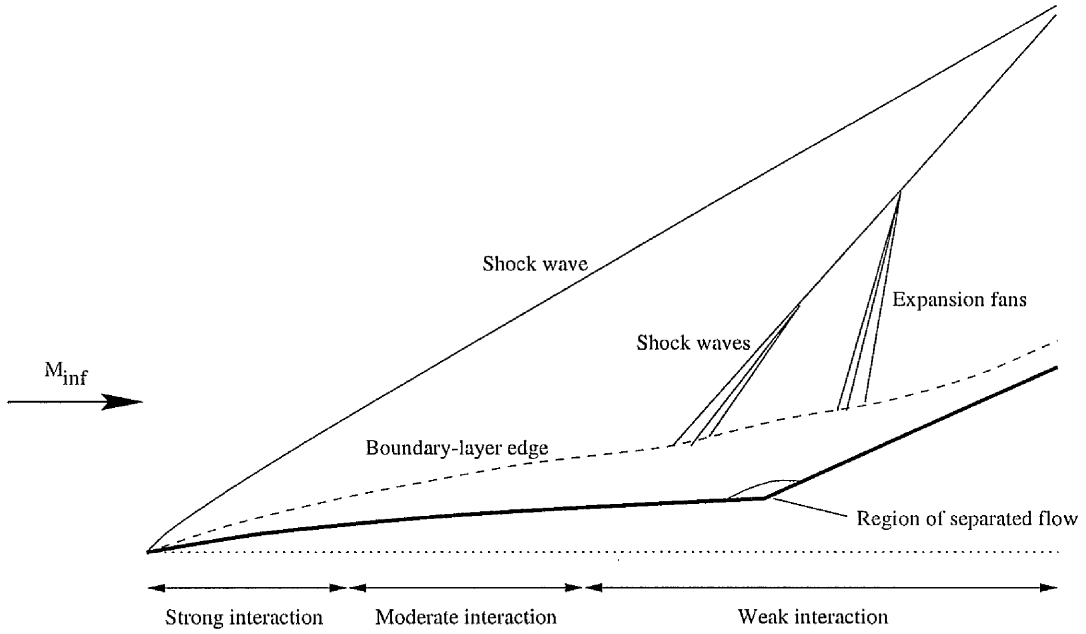

Figure 1.1: The hypersonic flow structure over a slender body at zero angle-of-attack (not to scale).

here. Hypersonic flows differ from subsonic or even low Mach number supersonic flows in many respects. Firstly, the temperature within the viscous boundary layer near to the body surface increases and the density decreases as the free-stream Mach number becomes large. This results in comparatively large amounts of viscous dissipation and heat transfer to the body surface, and it is for this reason that re-entry vehicles must be protected from the generated heat using special tiles or ablative materials. In addition, a relatively strong shock wave is generated near the leading-edge, as can be clearly seen in experiments (see Figs. 1.2 and 1.3).

The extreme viscous dissipation within hypersonic boundary layers can create temperatures high enough to cause chemical reactions, dissociation or even

ionization within the gas. The high temperature and low density within a hypersonic boundary layer causes it to be orders of magnitude thicker than low speed boundary layers at the same Reynolds number. Consequently, the boundary layer can exert a major displacement effect on the inviscid flow outside the boundary layer, thus causing a given body shape to appear thicker than it really is. The changes in the inviscid flow in turn feed back to affect the growth of the boundary layer downstream. This phenomenon, which is known as *viscous interaction*, can have important effects on the pressure distribution, and hence the lift, drag and stability on hypersonic vehicles. Very close to the leading-edge tip there exists a merged region – also known as the *shock layer* – in which the shock wave and viscous boundary layer are virtually indistinguishable. Furthermore, hypersonic boundary layers have a well-defined edge where the appropriately scaled gas temperature and viscosity vanish, which is in sharp contrast to low speed flows.

For simplicity, real gas effects shall be neglected throughout this thesis and the gas assumed to obey the perfect gas law. In addition, vorticity and entropy layer effects will also not be taken into account, and the flow shall be assumed to be laminar throughout. Nevertheless, these aspects are extremely important for the overall vehicle design and performance (for further details concerning these effects, please refer to the above cited references and also to Bertin 1989 and Dorrance 1962).

1.2 Fundamental Flow Parameters

It is important to introduce several non-dimensional parameters that characterize the nature of the flow. It should be noted that throughout this thesis, the streamwise and transverse coordinates are represented by x and y respectively, with corresponding velocity components u and v. In addition p is the pressure, ρ the density, T the temperature and μ the viscosity. Quantities with a subscript

'∞' are used to denote free-stream conditions. For convenience the acronyms '2D' and 'AXI' will be used to refer to two-dimensional or axially-symmetric cases respectively, and the integer j is defined as:

$$j = \begin{cases} 0 & \text{for 2D flows,} \\ 1 & \text{for AXI flows.} \end{cases} \tag{1.1}$$

The mainstream Mach and Reynolds numbers are defined respectively by:

$$M_\infty = u_\infty \left(\frac{\gamma p_\infty}{\rho_\infty} \right)^{-1/2}, \qquad \mathrm{Re}_\infty = \frac{\rho_\infty u_\infty L}{\mu_\infty}, \tag{1.2}$$

where L is a characteristic length scale of the body. These two fundamental flow parameters are assumed to be large, but such that the *small perturbation parameter* ϵ is small, namely[1]

$$\epsilon = M_\infty^{1/2} \mathrm{Re}_\infty^{-1/4} \ll 1. \tag{1.3}$$

Furthermore, the ratio of specific heats γ and the Prandtl number Pr are defined respectively by

$$\gamma = \frac{c_p}{c_v}, \qquad \mathrm{Pr} = \frac{\mu c_p}{k}. \tag{1.4}$$

where k is the thermal conductivity. For air at standard atmospheric conditions $\gamma = 1.4$ and $\mathrm{Pr} \approx 0.725$.

One of the most important parameters in hypersonic flow theory is the *hypersonic viscous interaction parameter* χ defined by:

$$\chi = M_\infty^3 \mathrm{Re}_\infty^{-1/2} C^{1/2}, \tag{1.5}$$

where C is the Chapman-Rubesin constant given by Eq. (2.7). This parameter characterizes the intensity of the viscous-inviscid interaction described in the

[1]It will be shown in Sec. 2.2 that for flows with strong viscous interaction, the boundary layer thickness is of the same order of magnitude as ϵ.

previous section (see also Sec. 1.3). Another fundamental flow parameter is the *hypersonic similarity parameter* $K = M_\infty \alpha$, where α is the body slenderness ratio. The hypersonic inviscid flow over two different but affinely related bodies are similar (in terms of non-dimensional variables) if the ratio of specific heats γ and K are the same (Anderson 1989). This result can be extended to hypersonic flows with viscous interaction, provided that K is defined in terms of the local inclination angle θ of the boundary layer edge, i.e.

$$K = M_\infty \theta. \tag{1.6}$$

It is also important to introduce the ratio Ω of the body thickness h to that of the boundary layer δ, i.e.:

$$\Omega = \frac{h}{\delta}, \tag{1.7}$$

If $\Omega \gg 1$, the AXI boundary layer equations reduce to an equivalent 2D problem using *Mangler's transformation* (see, for example, Hayes & Probstein 1959 and Yasuhara 1962). However if $\Omega \sim 1$ or $\Omega \ll 1$ (as would be the case for a vanishingly thin needle), then Mangler's transformation is not applicable and transverse curvature effects can not be neglected.

1.3 Hypersonic Viscous Interaction

In this section, the theory of viscous-inviscid interaction in hypersonic flows shall be described. For a more complete discussion including a comprehensive reference list, please refer to Anderson (1989), Cheng (1993), Mikhailov *et al.* (1971) and also to the other references previously cited above.

1.3.1 Strong Interaction Regime

This case occurs when $\chi \gg 1$, and is of particular importance near the leading edge tip of a slender body, as shown in Figs. 1.1 and 2.1. If the thickness of the

boundary layer is of the same order of magnitude, or even much greater than, that of the body (i.e. $\Omega \sim 1$ or $\Omega \ll 1$), it can be shown that the local inclination angle θ of the boundary layer edge can be estimated by (see Sec. 2.2):

$$\theta \sim \epsilon = M_\infty^{1/2} \mathrm{Re}_\infty^{-1/4}. \tag{1.8}$$

As pointed out by Bush & Cross (1967), this approximation differs from the classical result given by Eq. (1.10) which is valid for flows with weak or moderate viscous interaction. It also follows from this estimate and Eq. (1.2) (with L replaced by x) that the boundary layer thickness $\delta \sim x\theta \sim x^{3/4}$. Furthermore, the pressure distribution for flows with strong viscous interaction can be approximated using the tangent-wedge/cone formula (see Sec. 2.3), which states that

$$p \propto \theta^2. \tag{1.9}$$

Using this approximation, it can be inferred that the leading-order pressure $p \sim x^{-1/2}$. Therefore the pressure gradient is favourable and the flow is not expected to separate from the body surface near the leading-edge tip.[2] It is also evident from Eqs. (1.5), (1.6) and (1.8) that the viscous interaction parameter $\chi \sim K^2$.

The hypersonic flow over flat plates with strong viscous interaction was considered by Lees (1953) and Stewartson (1955b). Solutions for the hypersonic flow over hot or cold flat plates have been computed by Werle *et al.* (1973) using an implicit finite-difference scheme. Kozlova & Mikhailov (1970) and Dudin (1978) have also computed flows with strong viscous interaction on a semi-infinite delta wing at zero angle-of-attack, and it can be shown that the problem can be reduced to a self-similar one which can be subsequently solved using techinqiues developed for two-dimensional flows.

[2]Flow separation may occur at non-zero angles-of-attack.

The asymptotic solution of the boundary layer equations for the flow over axially-symmetric bodies has been obtained by Glauert & Lighthill (1955) and Stewartson (1955a) for incompressible flows. Later, Wei (1964) considered the self-similar problem at moderate supersonic speeds and Stewartson (1964) investigated the hypersonic flow with strong viscous interaction near the nose of a very slender sharp cone. Self-similar solutions for the flow over slender AXI bodies with surface shapes of the form $y_s \propto x^{3/4}$ have been obtained by Yasuhara (1962) and Ellinwood & Mirels (1968), under the assumption that $\Omega \sim 1$. However, it appears that no solutions have so far been obtained for vanishingly thin AXI needles (i.e. for which $\Omega \to 0$), and this problem shall be addressed in Chapter 3.

1.3.2 Moderate Interaction Regime

From Fig. 1.1, it is clear that there must exist a transitional region where the viscous interaction is moderate (i.e. $\chi \sim 1$). A number of solutions have already been obtained for this case, such as the computational results of Dewey (1963), who obtained solutions of the boundary layer equations with cross flow using the local similarity method. The hypersonic flow over a finite delta wing at zero angle-of-attack has been computed by Dudin (1983) using a finite-difference scheme which takes into account the pressure on the wing trailing edge (see also Walker *et al.* 1993, pages 68–71). In contrast to the strong interaction regime, the main obstacle posed by flows with moderate viscous interaction is that they do not admit self-similar solutions, and therefore the full three-dimensional problem should be considered. Khorrami & Smith (1994) have also computed the hypersonic flow over 2D flat plates and thin aerofoils using a multi-sweeping method to solve the equations in both the inviscid and viscous layers simultaneously.

Talbot *et al.* (1958) have measured the self-induced pressure on a 3^o and 5^o semi-vertex cone experimentally in a hypersonic flow with $0.5 < \chi < 2.3$ and

$0.9 < \chi < 3.5$ respectively. It was shown that the tangent-cone approximation (see Sec. 2.3) predicts self-induced pressures which are only 10 to 20 percent higher than the measured values.

1.3.3 Weak Interaction Regime

This case occurs when $\chi \ll 1$, and is of particular importance far downstream of the leading edge or nose, as shown in Fig. 1.1. It can be verified that the boundary layer inclination angle θ for the hypersonic flow past a flat plate can be estimated by:

$$\theta \sim M_\infty^2 \mathrm{Re}_\infty^{-1/2}, \tag{1.10}$$

(see, for example, Anderson 1989 and Dorrance 1962). It follows using this estimate and Eq. (1.2) (with L replaced by x) that the boundary layer develops a parabolic profile since $\delta \sim x\theta \sim x^{1/2}$. It can also be inferred from Eqs. (1.5), (1.6) and (1.10) that $\chi \sim K$.

If the thickness of the boundary layer is negligible in comparison to that of the body (i.e. $\Omega \gg 1$), it is expected that the pressure distribution may be calculated using the inviscid equations of motion, and that the boundary layer displacement effect should be of secondary importance. This is the case for the flow over blunt bodies, and to leading-order

$$\theta \sim \frac{\mathrm{d}y_s}{\mathrm{d}x}, \tag{1.11}$$

where $y_s(x)$ is the body contour geometry.

Numerous self-similar, parabolized and full Navier-Stokes solutions for the hypersonic flow with weak viscous interaction past flat plates and thin aerofoils have been obtained by a number of investigators (see, for example, Anderson 1989 and 1995, Bertin *et al.* 1989 and Mikhailov *et al.* 1971 for further details). In particular, self-similar solutions for the flow over bodies of power law shape are

well known (see Hayes & Probstein 1959). Inger (1995) has recently considered another type of similarity solutions in the case of exponentially shaped bodies. Ruban & Sychev (1973) have also computed the three-dimensional flow over a two-dimensional aerofoil with three-quarter power-law generator and with various trailing edge boundary conditions.

It was shown by Neiland (1969), Stewartson & Williams (1969), Messiter (1970) and Sychev (1972) that viscous-inviscid interaction in a region of weak global viscous interaction can be described in terms of a local multi-layer structure known as the *triple-deck*, as shown in Fig. 5.1, and numerous solutions of the triple-deck equations have been obtained (see Sec. 1.5 for further details).

1.4 Upstream Influence Effect

An important property of supersonic and hypersonic boundary layers is their ability, under certain circumstances, to transmit perturbations upstream through the subsonic part of the boundary layer. This implies that the solution at a particular streamwise location can not be determined uniquely without consideration of the downstream conditions, thus reflecting the true elliptic nature of the Navier-Stokes equations. This is rather surprising, since the governing equations in the viscous and inviscid layers are of parabolic and hyperbolic type respectively, and at first sight it would appear that the flow over the entire body could be computed using a downstream marching technique with simultaneous matching between the solutions in both layers at the boundary layer edge.

This upstream influence effect has been a major problem in the computation of viscous hypersonic flows – particularly for flows with moderate or strong viscous interaction – and can cause a nonlinear breakdown of the solutions if numerical marching is used purely in the downstream direction. However, Khorrami & Smith (1994) have recently developed a multi-sweeping method to compute the

hypersonic boundary layer over flat plates and thin airfoils. This method prevents nonlinear breakdown of the numerical marching procedure by directly bringing into effect the upstream influence.

The upstream propagation of disturbances within supersonic boundary layers was first observed in the experiments of Ferri (1939), Ackeret (1947), Chapman *et al.* (1958) and others. In these investigations it was observed that an oblique shock wave incident on a boundary layer could cause the flow to separate well upstream of the point of intersection of the shock and boundary layer. A similar situation can also occur, for example, for the flow over a compression ramp or forward facing step. The theoretical description of this behaviour was first presented by Lighthill (1953), who showed that the viscous-inviscid interaction plays a key rôle in the upstream influence effect. Using the equations of the supersonic triple-deck formulation, solutions of the boundary layer equations can be sought in the following form (see Stewartson 1974):

$$\left.\begin{aligned} u &= y - q\,\mathrm{e}^{\sigma x} f'(y) + \cdots, \\ v &= q\sigma\,\mathrm{e}^{\sigma x} f(y) + \cdots, \\ p &= q\,\mathrm{e}^{\sigma x} + \cdots, \end{aligned}\right\} \quad \text{as} \quad x \to -\infty, \tag{1.12}$$

where the positive eigenvalue σ is to be determined and q is an arbitrary constant. In addition, $f(y)$ satisfies the following boundary conditions:

$$f(0) = f'(0) = 0, \quad f'(\infty) = \sigma^{-1}. \tag{1.13}$$

It can be shown that

$$f'(y) = -\frac{\sigma^{2/3}}{\mathrm{Ai}(0)} \int_0^y \mathrm{Ai}(\sigma^{1/3} z)\,\mathrm{d}z, \tag{1.14}$$

where

$$\sigma = \left\{ \frac{3^{7/6}\Gamma(-1/3)}{2\pi} \right\}^{3/4} \approx 0.8272. \tag{1.15}$$

Since σ is positive, it is concluded that upstream influence does exist and that it decays exponentially as $x \to -\infty$.

The upstream influence effect associated with hypersonic boundary layers with strong viscous interaction was first discovered by Neiland (1970), who considered the flow over an insulated flat plate under the assumption of a linear temperature-viscosity law and a Prandtl number of unity. It was shown that the streamwise extent Δx of the upstream propagation of disturbances is of the order

$$\Delta x \sim \chi^{3/4}. \tag{1.16}$$

Thus, in contrast to flows with weak global viscous interaction, the upstream influence effect for the case $\chi \gg 1$ affects the entire flow up to the leading-edge. In addition, by making use of the tangent-wedge approximation for the pressure distribution, Neiland (1970) showed that there exists a non-uniqueness in the asymptotic expansion for the pressure:

$$p = p_0 x^{-1/2}\{1 + \cdots + q x^{\sigma - 1/2} + \cdots\} \quad \text{as} \quad x \to 0^+, \tag{1.17}$$

where p_0 is a constant which can be computed by solving the appropriate self-similar equations, and q is an arbitrary constant. The eigenvalue σ characterizes the intensity of the upstream transmission of disturbances and was found to be approximately 25.3. Werle *et al.* (1973) extended Neiland's (1970) original work to include the effects of non-adiabatic walls. These results were later confirmed by Brown & Stewartson (1975a), who solved the equations in both the viscous and inviscid layers simultaneously, and concluded that the tangent-wedge formula yields remarkably accurate results.

1.5 Asymptotic Theory of Separated Flows

Flow separation can lead to quite adverse effects on the performance of aircraft and vehicles capable of hypersonic flight, and may result in excessively high heat transfer rates at the reattachment point. For a more comprehensive discussion of separated flows, see Bos (1998), Cassel *et al.* (1995, 1996), Kerimbekov *et al.* (1994) and Sychev *et al.* (1998).

It turns out that the interaction between the boundary and inviscid layers plays a crucial rôle in the separation process. If the flow separates in a region of weak viscous interaction, the separation and reattachment process can be described using an asymptotic theory based on the triple-deck structure. The main difference between this theory and the classical interactive strategy of Prandtl (1904) is that the pressure $p(x)$ is unknown in advance and for 2D flows is related to the displacement thickness $A(x)$ and surface geometry $f(x)$ via the *Ackeret formula*, which for supersonic or hypersonic flows without wall cooling takes the form:

$$p(x) = -\frac{\mathrm{d}A}{\mathrm{d}x} + \frac{\mathrm{d}f}{\mathrm{d}x}, \tag{1.18}$$

(see, for example, Ashley & Landahl (1965) for a derivation of this relation). In order to take upstream influence effects into account, the boundary conditions far downstream from the leading edge are also required in order to solve the triple-deck equations, an exception being the hypersonic flow past compression ramps with strong supercritical wall cooling (see Sec. 6.2.2).

Triple-deck theory has subsequently been applied to many problems spanning the full range of flow speeds from subsonic to hypersonic. The effects of wall cooling on the triple-deck structure have also been investigated (see Chapter 5 for further details). Numerical solutions of the triple-deck equations for the flow over 2D compression ramps have been obtained by numerous authors, most recently by

Cassel *et al.* (1995, 1996) and Bos (1998). These results show that a separation zone develops near the corner for ramp angles greater than a certain critical value. Gajjar & Smith (1983) have also considered the case of free–interactions. Solutions for supersonic AXI flows have been obtained by Kluwick *et al.* (1984) who solved the governing equations in both the lower viscous sublayer and inviscid region simultaneously. In addition, the separated flow past a trailing edge at incidence in supersonic flow has been investigated by Elliott& Smith (1986).

It will be shown in Chapter 5 that the lower-deck sublayer for the flow over bodies with strong wall cooling reduces to a classical Prandtl boundary layer with prescribed pressure gradient. However, it is well known that a Goldstein (1948) singularity is usually encountered at the separation point in any situation where the pressure distribution is known in advance. The nature and structure of this singularity was first described by Landau & Lifschitz (1944), who showed that the asymptotic behaviour of the skin friction τ_s immediately upstream of the separation point $x = x_s$ is given by:

$$\tau_s(x) \sim (x_s - x)^{1/2} \quad \text{as} \quad x \to x_s^-. \tag{1.19}$$

Later, Goldstein (1948) demonstrated that the solution of the boundary layer equations can not be continued downstream of x_s. However, under certain circumstances (such as the flow near the leading-edge of an aerofoil at a critical angle-of-attack), a weaker singularity may be encountered in which the skin friction vanishes linearly at x_s (see Werle & Davis 1972 and Ruban 1981, 1982). This is sometimes referred to as *marginal separation*, and does not preclude the possibility of continuation of the solution downstream of x_s (see also Appendix C).

It should be emphasized that triple-deck theory is not in general applicable in a region of strong global viscous interaction (i.e. $\chi \gg 1$). Nevertheless, Brown *et al.* (1975b) have developed a Newtonian version of the theory (i.e. γ close to unity) which makes use of the tangent-wedge formula in place of Eq. (1.18) as the crucial pressure-displacement relation.

1.6 Outline of Thesis

This thesis is divided into two main parts. The first part deals with the hypersonic flow near the leading-edge of 2D or AXI slender bodies with strong viscous-inviscid interaction. The second part is mainly devoted to the hypersonic flow over compression or expansion ramps in a region of weak viscous interaction and with strong wall cooling. Although the same governing equations of gas dynamics are valid over the entire body, the crucial pressure-displacement relation differs in both of these regions.

Chapter 2 introduces the hypersonic boundary layer equations with strong viscous interaction for values of the ratio Ω of the body to the boundary layer thickness spanning the full range of values from zero to infinity. In addition, the tangent wedge/cone approximation shall be employed as a means of determining the pressure distribution, and transverse curvature effects for the AXI case are fully taken into account. The conditions for self-similarity are also discussed, and it will be shown that self-similar solutions for the case $\Omega \sim 1$ or $\Omega \ll 1$ exist only for three-quarter power-law bodies, flat plates or vanishingly thin AXI needles.

Chapter 3 is mainly devoted to the flow over three-quarter power-law bodies, and numerical solutions are obtained for the resulting self-similar equations. The results for vanishingly thin AXI needles are believed to be the first ever obtained. In addition, new semi-analytical relationships for the determination of the boundary layer thickness for different body thicknesses are derived. The upstream influence effect is represented in the form of an eigen-function perturbation whose intensity is dependent upon an eigenvalue σ. Although upstream influence in hypersonic flows was discovered almost thirty years ago, results for the eigenvalue σ have so far only been obtained for the 2D flat plate case with a Prandtl number of unity. In this chapter, numerical results are obtained for various body thicknesses, temperature factors, Prandtl numbers and ratio of specific

heats for both 2D and AXI flows. Asymptotic results for very hot bodies are also derived, and the results are compared with existing solutions.

Chapter 4 considers relatively thick power-law bodies of the form $y_s = rx^\alpha$, where $\alpha < 3/4$. It is shown that the parameter Ω is much greater than unity for this choice of body contour. Furthermore, it is expected that the upstream influence effect should decay exponentially near the leading edge and that its effects are most strongly felt in a thin viscous sublayer near to the surface. Analytical results are obtained for the thickness of the sublayer and also for the eigenvalue ω. It is shown that ω is positive, thus proving that the upstream influence does indeed decay exponentially as the leading-edge is approached. Finally, numerical solutions of the self-similar equations are used to correlate the analytical results for various values of α, γ, Pr and temperature factor g_s.

Chapter 5 discusses the hypersonic flow over compression or expansion corners with wall cooling for both 2D and AXI cases in which the parameter Ω is much greater than unity. The influence of the surface temperature is considered, and the equations for the strong wall cooling case are formulated.

Chapter 6 treats the numerical solution of the inviscid upper-deck equations using both the Method of Characteristics and finite-difference 'Leap-frog' method. The resulting pressure distribution is employed in the computation of the flow in the viscous lower deck using a fully-implicit downstream marching technique. New numerical results are obtained for both 2D and AXI cases, and the effects of varying the body radius or ramp angle are discussed. In addition, new self-similar solutions are determined for the flow far downstream of the ramp corner for flows without separation, and also for cases exhibiting incipient separation.

Chapter 7 is devoted to the flow separation phenomenon occurring in hypersonic flows over 2D compression ramps with strong subcritical wall cooling. It is surprising that no numerical solutions have so far been obtained for this case,

owing to the de-stabilising effect of subcritical wall cooling. An asymptotic theory is employed in order to remove the Goldstein singularity, and the resulting nonlinear interaction problem is solve numerically using a novel unsteady algorithm developed by the author. In addition, the asymptotic solution far upstream and downstream of the interaction region is derived, and it shall be shown that the numerical solution is in very good agreement with both of these analytical results. It is also shown that the asymptotic theory considered here, as well as marginal separation theory, can both be extended to describe the separation process occurring in axially-symmetric flows.

All the numerical results presented in this thesis were obtained using FORTRAN 90 computer codes written exclusively by the author, and run on a DEC Alpha workstation using double precision accuracy. Unless otherwise stated, all the solutions presented here are properly converged to within the required accuracy, and also appear to be grid independent.[3]

[3]Discrepancies in the numerical results could of course appear if the grid being employed is either too coarse or too fine.

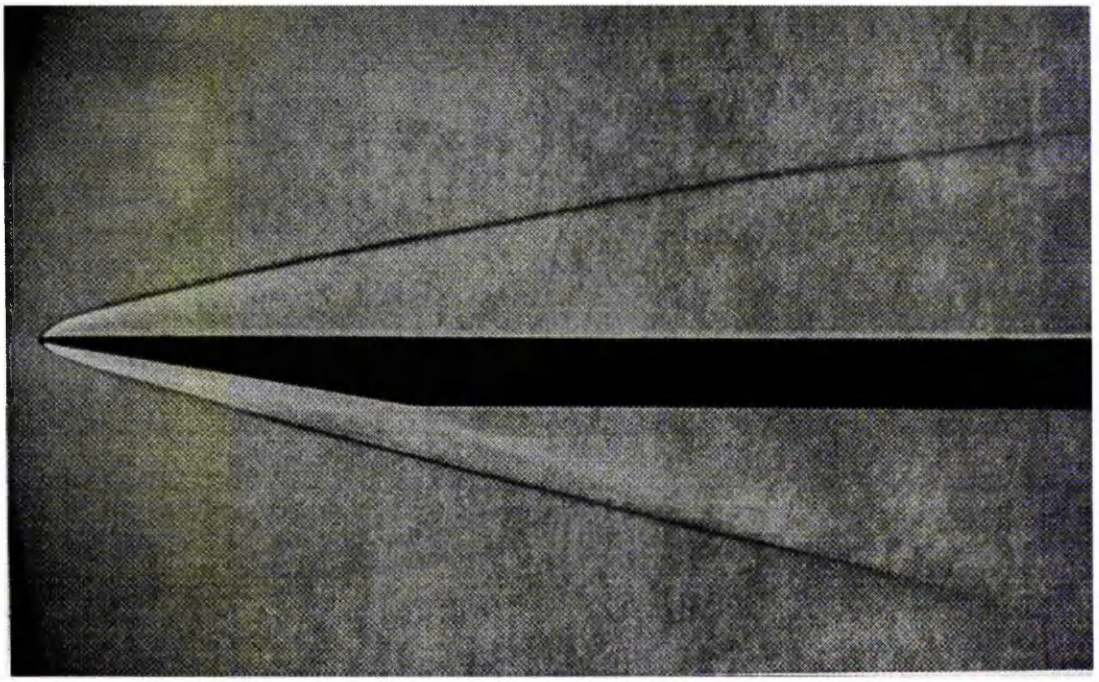

Figure 1.2: Hypersonic flow past a blunted flat plate in air at $M_\infty = 13.8$. (*Crown copyright photo from Cox & Crabtree 1965.*)

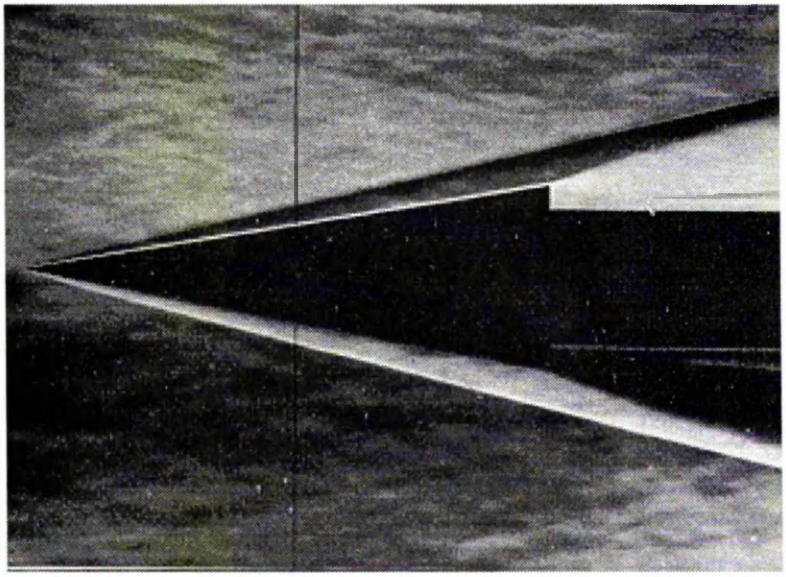

Figure 1.3: Hypersonic flow past a sharp 10^o cone in air at $M_\infty = 6.85$. (*Photo from Chernyi 1961.*)

Part I

Hypersonic Flow over Very Slender Bodies with Strong Viscous Interaction

Chapter 2

Hypersonic Boundary Layer Equations

2.1 Introduction

In this chapter, the hypersonic flow of an ideal gas near the leading-edge of a very slender 2D or AXI body oriented parallel to the upstream flow will be investigated, as shown in Fig. 2.1. If h and L are the characteristic height and length of the body respectively, then the *slenderness ratio* $d = h/L$ is assumed small in the sense that

$$d \sim \epsilon = M_\infty^{1/2} \mathrm{Re}_\infty^{-1/4} \ll 1. \tag{2.1}$$

The equations of the body surface y_s and boundary layer edge y_b will be taken respectively as:

$$y_s = Lds(x/L), \qquad y_b = Lb(x/L)s(x/L), \tag{2.2}$$

where the functions s and b are arbitrary to start off with. In addition, the viscous-inviscid interaction is expected to be strong, i.e.

$$\chi = M_\infty^3 \mathrm{Re}_\infty^{-1/2} C^{1/2} \gg 1. \tag{2.3}$$

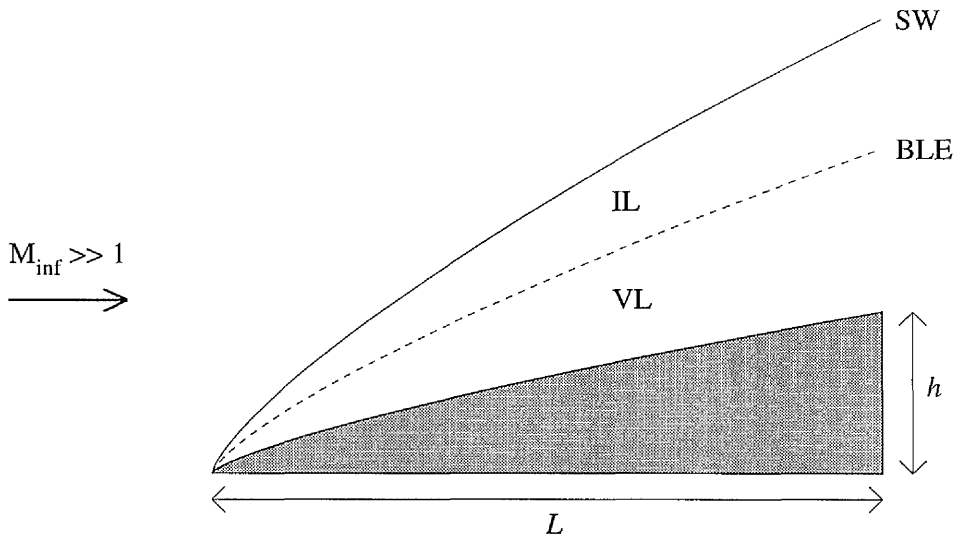

Figure 2.1: Schematic of the hypersonic flow near the leading edge of a slender body (not to scale). SW and BLE indicate the shock wave and boundary layer edge; IL and VL are the inviscid and viscous layers.

The equations of continuity, streamwise momentum and energy which govern the flow within the boundary layer are given respectively by (see, for example, Hayes & Probstein 1959):

$$\frac{\partial}{\partial x}\left(\rho u y^j\right) + \frac{\partial}{\partial y}\left(\rho v y^j\right) = 0, \tag{2.4}$$

$$\rho\left(u\frac{\partial u}{\partial x} + v\frac{\partial u}{\partial y}\right) = -\frac{\partial p}{\partial x} + \frac{1}{y^j}\frac{\partial}{\partial y}\left(y^j \mu \frac{\partial u}{\partial y}\right), \tag{2.5}$$

$$\rho\left(u\frac{\partial h}{\partial x} + v\frac{\partial h}{\partial y}\right) = u\frac{\partial p}{\partial x} + \frac{1}{y^j}\frac{\partial}{\partial y}\left(y^j \frac{\mu}{\mathrm{Pr}}\frac{\partial h}{\partial y}\right) + \mu\left(\frac{\partial u}{\partial y}\right)^2. \tag{2.6}$$

In addition it can be inferred from the transverse momentum equation that the pressure is a function of x only throughout the boundary layer. The perfect gas

equation of state and linear temperature-viscosity law are given by:

$$p = \rho \mathcal{R} T, \quad \frac{\mu}{\mu_\infty} = C \frac{T}{T_\infty}, \tag{2.7}$$

where $\mathcal{R}$ is the universal gas constant and C is the Chapman-Rubesin constant. Furthermore, the total enthalpy H is related to the static enthalpy h by:

$$H = h + \frac{u^2 + v^2}{2}, \quad h = \frac{p}{\lambda \rho}, \tag{2.8}$$

where

$$\lambda = \frac{\gamma - 1}{\gamma}. \tag{2.9}$$

The no-slip conditions on the body surface imply that

$$u = v = 0 \quad \text{at} \quad y = y_s(x). \tag{2.10}$$

The surface condition for the enthalpy is given by:

$$\left.\begin{array}{l} h = h_s \quad \text{(heat transfer case) } \textit{or} \\ \partial h / \partial y = 0 \quad \text{(thermally insulated case)} \end{array}\right\} \quad \text{at} \quad y = y_s(x), \tag{2.11a}$$

where h_s is the body surface enthalpy. The conditions at the outer edge of the boundary layer can be determined using the Rankine-Hugoniot shock relations in the hypersonic limit $M_\infty \to \infty$ (see, for example, Anderson 1989):

$$\frac{p}{p_\infty} \to \frac{2\gamma}{\gamma + 1} M_\infty^2 \sin^2 \beta, \tag{2.12a}$$

$$\frac{\rho}{\rho_\infty} \to \frac{\gamma + 1}{\gamma - 1}, \tag{2.12b}$$

$$\frac{T}{T_\infty} \to \frac{2\gamma(\gamma - 1)}{(\gamma + 1)^2} M_\infty^2 \sin^2 \beta, \tag{2.12c}$$

$$\frac{u}{u_\infty} \to 1 - \frac{2 \sin^2 \beta}{\gamma + 1}, \tag{2.12d}$$

$$\frac{v}{u_\infty} \to \frac{\sin(2\beta)}{\gamma + 1}, \tag{2.12e}$$

where β is the shock wave inclination angle. By making use of the equation of state (2.8), it follows that the required boundary conditions at the outer edge of the boundary layer are, to leading-order,

$$u = u_\infty, \quad h = \frac{2\gamma}{(\gamma+1)^2} u_\infty^2 \sin^2\beta \quad \text{at} \quad y = y_b(x). \tag{2.13}$$

2.2 Estimates for Hypersonic Flows

It is very useful in the investigation of hypersonic flows to obtain simple order of magnitude estimates for the flow variables within the boundary layer. By comparing the convective, viscous and mechanical energy dissipation terms in the energy equation (2.6), it can be inferred that

$$h = c_p T \sim u_\infty^2. \tag{2.14}$$

It follows from Eq. (2.7) that the viscosity can be estimated by

$$\mu \sim \mu_\infty M_\infty^2. \tag{2.15}$$

For hypersonic flows with strong viscous interaction, the shock wave inclination angle β is of the same order-of-magnitude as the local inclination angle θ of the boundary layer edge. Moreover, since θ is relatively small, it follows from Eq. (2.12a) that the pressure can be estimated by:

$$p \sim \gamma p_\infty M_\infty^2 \theta^2 = \rho_\infty u_\infty^2 \theta^2. \tag{2.16}$$

An estimate for the density can now be found using the equation of state Eq. (2.7a) yielding:

$$\rho \sim \rho_\infty \theta^2. \tag{2.17}$$

A comparison of the convective and viscous terms in the momentum equation (or equivalently the convective and heat transfer terms in the energy equation)

shows that:

$$\frac{\rho u}{\Delta x} \sim \frac{\mu}{(\Delta y)^2}. \tag{2.18}$$

Using the above results, as well as the definition of the Reynolds number Re_∞ given by Eq. (1.2), it can be shown that an estimate for the boundary layer thickness δ is given by:

$$\delta \sim L M_\infty^{1/2} \mathrm{Re}_\infty^{-1/4}. \tag{2.19}$$

Hence, the slope θ of the outer edge of the boundary layer is found to be of the same order-of-magnitude as the small perturbation parameter ϵ, i.e.:

$$\theta \sim \frac{\delta}{L} \sim \epsilon = M_\infty^{1/2} \mathrm{Re}_\infty^{-1/4}. \tag{2.20}$$

It should be noted that the requirements that $\epsilon \ll 1$ and $\chi \gg 1$ both imply that

$$\mathrm{Re}_\infty^{1/6} \ll M_\infty \ll \mathrm{Re}_\infty^{1/2}, \tag{2.21}$$

which is valid for most hypersonic flow conditions, such as that encountered during the atmospheric re-entry from orbit.

These simple order-of-magnitude estimates suggest the use of the following non-dimensional scaled variables within the boundary layer:

$$x = L\hat{x}, \quad y = L\epsilon\hat{y}, \quad u = u_\infty \hat{u}, \quad v = u_\infty \epsilon \hat{v}, \tag{2.22a}$$

$$h = u_\infty^2 \hat{h}, \quad H = u_\infty^2 \hat{H}, \quad p = \gamma p_\infty M_\infty^2 \epsilon^2 \hat{p}, \tag{2.22b}$$

$$\rho = \rho_\infty \epsilon^2 \hat{\rho}, \quad \mu = \mu_\infty M_\infty^2 \hat{\mu}, \quad T = \gamma T_\infty M_\infty^2 \hat{T}. \tag{2.22c}$$

In addition, the slenderness ratio d and the function $b(x)$ defined by Eq. (2.2) must also be scaled according to:

$$d = \epsilon r, \quad b(x/L) = \epsilon \hat{b}(\hat{x}). \tag{2.23}$$

It can be inferred from Eq. (2.13) and from the first of Eqs. (2.22b) that the scaled enthalpy at the boundary layer edge is given by:

$$\hat{h} \sim \frac{2\gamma\epsilon^2}{(\gamma+1)^2} \ll 1. \tag{2.24}$$

Therefore, for hypersonic flows, the scaled enthalpy and viscosity should vanish at the outer edge of the boundary layer, and thus the position of this edge can be determined precisely. This is in sharp contrast to subsonic or supersonic flows with small freestream Mach numbers. Moreover, the density within a hypersonic boundary layer is relatively small and can be thought of as a quasi-vacuum. Upon substitution of Eqs. (2.22) into Eqs. (2.4)–(2.6), it can be shown that the boundary layer equations remain invariant. Therefore, for convenience, **the superscript ' ˆ ' will be dropped and the equations considered to be scaled and non-dimensional.** The scaled perfect gas equation of state and linear temperature-viscosity law given by Eq. (2.7) can be written in the form:

$$p = \rho T, \qquad \mu = \gamma C T, \tag{2.25}$$

and from Eq. (2.8), the scaled total enthalpy H can be expressed to leading-order as

$$H = h + \frac{1}{2}u^2, \qquad h = \frac{p}{\lambda\rho}. \tag{2.26}$$

It is useful to express the scaled energy equation (2.6) in terms of the total enthalpy H with the help of the streamwise momentum equation (2.5), and the resulting equation can be written in the form:

$$\rho\left(u\frac{\partial H}{\partial x} + v\frac{\partial H}{\partial y}\right) = \frac{1}{y^j}\frac{\partial}{\partial y}\left\{y^j\mu\left(\nu u\frac{\partial u}{\partial y} + \frac{1}{\mathrm{Pr}}\frac{\partial H}{\partial y}\right)\right\}, \tag{2.27}$$

where

$$\nu = 1 - \frac{1}{\mathrm{Pr}}. \tag{2.28}$$

In addition, the equations for the body and boundary layer edge position given by Eq. (2.2) become

$$y_s = rs(x), \qquad y_b = b(x)s(x). \tag{2.29}$$

The boundary conditions at the body surface are given by:

$$u = v = 0, \quad H = g_s \quad \text{or} \quad \frac{\partial H}{\partial y} = 0 \quad \text{at} \quad y = y_s(x), \tag{2.30}$$

where $g_s = h_s/u_\infty^2$ is the *temperature factor*. At the boundary layer edge,

$$u = 1, \quad H = 1/2 \quad \text{at} \quad y = y_b(x). \tag{2.31}$$

For the special case of the flow past an insulated body with $\mathrm{Pr} = 1$, it follows from Eqs. (2.27) and (2.31) that

$$H = h + \frac{1}{2}u^2 = \frac{1}{2}, \tag{2.32}$$

which is known as *Crocco's Integral*. A similar integral can be obtained under the assumption that the Prandtl number is small (i.e. $\mathrm{Pr} \to 0$), in which case the constant $\nu \to -\infty$. In this case it can be shown that the solution to Eq. (2.27) is given by:

$$H = \frac{1}{2}u^2. \tag{2.33}$$

2.3 Tangent Wedge/Cone Approximation

The pressure distribution on the surface of a slender body in a hypersonic flow can be approximated using the so-called *tangent wedge/cone formula*. This states that the local surface pressure is approximately equal to the exact value of the pressure on a wedge or cone having the same inclination to the oncoming flow direction under the same freestream conditions. The experimental results of Talbot *et al.* (1958) for the hypersonic flow over a slender cone with moderate viscous

interaction show that the tangent cone method predicts self-induced pressures which are only 10 to 20 percent higher than the measured values. However, it is expected that this approximation yields more accurate results as $\chi \to \infty$.

It can be shown (see Chernyi 1961 and Cox & Crabtree 1965) that the pressure coefficient C_p on the surface of a body in inviscid hypersonic flow can be approximated by:

$$C_p = \frac{p - p_\infty}{\frac{1}{2}\rho_\infty {u_\infty}^2} = 2\kappa(\gamma)\phi^2, \tag{2.34}$$

where the function $\kappa(\gamma)$ is given by

$$\kappa(\gamma) = \begin{cases} \frac{\gamma+1}{2} & \text{for 2D flows,} \\ \frac{(\gamma+1)(\gamma+7)}{(\gamma+3)^2} & \text{for AXI flows,} \end{cases} \tag{2.35}$$

and ϕ is the local surface inclination to the upstream flow. If $\gamma = 1$ and ϕ is small, this approximation reduces to the *Newtonian formula* (see Anderson 1989 and Cox & Crabtree 1965), namely

$$C_p = 2\sin^2\phi \sim 2\phi^2. \tag{2.36}$$

In order to apply this formula to flows with strong viscous-inviscid interaction, the slope ϕ of the body surface should be replaced by the local slope θ of the outer edge of the comparatively thick boundary layer. Therefore, Eq. (2.34) can be written in terms of the scaled pressure defined by Eq. (2.22b):

$$\hat{p} = \frac{1}{\gamma K^2} + \left(\frac{\theta}{\epsilon}\right)^2 \kappa(\gamma), \tag{2.37}$$

where $K = M_\infty \epsilon$. For small values of θ,

$$\theta \sim \tan\theta = \frac{\mathrm{d}y_b}{\mathrm{d}x} = \epsilon \frac{\mathrm{d}}{\mathrm{d}\hat{x}} \left\{ b(\hat{x}) s(\hat{x}) \right\}. \tag{2.38}$$

Since $K^2 \sim \chi \gg 1$ for flows with strong viscous-inviscid interaction (see Sec. 1.3), it follows that to leading-order

$$p = \kappa(\gamma) \left\{ \frac{\mathrm{d}}{\mathrm{d}x} \left[b(x) s(x) \right] \right\}^2, \tag{2.39}$$

where the superscript '^' has been dropped for convenience. It should be noted that the boundary layer edge position $y_b(x) = b(x)s(x)$ is unknown in advance and depends upon the solution in both the viscous and inviscid layers. The above formula allows the determination of the pressure distribution without recourse to the solution of the full Euler Equations, and it is also invaluable in developing self-similar solutions of the boundary layer equations. Finally, it is important to understand that for flows with weak viscous-inviscid interaction, the *Ackeret* (or related) formula given by Eq. (1.18) should be used instead.

2.4 Self-Similarity Requirements

It is convenient to define a stretched transverse coordinate η by

$$\eta = \frac{1}{G(x)} \int_{y_s}^{y} \xi^j \rho(x, \xi) \, \mathrm{d}\xi, \tag{2.40}$$

where $G(x)$ is an unknown function to be determined by similarity requirements as part of the solution. This transformation was originally employed by Dorodnitsyn (1942) for the compressible flow over a flat plate, and enables the governing equations of gas dynamics to be expressed in quasi-incompressible form. Moreover, the use of Dorodnitsyn variables avoids problems associated with the relative low temperature and high density conditions in the intermediate layer between the inviscid flow and boundary layer, at least for linear temperature-viscosity laws.

It is convenient to introduce the stream function ψ such that

$$\frac{\partial \psi}{\partial y} = \rho u y^j, \qquad \frac{\partial \psi}{\partial x} = -\rho v y^j. \tag{2.41}$$

Restricting attention to the scaled momentum equation to start off with, it can be shown that Eq. (2.5) can be written as

$$\frac{1}{G}\left(\frac{\partial \psi}{\partial \eta}\frac{\partial u}{\partial x} - \frac{\partial \psi}{\partial x}\frac{\partial u}{\partial \eta}\right) = -\lambda\left(H - \frac{1}{2}u^2\right)\frac{1}{p}\frac{\mathrm{d}p}{\mathrm{d}x} + \frac{\gamma C p}{G^2(x)}\frac{\partial}{\partial \eta}\left(y^{2j}\frac{\partial u}{\partial \eta}\right), \tag{2.42}$$

where y is now considered to be a function of both x and η (cf. Eq. (2.43b)). It should be noted that the density ρ and viscosity μ have been eliminated by making use of the equation of state and linear temperature-viscosity law given by Eq. (2.25)

A self-similar solution of the above equation will now be sought in the form

$$u = \bar{u}(\eta), \qquad H = \bar{H}(\eta), \tag{2.43a}$$

$$\psi = G(x)\bar{\psi}(\eta), \quad y = s(x)\bar{y}(\eta), \tag{2.43b}$$

$$p = [s'(x)]^2\bar{p}, \qquad \rho = [s'(x)]^2\bar{\rho}(\eta), \tag{2.43c}$$

where $s(x)$ is the body surface contour and $G(x)$ is the unknown function defined in Eq. (2.40). In this section, a prime ($'$) will be used to denote differentiation with respect to x. The form of the solutions given by Eqs. (2.43c) for the pressure and density are suggested by the tangent-wedge/cone formula (2.39). It can be easily shown from the definition of the stream function Eq. (2.41a) and the first of Eqs. (2.43b) that

$$u = \bar{u} = \frac{\partial\bar{\psi}}{\partial\eta}. \tag{2.44}$$

Hence the momentum equation becomes:

$$-\bar{\psi}\frac{\mathrm{d}^2\bar{\psi}}{\mathrm{d}\eta^2}\frac{G'}{G} = -\lambda\left[2\bar{H} - \left(\frac{\mathrm{d}\bar{\psi}}{\mathrm{d}\eta}\right)^2\right]\frac{s''}{s'} + \gamma C\bar{p}\frac{\mathrm{d}}{\mathrm{d}\eta}\left(\bar{y}^{2j}\frac{\mathrm{d}^2\bar{\psi}}{\mathrm{d}\eta^2}\right)\frac{s^{2j}(s')^2}{G^2}. \tag{2.45}$$

For self-similarity, this equation must be independent of x, and this requires that $G(x)$ satisfies the following conditions:

$$\frac{G'}{G} \sim \frac{s''}{s'}, \tag{2.46}$$

$$G^2 \sim \frac{(s')^3 s^{2j}}{s''}. \tag{2.47}$$

With this choice of $G(x)$, Eq. (2.45) reduces to the following ordinary differential equation:

$$\gamma C\bar{p}\frac{\mathrm{d}}{\mathrm{d}\eta}\left(\bar{y}^{2j}\frac{\mathrm{d}^2\bar{\psi}}{\mathrm{d}\eta^2}\right) + \bar{\psi}\frac{\mathrm{d}^2\bar{\psi}}{\mathrm{d}\eta^2} - \lambda\left\{2\bar{H} - \left(\frac{\mathrm{d}\bar{\psi}}{\mathrm{d}\eta}\right)^2\right\} = 0. \tag{2.48}$$

The distribution of $\bar{y}(\eta)$ may be determined by considering the definition of η given by Eq. (2.40), which can be written in the form:

$$\frac{\partial \eta}{\partial y} = \frac{y^j \rho}{G}. \tag{2.49}$$

This equation can be expressed in terms of the self-similar variables defined by Eqs. (2.43) as follows:

$$\frac{\mathrm{d}\bar{y}}{\mathrm{d}\eta} = \frac{\lambda}{\bar{\rho}\bar{y}^j}\left[\bar{H} - \frac{1}{2}\left(\frac{\mathrm{d}\bar{\psi}}{\mathrm{d}\eta}\right)^2\right]\left\{\frac{G}{s^{j+1}(s')^2}\right\}. \tag{2.50}$$

For self-similarity, the expression in braces in the foregoing equation must be a constant, and this yields a second expression for the function $G(x)$:

$$G \sim s^{j+1}(s')^2. \tag{2.51}$$

Equations (2.47) and (2.51) can now be combined yielding the following equation for $s(x)$:

$$s^2 s' s'' = c, \tag{2.52}$$

where c is an arbitrary constant. Hence, for a self-similar solution to exist, the body contour $s(x)$ must satisfy Eq. (2.52).[1] For the special case $c = 0$, this equation has the trivial solution $s(x) = 0$, which corresponds to a flat plate or vanishingly thin needle. The only non-trivial solution satisfying the boundary conditions $s(0) = 0$ and $s(1) = 1$ is given by $s(x) \sim x^{3/4}$. This choice of body contour ensures self-similarity for both 2D and AXI flows. Although this fundamental fact has been known for several decades, the analysis employed here for arbitrary bodies shall prove useful in Chapter 4. Finally, the function $G(x)$ can be found using either Eq. (2.47) or (2.51), and it should be noted that $G(x)$ is unique to within a multiplicative constant. It should also be noted that Eq. (2.46) is identically satisfied for power law bodies of the form $s(x) = x^\alpha$.

[1] To the best of the author's knowledge, this equation has never been derived before.

Chapter 3

Formulation for Three-Quarter Power-Law Bodies

3.1 Introduction

This chapter shall focus on the solution of the interactive hypersonic boundary layer equations for surface geometries of the form:

$$y_s(x) = rx^{3/4}, \tag{3.1}$$

where r is an $O(1)$ slenderness ratio. From Eqs. (2.43a–c), this choice of body contour suggests that the solution of the boundary layer equations should be sought in the following form:

$$u = \bar{u}(x,\eta), \qquad H = \bar{H}(x,\eta), \tag{3.2a}$$

$$\psi = G(x)\bar{\psi}(x,\eta), \quad y = x^{3/4}\bar{y}(x,\eta), \tag{3.2b}$$

$$p = x^{-1/2}\bar{p}(x), \qquad \rho = x^{-1/2}\bar{\rho}(x,\eta). \tag{3.2c}$$

Functions with a superscript '$\bar{}$' are now assumed to be dependent on x as well as η. In accord with Eq. (2.51), the function $G(x)$ is chosen as:

$$G(x) = 2^{1-j}\sqrt{\gamma C p_0}\, x^n = \begin{cases} 2\sqrt{\gamma C p_0}\, x^{1/4} & \text{for 2D flows,} \\ \sqrt{\gamma C p_0}\, x & \text{for AXI flows,} \end{cases} \tag{3.3}$$

where $n = (1+3j)/4$ and p_0 is the self-similar pressure coefficient given by Eq. (3.21). It should be noted that an affine transformation has been incorporated into the definition of $G(x)$ such that the resulting momentum and energy equations are independent of both p_0 and C, and the factor of 2^{1-j} has been introduced for convenience.

The momentum equation (2.5) becomes

$$x\left(\frac{\partial\bar{\psi}}{\partial\eta}\frac{\partial^2\bar{\psi}}{\partial\eta\partial x} - \frac{\partial\bar{\psi}}{\partial x}\frac{\partial^2\bar{\psi}}{\partial\eta^2}\right) - n\bar{\psi}\frac{\partial^2\bar{\psi}}{\partial\eta^2} = \frac{\lambda}{4}\left[2\bar{H} - \left(\frac{\partial\bar{\psi}}{\partial\eta}\right)^2\right]\left[1 - \frac{2x}{\bar{p}}\frac{\mathrm{d}\bar{p}}{\mathrm{d}x}\right] + n\frac{\bar{p}}{p_0}\frac{\partial}{\partial\eta}\left(\bar{y}^{2j}\frac{\partial^2\bar{\psi}}{\partial\eta^2}\right). \tag{3.4}$$

Similarly the transformed energy equation (2.27) is given by

$$x\left(\frac{\partial\bar{\psi}}{\partial\eta}\frac{\partial\bar{H}}{\partial x} - \frac{\partial\bar{\psi}}{\partial x}\frac{\partial\bar{H}}{\partial\eta}\right) - n\bar{\psi}\frac{\partial\bar{H}}{\partial\eta} = n\frac{\bar{p}}{p_0}\frac{\partial}{\partial\eta}\left[\bar{y}^{2j}\left(\nu\frac{\partial\bar{\psi}}{\partial\eta}\frac{\partial^2\bar{\psi}}{\partial\eta^2} + \frac{1}{\mathrm{Pr}}\frac{\partial\bar{H}}{\partial\eta}\right)\right]. \tag{3.5}$$

The relationship between $\bar{y}$ and η, for $j = 0$ or 1 is:

$$\frac{\partial}{\partial\eta}\left(\bar{y}^{1+j}\right) = \frac{\lambda\sqrt{\gamma C p_0}}{\bar{p}}\left[2\bar{H} - \left(\frac{\partial\bar{\psi}}{\partial\eta}\right)^2\right], \tag{3.6}$$

which shall be referred to henceforth as the *displacement equation*. Finally, the tangent wedge/cone formula Eq. (2.39) can be written as

$$\bar{p} = \kappa(\gamma)\left\{\frac{3}{4}b(x) + xb'(x)\right\}^2. \tag{3.7}$$

The boundary conditions at the body surface ($\eta = 0$) are:

$$\bar{y} = r, \quad \bar{\psi} = \frac{\partial\bar{\psi}}{\partial\eta} = 0, \quad \bar{H} = g_s \quad \text{or} \quad \frac{\partial\bar{H}}{\partial\eta} = 0, \tag{3.8}$$

and the conditions at the boundary layer edge ($\eta = \infty$) are given by:

$$\bar{y} = b(x), \quad \frac{\partial \bar{\psi}}{\partial \eta} = 1, \quad \bar{H} = 1/2. \tag{3.9}$$

It is convenient for AXI flows to define the *area function* Λ by:

$$\bar{\Lambda}(\eta) = \{\bar{y}(\eta)\}^2, \tag{3.10}$$

which represents the area of a circular annulus between the body and boundary layer edge.

Equations (3.4)–(3.9) constitute a system of four nonlinear coupled equations for the four unknown functions $\bar{\psi}$, $\bar{H}$, $\bar{y}$ (or $\bar{\Lambda}$) and $\bar{p}$. In order to investigate the upstream propagation of disturbances, the solution of the foregoing equations shall be sought in the following asymptotic form:

$$\bar{\phi}(x, \eta) = \phi_0(\eta) + \cdots + qx^\sigma \phi_1(\eta; \sigma) + \cdots \quad \text{as} \quad x \to 0^+. \tag{3.11}$$

The quantity ϕ represents ψ, H, y or Λ, and q is an arbitrary constant representing the amplitude of the perturbations. The positive constant σ is an unknown eigenvalue which characterizes the intensity of the upstream transmission of disturbances through the subsonic part of the boundary layer. The smaller the value of σ, the more pronounced the upstream influence effect. Functions with a subscript '0' represent the self-similar (leading-order) solutions, whilst those with a subscript '1' represent the first eigen (perturbation) solutions. In addition, the pressure and boundary layer edge positions are expressed as:

$$\bar{p}(x) = p_0(1 + \cdots + qx^\sigma + \cdots), \tag{3.12}$$

$$\bar{b}(x) = b_0 + \cdots + qx^\sigma b_1 + \cdots. \tag{3.13}$$

The following relations also hold for the AXI case:

$$y_0 = \sqrt{\Lambda_0}, \qquad y_1 = \frac{\Lambda_1}{2\sqrt{\Lambda_0}}. \tag{3.14}$$

Substitution of the above expansions into the transformed boundary layer equations (3.4)–(3.9), and equating powers of x^σ, yields two systems of equations which will be given in the next two sections. It is important to note that the constant q is left completely undetermined from these equations and can in principle be used to impose a boundary condition far downstream of the leading edge, such as the presence of a compression ramp.

3.2 Self-Similar Equations

The self-similar momentum, energy and displacement equations for 2D flows are:

$$\psi_0''' + \psi_0\psi_0'' + \lambda\left[2H_0 - (\psi_0')^2\right] = 0, \tag{3.15}$$

$$\mathrm{Pr}^{-1}\, H_0'' + \psi_0 H_0' + \nu(\psi_0'\psi_0'')' = 0, \tag{3.16}$$

$$y_0(\eta) = r + M\mathcal{I}_0(\eta), \tag{3.17}$$

where a prime ($'$) is now used to denote differentiation with respect to η. The corresponding equations for the AXI case are given by:

$$(\Lambda_0\psi_0'')' + \psi_0\psi_0'' + \frac{\lambda}{4}\left[2H_0 - (\psi_0')^2\right] = 0, \tag{3.18}$$

$$\mathrm{Pr}^{-1}(\Lambda_0 H_0')' + \psi_0 H_0' + \nu(\Lambda_0\psi_0'\psi_0'')' = 0, \tag{3.19}$$

$$\Lambda_0(\eta) = r^2 + M\mathcal{I}_0(\eta). \tag{3.20}$$

The leading-order pressure p_0 and boundary layer edge positions b_0 are related via the tangent wedge/cone formula given by Eq. (3.7) which gives:

$$p_0 = \frac{9}{16}\kappa(\gamma)b_0^2, \tag{3.21}$$

where

$$b_0 = y_0(\infty). \tag{3.22}$$

In these equations, the displacement integral $\mathcal{I}_0$ and the unknown constant M are defined respectively by:

$$\mathcal{I}_0(\eta) = \int_0^\eta 2H_0 - (\psi_0')^2 \, \mathrm{d}\eta, \tag{3.23}$$

$$M = \lambda\sqrt{\frac{\gamma C}{p_0}}. \tag{3.24}$$

These equations must be solved subject to the boundary conditions:

$$\psi_0(0) = \psi_0'(0) = 0, \qquad \psi_0'(\infty) = 1, \tag{3.25a}$$

$$H_0(0) = g_s \quad \text{or} \quad H_0'(0) = 0, \qquad H_0(\infty) = 1/2. \tag{3.25b}$$

The leading-order boundary layer thickness is given by $\delta_0 = b_0 - r$ and the pressure distribution along the body is $p(x) = p_0 x^{-1/2}$. Finally, the skin friction τ_s and surface heat transfer q_s are defined by:

$$\tau_s(x) = \left(\mu\frac{\partial u}{\partial y}\right)_{y=y_s}, \quad q_s(x) = \left(k\frac{\partial T}{\partial y}\right)_{y=y_s}. \tag{3.26}$$

In order to take into account the displacement effect of the boundary layer into these expressions, the body surface $y_s = rx^{3/4}$ has been replaced by the effective surface formed by both the body and boundary layer thicknesses, i.e. $y_b = b_0 x^{3/4}$, and it can be shown that to leading-order:

$$\tau_s(x) = \tau_0 x^{-3/4}, \quad q_s(x) = q_0 x^{-3/4}, \tag{3.27}$$

where

$$\tau_0 = 2^{j-1}\sqrt{\gamma C p_0}\, b_0^j\, \psi_0''(0), \tag{3.28}$$

$$q_0 = 2^{j-1}\,\mathrm{Pr}^{-1}\,\sqrt{\gamma C p_0}\, b_0^j\, H_0'(0). \tag{3.29}$$

The quantities $\psi_0''(0)$ and $H_0'(0)$ are determined from a numerical solution of the self-similar equations.

JOHN RYLANDS
UNIVERSITY
LIBRARY OF
MANCHESTER

3.3 Eigen-Equations

The eigen momentum, energy and displacement equations for 2D flows are given by:

$$\begin{aligned}\psi_1''' + \psi_0\psi_1'' - (4\sigma+2\lambda)\psi_0'\psi_1' + (4\sigma+1)\psi_0''\psi_1 \\ = 2\lambda\left\{\sigma\left[2H_0 - (\psi_0')^2\right] - H_1\right\} - \psi_0''',\end{aligned} \tag{3.30}$$

$$\begin{aligned}\mathrm{Pr}^{-1}\, H_1'' + \psi_0 H_1' - 4\sigma\psi_0' H_1 \\ = -\frac{\nu}{2}\left[(\psi_0')^2 + 2\psi_0'\psi_1'\right]'' - \mathrm{Pr}^{-1}\, H_0'' - (4\sigma+1)\psi_1 H_0',\end{aligned} \tag{3.31}$$

$$y_1(\eta,\sigma) = M[\mathcal{I}_1(\eta,\sigma) - \mathcal{I}_0(\eta)]. \tag{3.32}$$

The corresponding equations for the AXI case are:

$$\begin{aligned}(\Lambda_0\psi_1'')' + \psi_0\psi_1'' - (\sigma+\frac{\lambda}{2})\psi_0'\psi_1' + (\sigma+1)\psi_0''\psi_1 \\ = \frac{\lambda}{2}\left\{\sigma\left[2H_0 - (\psi_0')^2\right] - H_1\right\} - \left\{(\Lambda_0+\Lambda_1)\psi_0''\right\}',\end{aligned} \tag{3.33}$$

$$\begin{aligned}\mathrm{Pr}^{-1}(\Lambda_0 H_1')' + \psi_0 H_1' - \sigma\psi_0' H_1 = -(\sigma+1)\psi_1 H_0' \\ - \left\{\nu\Lambda_0(\psi_0'\psi_1'' + \psi_0''\psi_1') + (\Lambda_0+\Lambda_1)(\nu\psi_0'\psi_0'' + \mathrm{Pr}^{-1}\, H_0')\right\}',\end{aligned} \tag{3.34}$$

$$\Lambda_1(\eta,\sigma) = M[\mathcal{I}_1(\eta,\sigma) - \mathcal{I}_0(\eta)]. \tag{3.35}$$

The integral $\mathcal{I}_1$ is defined by

$$\mathcal{I}_1(\eta,\sigma) = 2\int_0^\eta H_1 - \psi_0'\psi_1'\,\mathrm{d}\eta. \tag{3.36}$$

These are three linear coupled equations for the three unknown functions ψ_1, H_1 and y_1 (or Λ_1). However, the unknown eigenvalue σ also appears in this system of equations, and it can be shown from Eq. (3.7) that σ satisfies the following equation:

$$\phi(\sigma) = 2\left(\sigma+\frac{3}{4}\right)b_1(\sigma) - \frac{3}{4}b_0 = 0, \tag{3.37}$$

where

$$b_1(\sigma) = y_1(\infty;\sigma). \tag{3.38}$$

These equations must be solved subject to the boundary conditions:

$$\psi_1(0) = \psi_1'(0) = 0, \qquad \psi_1'(\infty) = 0, \tag{3.39a}$$

$$H_1(0) = 0 \quad \text{or} \quad H_1'(0) = 0, \qquad H_1(\infty) = 0. \tag{3.39b}$$

3.4 The Boundary Layer Thickness

For 2D flows, the momentum and energy equations (3.15) and (3.16) can be solved independently of Eqs. (3.17) and (3.21). Moreover, the latter equations have a remarkably simple analytic solution which shall now be derived. Since the leading-order boundary layer edge position $b_0 = y_0(\infty)$, it follows from Eq. (3.17) that

$$b_0 = r + MJ_0, \quad \text{where} \quad J_0 = \mathcal{I}_0(\infty). \tag{3.40}$$

With the help of Eq. (3.21), the unknown constant M, which was defined by Eq. (3.24), can be expressed in the form:

$$M = \frac{N}{b_0}, \quad \text{where} \quad N = \frac{4}{3}\lambda\sqrt{\frac{\gamma C}{\kappa(\gamma)}}, \tag{3.41}$$

and N is a known constant. These last two expressions yield the following quadratic equation for b_0:

$$b_0^2 - rb_0 - NJ_0 = 0. \tag{3.42}$$

The only physically acceptable solution to this equation is

$$b_0 = \frac{r + \sqrt{r^2 + 4NJ_0}}{2}. \tag{3.43}$$

This remarkably simple formula enables b_0 to be computed for any slenderness ratio r as soon as the momentum and energy equations have been solved, and Eq. (3.43) has been incorporated into the numerical algorithm which will be

described in Sec. 3.5. In particular, the boundary layer thickness on a flat plate (i.e. $r = 0$) predicted by this formula is $\delta_0 = \sqrt{NJ_0}$. Furthermore, by defining two new scaled variables B and R by

$$b_0 = B\sqrt{NJ_0}, \qquad r = R\sqrt{NJ_0}, \tag{3.44}$$

the solution (3.43) can be expressed in the form:

$$B = \frac{R + \sqrt{R^2 + 4}}{2}. \tag{3.45}$$

It is clear that B represents the *ratio* of the true boundary layer edge position to the flat plate boundary layer thickness $\delta_0 = \sqrt{NJ_0}$. Similarly, R is the *ratio* of the slenderness ratio r to δ_0. For example, if $R = 1$ (i.e. the body has the same thickness as the flat plate boundary layer), then Eq. (3.45) yields $B = (1+\sqrt{5})/2$ (i.e. the boundary layer edge position exceeds the body thicknesses by a factor of approximately 1.62).

A similar argument for AXI flows shows that the leading-order boundary layer edge position b_0 and slenderness ratio r are related via the following cubic equation:

$$b_0^3 - r^2 b_0 - NJ_0 = 0, \tag{3.46}$$

However, in contrast to the 2D case, the momentum and energy equations (3.18) and (3.19) cannot be solved independently of Eqs. (3.20) and (3.21). Thus, Eq. (3.46) cannot be used to determine b_0 for different values of r (since J_0 is itself a function of r), and the full system of equations must be solved simultaneously for ψ_0, H_0, Λ_0 and p_0 (and hence b_0). This suggests that the solution is strongly dependent upon the value of the slenderness ratio r. Nonetheless, Eq. (3.46) may be used to check the final numerical solution, and can be made independent of J_0 by introducing the scaled variables:

$$b_0 = B\sqrt[3]{NJ_0}, \qquad r = R\sqrt[3]{NJ_0}. \tag{3.47}$$

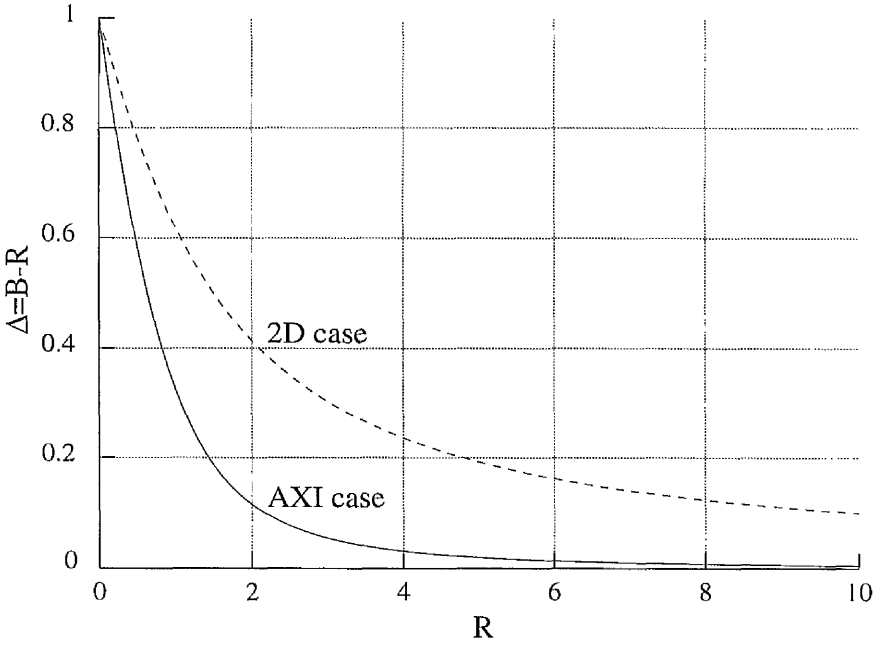

Figure 3.1: Theoretical scaled boundary layer thickness $\Delta = B - R$ for various body thicknesses R.

Substitution of this transformation into Eq. (3.46) yields the following equation:

$$B^3 - R^2 B - 1 = 0. \tag{3.48}$$

The analytic results given by Eqs. (3.45) and (3.48), which to the best of the author's knowledge have never been derived before, permit the scaled boundary layer thickness $\Delta = B - R$ to be determined *prior* to any numerical solution of the self-similar equations. Figure 3.1 shows the variation of Δ with R. The distribution of $B(R)$ for the 2D case is given by Eq. (3.45), whilst for the AXI case Eq. (3.48) was solved using the Newton-Raphson technique. It is evident that the boundary layer is in general thinner for the AXI case since the flow curves around the body, and this is known as the *three-dimensional relieving effect.* Also notice that Δ decreases monotonically as R increases, and it follows from Eq. (3.45) or

(3.48) that $\Delta \to 0$ as $R \to \infty$.

For very small Prandtl numbers, the energy equation has the simple integral given by Eq. (2.33), from which it follows that $J_0 = \mathcal{I}_0(\infty) = 0$. It can therefore be deduced from Eq. (3.43) or (3.46) that $b_0 = r$, i.e. the boundary layer thickness is negligible. Similarly for the special case $\gamma = 1$, the constant $N = 0$ and it also follows that $b_0 = r$.

3.5 Numerical Algorithm

The self-similar and eigen-equations derived in Secs. 3.2 and 3.3 were solved using a second-order accurate finite-difference scheme, and only a brief description of the numerical method will be given in this section.

It is convenient to express the momentum equation as a second-order equation for the streamwise velocity $u = \partial\psi/\partial\eta$. The self-similar equations thus constitute a system of five nonlinear coupled equations for the functions ψ_0, u_0, H_0, y_0 (or Λ_0 for AXI flows) and the unknown constant p_0. For the 2D case, the momentum and energy equations (3.15)–(3.16) were solved simultaneously using the global finite-difference method described in Appendix A.2, which is based on a quasi-Newton iteration procedure. The streamfunction ψ_0 and the integral $\mathcal{I}_0(\eta)$ were computed using the Trapezoidal rule. Once these equations have been solved, the boundary layer edge position b_0 was determined using Eq. (3.43). For the AXI case, the entire system of equations (3.18)–(3.25) were solved simultaneously. The implementation of the method described in Appendix A.2 for the solution of these equations is best described by considering the AXI momentum equation (3.18), which can be written in the form:

$$w''' = \phi(w, x, y, z) = \frac{0.25\,\lambda(y^2 - 2H_0) - (w + \Lambda_0')z}{\Lambda_0}, \tag{3.49}$$

where, in order to be consistent with the notation of Appendix A.2,

$$w = \psi_0, \quad y = w' = u_0, \quad z = y' = w'', \quad 0 \leq \eta \leq \eta_{\max}. \tag{3.50}$$

Once the function ϕ has been identified, the solution for $y(\eta)$ can be computed iteratively by solving the system of tri-diagonal equations (A.11)–(A.12). It should be noted that the condition $H_0'(0) = 0$ for insulated bodies was approximated using a second-order accurate forward-difference quotient (see Eqs. (A.13)–(A.15)).

Once the self-similar solutions have been computed, the eigen-equations were solved using a method similar to that described above. However, these equations involve the unknown eigenvalue σ, which was determined as a root of Eq. (3.37). This equation can be solved using the Bisection or Newton-Secant algorithms, although the former method was preferred since it guarantees convergence to within any specified accuracy ϵ, provided the true value of σ lies within the interval specified by the two starting approximations. This is particularly useful for cases in which the eigenvalue is very large.

The numerical algorithm described here is globally second-order accurate, and was found to be very robust. The solution was assumed to converge only when the maximum change between successive iterations was less than a specified tolerance level ϵ, which was taken as 10^{-7} for all of the solutions presented here. The initial velocity and enthalpy profiles used to start the iteration were chosen as $u_0^* = \tanh \eta$ and $H_0^* = 0.5$. Unless otherwise specified, all the numerical results presented in this chapter have been obtained using a uniform grid consisting of 1000 mesh points, and the maximum value of η was taken as 10. Solutions have also been computed using various other mesh sizes, and the results appear to be grid independent provided $\eta_{\max}$ is chosen large enough.

3.6 Self-Similar Results & Discussion

Self-similar and eigen-results have been obtained by the author for numerous different cases, and it is only possible to present a few of them in this thesis. In particular, solutions will be presented showing the effect of varying one or more of the *reference conditions*:

$$r = 1, \quad g_s = 0.5, \quad \gamma = 1.4, \quad \mathrm{Pr} = 0.725. \tag{3.51}$$

The last two parameters are valid for air at standard atmospheric conditions, and the Chapman-Rubesin constant C was taken as unity for all of the solutions shown here. Unless otherwise stated, the following symbols have been used in Figs. 3.2–3.6:

- 2D case (- - -),
- AXI case (—),
- AXI insulated case (o o o).

3.6.1 Boundary layer thickness & pressure distribution

Figures 3.2 (a)–(d) show the effect of varying the slenderness ratio r or surface enthalpy g_s on the leading-order boundary layer thickness δ_0 and pressure p_0. It is apparent that δ_0 decreases monotonically as r increases, and that the AXI boundary layer is thinner than the corresponding 2D case for all of the results shown here, thus confirming the theoretical result shown in Fig. 3.1. It is also evident from Fig. 3.2 (b) that the effect of surface heating is to increase the boundary layer thickness. Solutions for the insulated case are shown in Figs. 3.2 (a) and (c) and Fig. 3.4 (a) for the AXI case only. It is evident that the effect of insulating the body is to decrease the boundary layer thickness by a small amount. The effect of varying r or g_s on the self-similar boundary layer edge position is also

shown schematically in Figs. 3.3 (a)–(c). To the best of the author's knowledge, the results shown in Fig. 3.3 (a) are the first solutions ever obtained for the AXI hypersonic flow over a vanishingly thin needle.

3.6.2 Skin friction & heat transfer

Figures 3.4 (a)–(d) show the effect of varying r or g_s on the self-similar skin friction τ_0 and surface heat transfer q_0 coefficients, which were both defined by Eq. (3.28). As expected for 2D flows, τ_0 and $|q_0|$ increase as r increases. However, an interesting observation from Figs. 3.4 (a) and (c) for the AXI case is that there exists an optimum radius r^* which results in minimum values for τ_0 and $|q_0|$. It should be emphasized that τ_0 and $|q_0|$ were evaluated at the boundary layer edge position y_b, rather than the true surface y_s, in order to take into account the displacement effect of the boundary layer[1] . Furthermore, it can be observed that τ_0 increases as g_s increases. A similar kind of behaviour can also be seen in the results for the surface heat transfer $|q_0|$, provided $g_s > 0.5$. It is also evident that both τ_0 and $|q_0|$ are greater for AXI flows.

3.6.3 Velocity & enthalpy profiles

Figures 3.5 (a)–(d) show typical velocity and static enthalpy (temperature) profiles for the AXI case with various surface enthalpies g_s. In view of the transformation given by Eq. (3.3), u_0 and h_0 have been plotted against the variable $\zeta = 2^{1-j}\sqrt{\gamma C p_0}\,\eta$. For cold surface temperatures, the enthalpy distribution reaches a maximum value near to the wall, after which it decreases to its prescribed cold surface value. For comparatively high temperature factors, the velocity profile exhibits an overshoot which becomes increasingly pronounced as g_s becomes large. This is believed due to the relative low density within the hot

[1]See also Chernyi (1961) for further details concerning the determination of body shapes with minimum drag for AXI inviscid hypersonic flows.

hypersonic boundary layer which allows the flow within the boundary layer to accelerate and exceed that of the external inviscid flow. It is easily verified that this effect is a natural consequence of the self-similar boundary layer equations as follows. Suppose $u_0 = \psi_0'$ reaches a maximum value at $\eta = \eta^\star$. Consequently $\psi_0''(\eta^\star) = 0$ and $\psi_0'''(\eta^\star) < 0$, and it can be inferred from the momentum equation (3.15) or (3.18) that this can only occur if $H_0(\eta^\star)$ is large enough. This implies that the surface enthalpy must exceed a certain critical value. The results of Emanuel (1994) and Yasuhara (1962) also show pronounced velocity overshoot.

Although not shown, the boundary layer profiles for the 2D case were found to be qualitatively similar to the AXI case, and that the velocity overshoot effect is considerably greater for 2D flows. Moreover, it can be inferred from the self-similar energy equation that velocity overshoot can also occur if the Prandtl number is small enough[2] . However, it remains unclear whether or not velocity overshoot is a true physical phenomenon, since real gas effects should be taken into account for very high surface enthalpies.

[2]Although not shown, this effect has been observed in the present numerical results.

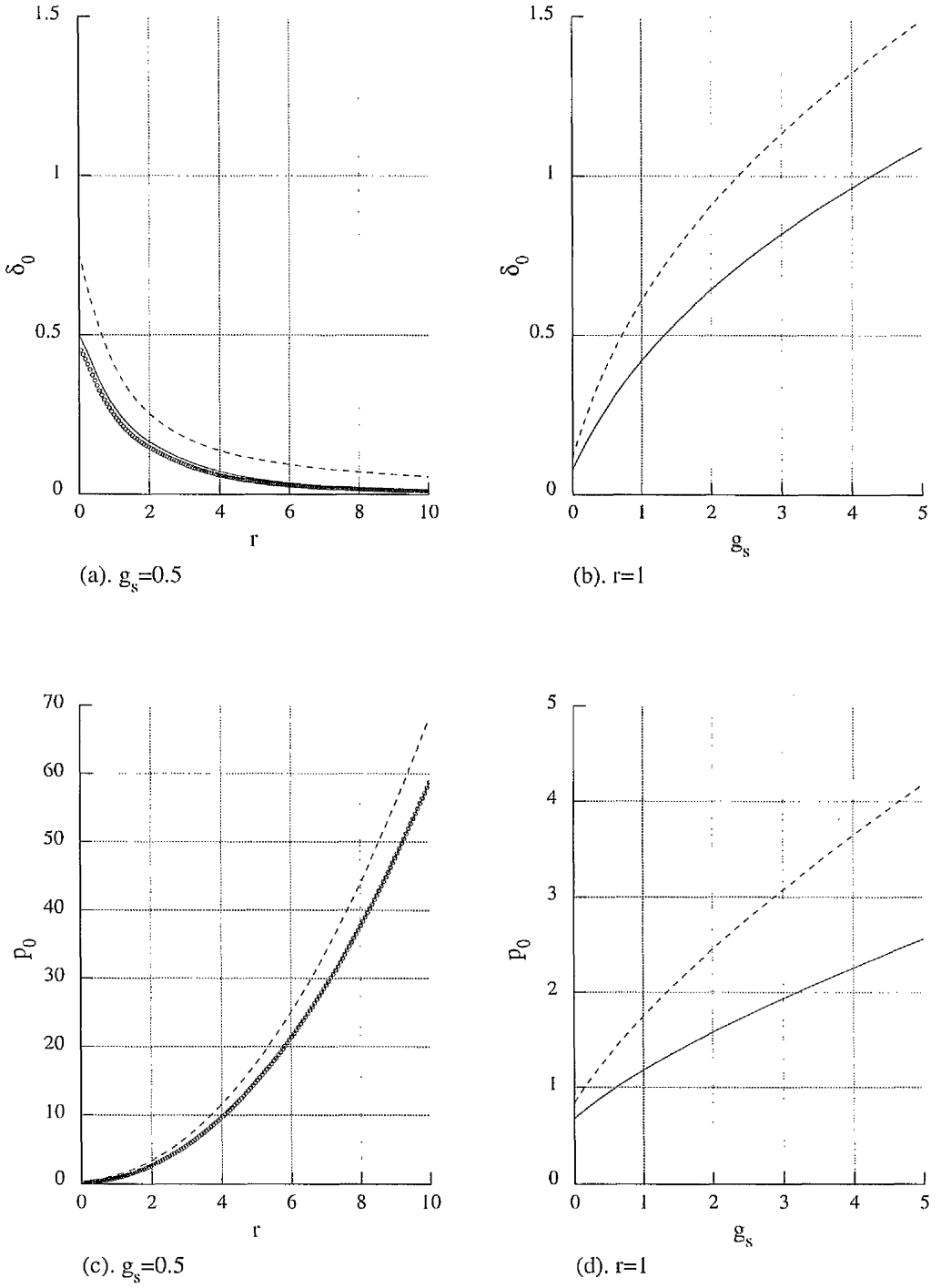

Figure 3.2: Effect of varying r or g_s on the boundary layer thickness δ_0 and pressure p_0 ($\gamma = 1.4$, $\mathrm{Pr} = 0.725$; for legend see page 55).

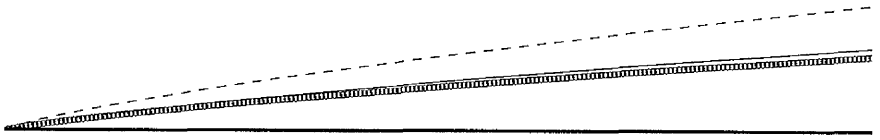

(a). r=0, g_s=0.5

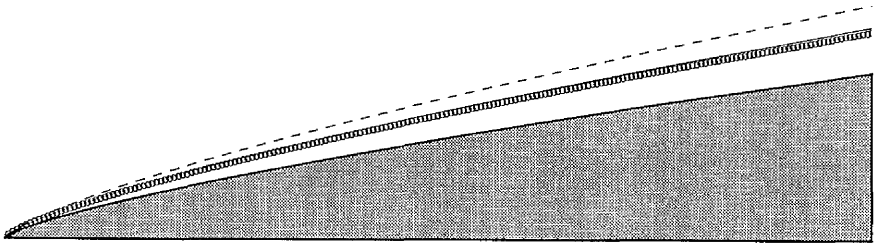

(b). r=1, g_s=0.5

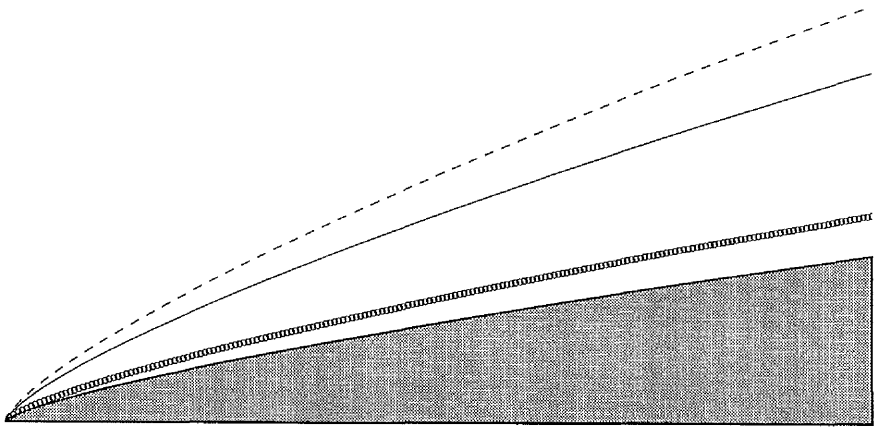

(c). r=1, g_s=5

Figure 3.3: Self-similar boundary-layer edge positions b_0 ($\gamma = 1.4$, $\mathrm{Pr} = 0.725$; for legend see page 55).

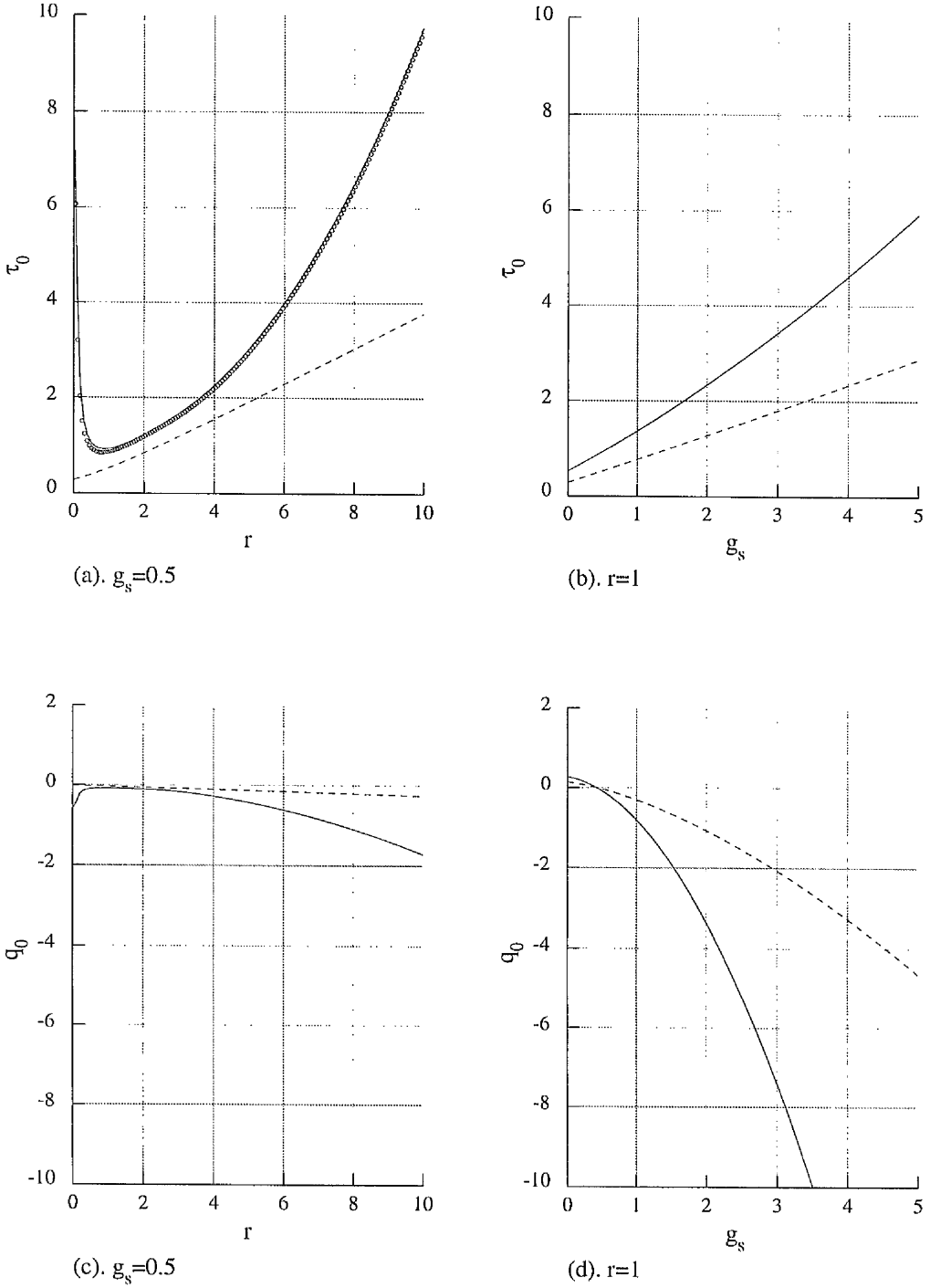

Figure 3.4: Effect of varying r or g_s on the skin friction τ_0 and surface heat transfer q_0 ($\gamma = 1.4$, $\mathrm{Pr} = 0.725$; for legend see page 55).

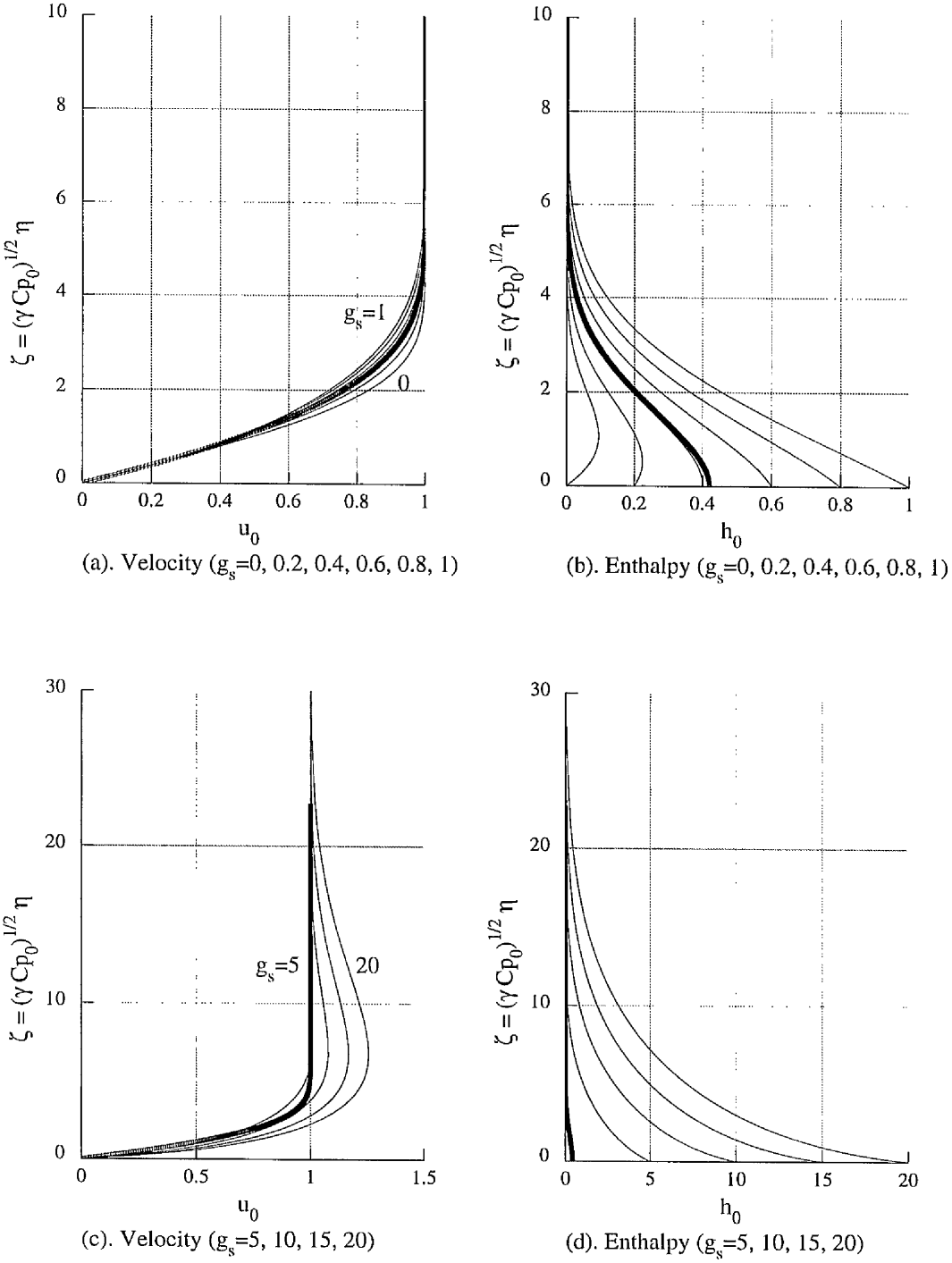

(a). Velocity (g_s=0, 0.2, 0.4, 0.6, 0.8, 1)

(b). Enthalpy (g_s=0, 0.2, 0.4, 0.6, 0.8, 1)

(c). Velocity (g_s=5, 10, 15, 20)

(d). Enthalpy (g_s=5, 10, 15, 20)

Figure 3.5: Velocity and enthalpy profiles for various surface enthalpies g_s (AXI case, $r = 1,\ \gamma = 1.4,\ \mathrm{Pr} = 0.725$). Insulated case ($\circ\ \circ\ \circ$).

3.7 Eigen-Results & Discussion

Figs. 3.6 (a)–(d) show the effect of varying one of the reference conditions (3.51) on the computed value of the upstream influence eigenvalue σ. Numerical investigations suggest that there *either* exists a unique positive eigenvalue (whose value depends on the input parameters) *or* that σ is infinitely large (in which case there is no upstream influence effect). Moreover, the smaller the value of σ, the greater the upstream influence effect.

3.7.1 Effect of varying r

As shown in Fig. 3.6 (a), σ increases monotonically as r becomes large, and this is a direct consequence of the fact that the boundary layer thickness decreases for increasing slenderness ratio. For the 2D case, σ decreases as $r \to 0$, and the upstream influence effect is felt most strongly for the flat plate case. On the other hand, AXI flows exhibit a rather surprising behaviour as $r \to 0$. The eigenvalue σ reaches a minimum value, after which it increases sharply and appears to become infinitely large at a critical value $r^* \approx 0.1131$ (see also Fig. 3.7 (a)). This behaviour suggests that the AXI boundary layer is *supercritical* for $r < r^*$, and does not permit the upstream propagation of disturbances. For $r > r^*$, the boundary layer will be referred to as being *subcritical*, and upstream influence is present. It should be noted that the value of r^* depends upon the input parameters, and varies from case to case. It is also evident that the upstream influence effect is almost always stronger for 2D flows, owing in part to their greater thickness.

3.7.2 Effect of varying g_s, γ or Pr

The variation of the surface enthalpy, ratio of specific heats and Prandtl number all appear to have similar effects on the value of σ, as shown in Figs. 3.6 (b)–(d).

In particular, σ decreases monotonically as g_s, γ or Pr increases for both 2D and AXI flows. The boundary layer also appears to be supercritical for g_s less than a certain critical value $g_s^* \approx 0.0207$ (see also Fig. 3.7 (b)).

It was shown in Sec. 3.4 that for very small Prandtl numbers (or for $\gamma = 1$), the boundary layer thickness is very small. This suggests that the upstream influence effect should be negligible for this regime, and this is indeed observed in the numerical solutions shown in Fig. 3.6 (c) and (d). Moreover, as $\mathrm{Pr} \to 0$, the value of σ for the 2D case exceeds that for the AXI case. A similar kind of behaviour is experienced for very hot surface temperatures, as will be discussed in the next section.

Solutions for the insulated case have also been obtained for the AXI case, and are shown in Fig. 3.6 (a). As expected, the effect of insulating the body is to reduce the upstream influence effect, since the boundary layer is thinner.

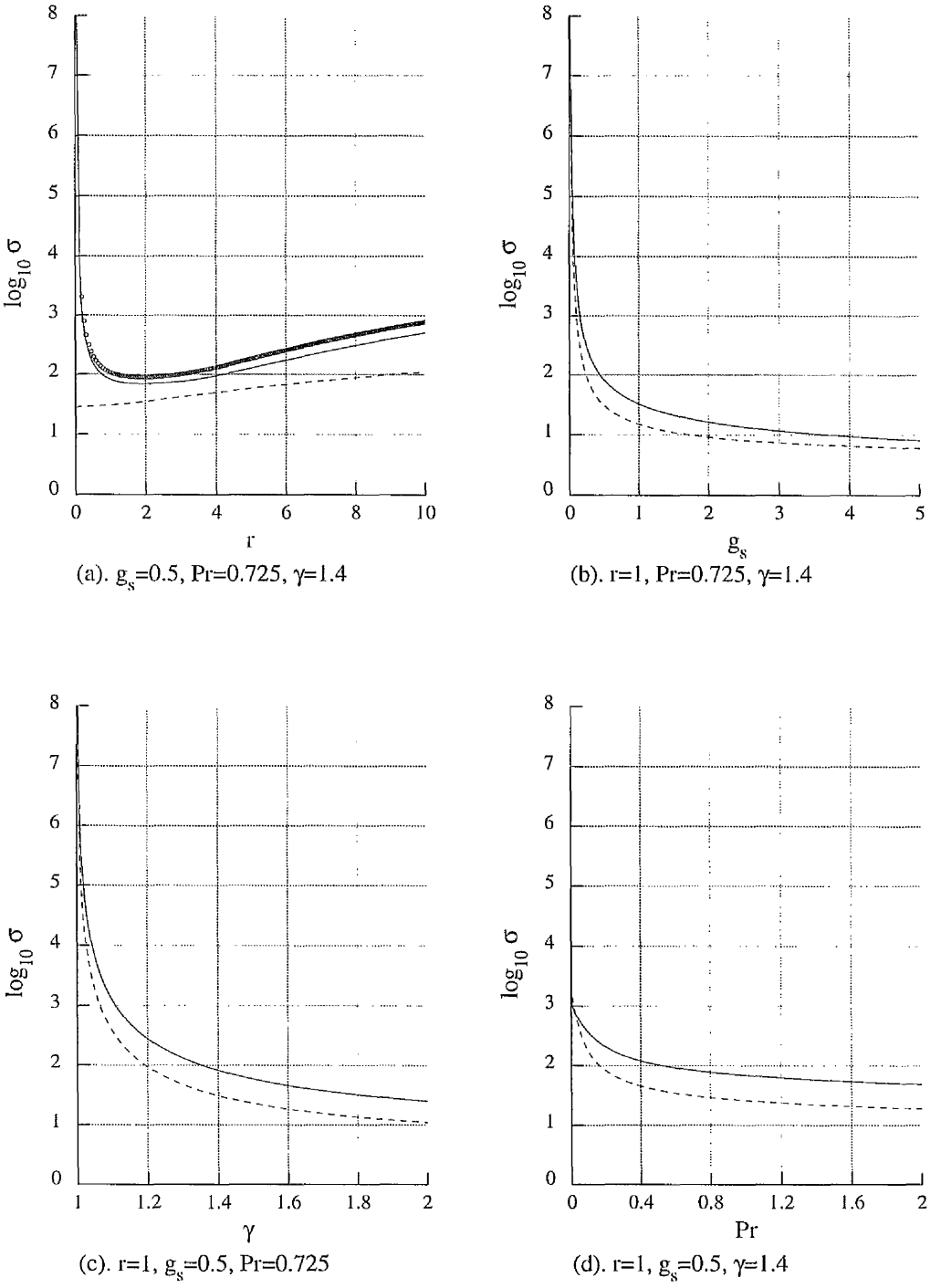

(a). g_s=0.5, Pr=0.725, γ=1.4

(b). r=1, Pr=0.725, γ=1.4

(c). r=1, g_s=0.5, Pr=0.725

(d). r=1, g_s=0.5, γ=1.4

Figure 3.6: Effect of varying the reference conditions (3.51) on the upstream influence eigenvalue σ (for legend see page 55).

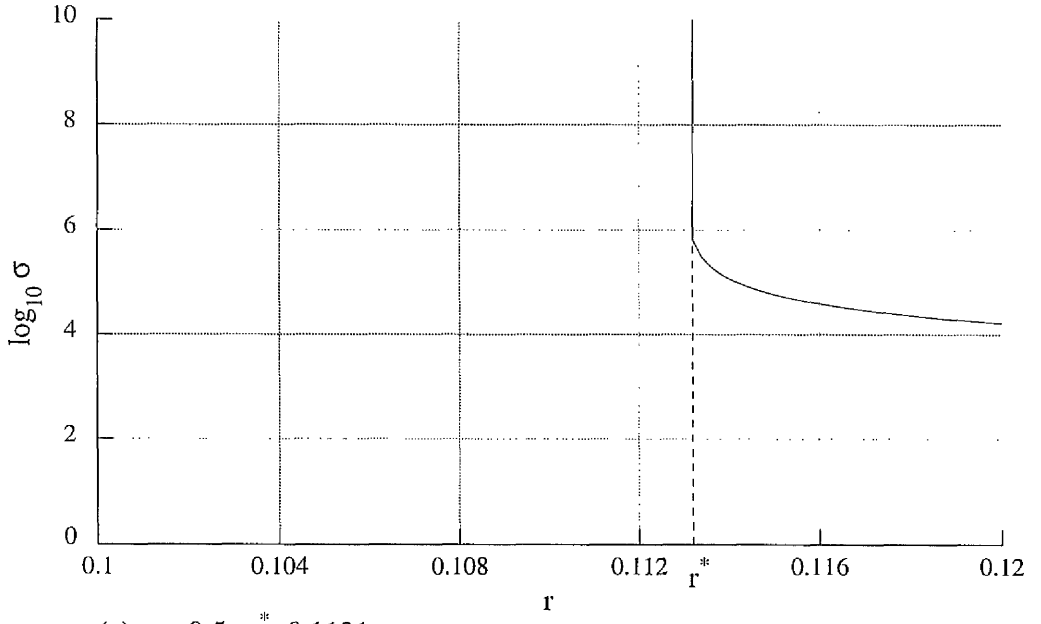

(a). g_s=0.5, r^*=0.1131

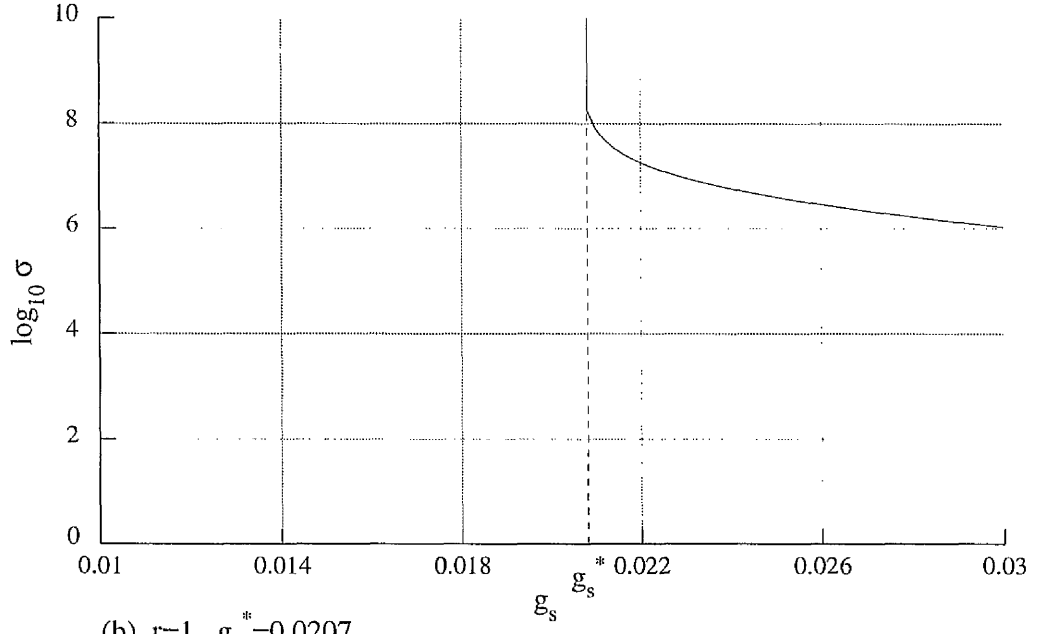

(b). r=1, g_s^*=0.0207

Figure 3.7: Upstream influence eigenvalue σ near the critical values r^* and g_s^* for the AXI case with $\gamma = 1.4$ and $\mathrm{Pr} = 0.725$.

3.8 Very Hot Bodies

It is well known that very high surface temperatures are experienced during hypersonic flight – such as during the atmospheric re-entry from orbit – and its effects are of particular importance near sharp leading edges. It is particularly interesting to determine the behaviour of the upstream influence eigenvalue σ for large values of the temperature factor g_s. Following the analysis of Brown & Stewartson (1975a) for the flat plate, the following scaled variables are indicated for 2D flows in the limit as $g_s \to \infty$:

$$\eta = g_s^{-1/4}\zeta, \quad y_i(\eta) = g_s^{3/8}\widehat{y}_i(\zeta) \tag{3.52a}$$

$$\psi_i(\eta) = g_s^{1/4}\widehat{\psi}_i(\zeta), \quad H_i(\eta) = g_s\widehat{H}_i(\zeta). \tag{3.52b}$$

for i=0 or 1, where ζ is $O(1)$ in a hot near-wall sublayer of thickness $g_s^{-1/4}$. Upon substitution of Eqs. (3.52) into the interactive self-similar and eigen boundary layer equations given in Secs. 3.2 and 3.3, it can be shown that the original equations remain unaltered, but that the boundary conditions become:

$$\widehat{\psi}_i(0) = \widehat{\psi}_i'(0) = 0, \quad \widehat{\psi}_i'(\infty) = 0, \tag{3.53a}$$

$$\widehat{H}_0(0) = 1, \quad \widehat{H}_1(0) = 0, \quad \widehat{H}_i(\infty) = 0. \tag{3.53b}$$

In addition, the body slenderness ratio r and boundary layer edge position b_i must be scaled according to

$$r = g_s^{3/8}\widehat{r}, \quad b_i = g_s^{3/8}\widehat{b}_i. \tag{3.54}$$

It thus follows that the leading-order boundary layer thickness $\delta_0 \sim g_s^{3/8}$, which can become relatively large for high surface temperatures.

For AXI flows, the following scaled variables must be used instead:

$$\eta = g_s^{1/8}\zeta, \quad \Lambda_i(\eta) = g_s^{3/4}\widehat{\Lambda}_i(\zeta) \tag{3.55a}$$

$$\psi_i(\eta) = g_s^{5/8}\widehat{\psi}_i(\zeta), \quad H_i(\eta) = g_s\widehat{H}_i(\zeta), \tag{3.55b}$$

which also result in the same equations as before, but with the original boundary conditions replaced by Eqs. (3.53a–b). In addition, it can be shown that the transformations given by Eq. (3.54) are also valid for the AXI case. It is evident from the first of Eqs. (3.55a) that the thickness of the hot near-wall sublayer for AXI flows is $O(g_s^{1/8})$, which is much greater than that for the corresponding 2D case which is $O(g_s^{-1/4})$.

Solutions for the hot surface limit $g_s \to \infty$ have been obtained for the case $r = 1$, $\gamma = 1.4$ and $\mathrm{Pr} = 0.725$.[3] The same numerical algorithm described in Sec. 3.5 has been used to solve the self-similar and eigen-equations for this case, but with the original boundary conditions replaced by Eqs. (3.53a–b). For the 2D case, it was found that $\sigma = 3.557$, whilst for the AXI case $\sigma = 2.293$ (accurate to three decimal places). These results suggest that for very hot bodies, the upstream influence effect is in fact greater for AXI flows. It is believed that this is mainly due to the fact that the boundary layer is thinner – and thus hotter – for AXI flows.

3.9 Comparison with Previous Studies

It is difficult to compare the present results with previously obtained solutions since the equations given by numerous authors were not scaled using the hypersonic estimates given in Sec. 2.2, and their formulations contained different parameters than those derived in this thesis. Moreover, results for the eigenvalue σ have only been previously obtained for the flow over a 2D flat plate (i.e. $r = 0$) and with a Prandtl number of unity. Nevertheless the results presented here appear to show the expected behaviour, and the self-similar solutions are in good qualitative agreement with those obtained by Yasuhara (1962). A useful check

[3]The maximum value of η was taken as 20 for these very hot body calculations, due to the comparatively large boundary layer thickness.

on the numerical results is to compute the surface enthalpy on an insulated flat plate for the special case $\gamma = 1.4$ and $\mathrm{Pr} = 0.725$. The present method yields $g_s = 0.4178$, which agrees to four decimal places with the value given by Khorrami & Smith (1994).

The analysis for the viscous layer employed in the present study is similar to the approach used by Brown & Stewartson (1975a), and differs in some respects from the original formulations of Neiland (1970) and Werle *et al.* (1973). Some aspects of the two approaches are not easily compared; in particular, the latter authors made use of the *Levy-Lees transformation* defined by:

$$\xi = \int_0^x \rho(x,y)\,\mathrm{d}x, \quad \eta = \frac{1}{\sqrt{2x}} \int_0^y \rho(x,z)\,\mathrm{d}z. \tag{3.56}$$

It is clear from Eq. (3.2c) that for self-similarity $\rho = x^{-1/2}\bar{\rho}(\eta)$, and it follows from the above equation that

$$\xi \sim \sqrt{x}. \tag{3.57}$$

Moreover, Neiland (1970) considers the following asymptotic expansion for the pressure:

$$p(\xi) = p_0\xi^{-1} + \cdots + p_1\xi^a + \cdots, \tag{3.58}$$

where a is an unknown eigenvalue. It can be inferred from the foregoing equations and Eqs. (3.2c) and (3.12) that a is related to the author's eigenvalue σ via the simple formula:

$$\sigma = \frac{a+1}{2}. \tag{3.59}$$

Neiland (1970) obtained a numerical solution of the self-similar and eigen equations[4] for the flow over a 2D flat plate with $g_s = 0.5$, $\gamma = 1.4$ and $\mathrm{Pr} = 1$ and found that $a = 49.6$, or equivalently $\sigma = 25.3$ from Eq. (3.59). By comparison,

[4]There appears to be a typographical error in the eigen-momentum equation in Neiland's 1970 paper.

the present algorithm yields $\sigma = 23.5$. It should be noted that Crocco's integral (cf. Eq. (2.32)) is valid for this special case.

Figure 3.8 compares the solutions obtained using the author's numerical code with those obtained by Brown & Stewartson (1975a) for the case of a 2D flat plate with various temperature factors g_s, under the assumption of a Prandtl number of unity. The latter solutions were obtained by solving the equations in the inviscid and viscous layers simultaneously, instead of using the tangent-wedge approximation for the determination of the pressure distribution. Also shown is the author's numerical result for very hot bodies:

$$\sigma \to 2.593 \quad \text{as} \quad g_s \to \infty, \tag{3.60}$$

which was obtained using the method described in Sec. 3.8, and the following asymptotic results which were obtained by Brown & Stewartson (1975a):

$$\sigma \sim 0.0014\, g_s^{-6} \quad \text{as} \quad g_s \to 0, \tag{3.61}$$

$$\sigma \to 3.2 \quad \text{as} \quad g_s \to \infty. \tag{3.62}$$

The two sets of results are in reasonably good agreement with each other, particularly for cold surface temperatures. This also verifies the fact that the tangent-wedge formula can be successfully used to determine the pressure distribution for flows with strong viscous interaction. However, it is apparent that the tangent-wedge approximation tends to overestimate the upstream influence effect for relatively large surface enthalpies. In addition, the author's results appear to suggest that σ becomes infinitely large for values of g_s less than a non-zero critical value g_s^*, in which case the flow becomes supercritical. This is in contradiction with Eq. (3.61), which is believed to be incorrect since it was derived in the double limit $\sigma \to \infty$ *and* $g_s \to 0$.

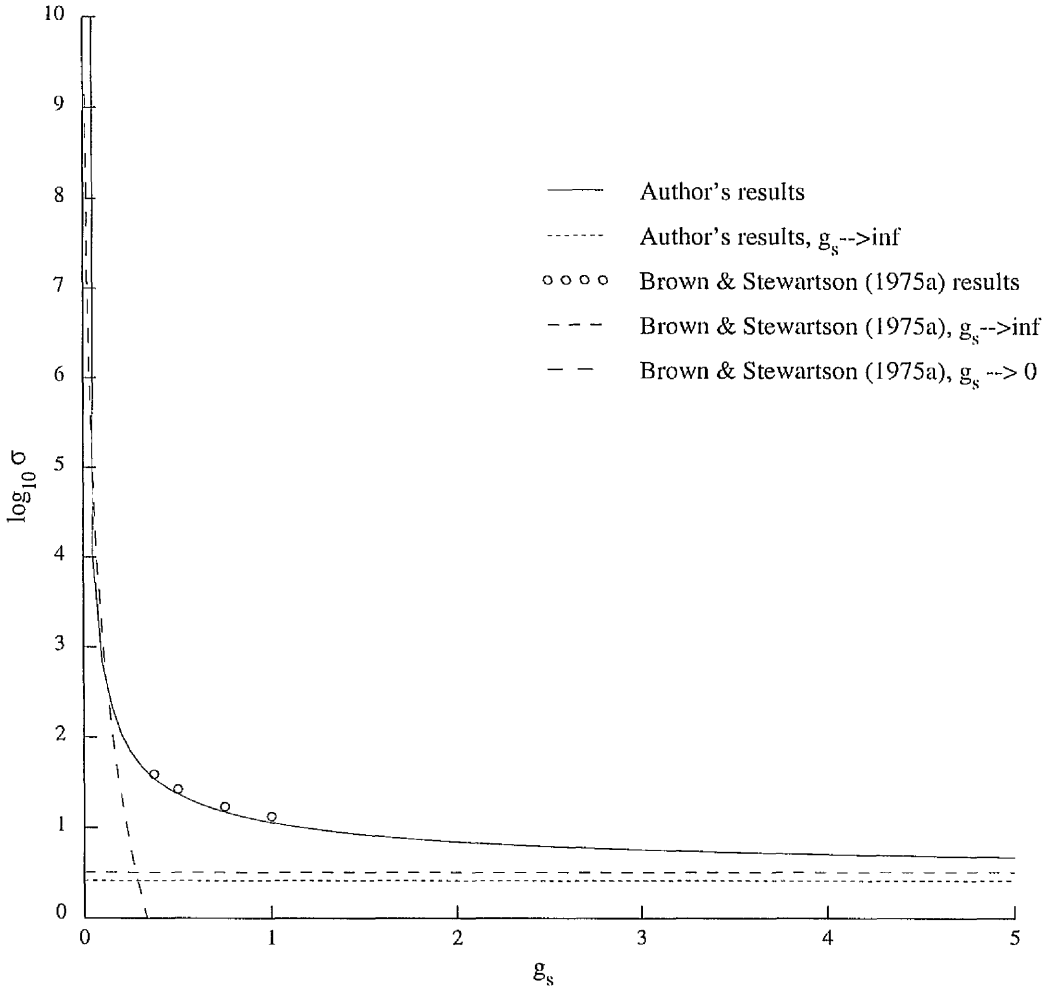

Figure 3.8: Comparison of the author's eigenvalue results with those of Brown & Stewartson (1975a) for the flow over a 2D flat plate (i.e. $r = 0$) with $g_s = 0.5,\ \gamma = 1.4,\ \mathrm{Pr} = 1$.

Chapter 4

Formulation for Relatively Thick Bodies

4.1 Introduction

Hitherto, the boundary layer thickness δ has been assumed to be of the same order of magnitude, or even much greater than, the body thickness h. Moreover, numerical results have been obtained in the previous chapter for bodies with surface shapes of the form $y_s(x) = rx^{3/4}$. In this chapter, analytical results shall be derived under the assumption that $\delta \ll h$. In this case, the boundary layer is two-dimensional to leading-order, and axially-symmetric curvature effects are only important within the inviscid layer. In contrast to the formulation used in the previous chapter, the leading-order pressure distribution is now known in advance and may be calculated using the tangent wedge/cone approximation given by Eq. (2.39), which to leading-order can be expressed in the following form:

$$p = \kappa(\gamma) r^2 \left(\frac{\mathrm{d}s}{\mathrm{d}x}\right)^2, \tag{4.1}$$

where the boundary layer edge position $y_b = b(x)s(x)$ has been replaced by the body surface $y_s = rs(x)$ due to the fact that the boundary layer thickness is assumed to be negligible. Nevertheless, the displacement effect of the boundary layer will be taken into account later in this chapter in order to analyse the nature of the upstream propagation of disturbances induced by the viscous-inviscid interaction.

It is convenient to introduce the *Prandtl transposition* (see, for example, Rosenhead 1963):

$$y = z + y_s(x), \quad v = w + uy_s'(x). \tag{4.2}$$

This leaves the *scaled* 2D continuity and momentum equations (2.4)–(2.6) unchanged, which in the transformed variables can be written as:

$$\frac{\partial}{\partial x}(\rho u) + \frac{\partial}{\partial z}(\rho w) = 0, \tag{4.3}$$

$$\rho\left(u\frac{\partial u}{\partial x} + w\frac{\partial u}{\partial z}\right) = -\frac{\mathrm{d}p}{\mathrm{d}x} + \frac{\partial}{\partial z}\left(\mu\frac{\partial u}{\partial z}\right), \tag{4.4}$$

$$\rho\left(u\frac{\partial H}{\partial x} + w\frac{\partial H}{\partial z}\right) = \frac{\partial}{\partial z}\left\{\mu\left(\nu u\frac{\partial u}{\partial z} + \frac{1}{\mathrm{Pr}}\frac{\partial H}{\partial z}\right)\right\}. \tag{4.5}$$

However, the boundary conditions become:

$$u = w = 0, \quad H = g_s \text{ or } \frac{\partial H}{\partial y} = 0 \quad \text{at} \quad z = 0, \tag{4.6}$$

$$u = 1, \quad H = 1/2 \quad \text{at} \quad z = \delta(x), \tag{4.7}$$

where $\delta(x)$ is the boundary layer thickness and g_s is the temperature factor.

The theory presented in this chapter is valid for arbitrary surface geometries $y_s(x)$, provided that the body is relatively thicker than the corresponding three-quarter power-law body. However, in order to simplify the subsequent analysis, only power-law bodies of the form:

$$y_s(x) = rx^\alpha, \quad \text{where} \quad \alpha < 3/4, \quad \alpha > 0 \tag{4.8}$$

shall be considered.

4.2 Self-Similar Equations

It is convenient to use the stream function ψ defined by:

$$\frac{\partial \psi}{\partial z} = \rho u, \qquad \frac{\partial \psi}{\partial x} = -\rho w, \tag{4.9}$$

and it is also useful to introduce a modified Dorodnitsyn variable η by:

$$\eta = \frac{1}{G(x)} \int_0^z \rho(x, \xi)\, \mathrm{d}\xi. \tag{4.10}$$

Following a procedure similar to that used in Sec. 2.4, a solution of the boundary layer equations shall be sought in the following form:

$$u = \bar{u}(x, \eta), \qquad H = \bar{H}(x, \eta), \tag{4.11a}$$

$$\psi = G(x)\bar{\psi}(x, \eta), \qquad z = x^{3/2-\alpha}\bar{z}(x, \eta), \tag{4.11b}$$

$$p = x^{2\alpha-2}\bar{p}(x), \qquad \rho = x^{2\alpha-2}\bar{\rho}(x, \eta). \tag{4.11c}$$

The functional form for the pressure and density are suggested from the tangent wedge/cone formula (4.1), whilst the solution for the transverse variable z shall be obtained in Sec. 4.5. It can be shown using Eqs. (4.8) and (4.11b) that the ratio Ω of the body to the boundary layer thickness is given by:

$$\Omega = \frac{y_s}{\delta} = \frac{r}{\delta_0} x^{2\alpha-3/2}. \tag{4.12}$$

Since Ω becomes large for $\alpha < 3/4$ as $x \to 0^+$, it follows that axially-symmetric transverse effects *within the boundary layer* can be neglected to leading-order (see also Sec. 1.2). However, transverse effects are still important in the inviscid flow outside the boundary layer, and therefore the only difference between 2D and AXI flows in the present theory is due to the differing definitions of the coefficient $\kappa(\gamma)$ in the tangent wedge/cone formula (see Eq. (2.35)).

Substitution of Eqs. (4.10) and (4.11) into the boundary layer equations (4.3)–(4.5) yields

$$\frac{\partial\bar{\psi}}{\partial\eta}\frac{\partial^2\bar{\psi}}{\partial\eta\partial x} - \frac{\partial\bar{\psi}}{\partial x}\frac{\partial^2\bar{\psi}}{\partial\eta^2} - \bar{\psi}\frac{\partial^2\bar{\psi}}{\partial\eta^2}\frac{G'}{G} = \lambda\left(\frac{1-\alpha}{x} - \frac{1}{2\bar{p}}\frac{\mathrm{d}\bar{p}}{\mathrm{d}x}\right)\left\{2\bar{H} - \left(\frac{\partial\bar{\psi}}{\partial\eta}\right)^2\right\} + \frac{\gamma C\bar{p}}{G^2}\frac{\partial^3\bar{\psi}}{\partial\eta^3}x^{2\alpha-2}, \quad (4.13)$$

$$\frac{\partial\bar{\psi}}{\partial\eta}\frac{\partial\bar{H}}{\partial x} - \frac{\partial\bar{\psi}}{\partial x}\frac{\partial\bar{H}}{\partial\eta} - \bar{\psi}\frac{\partial\bar{H}}{\partial\eta}\frac{G'}{G} = \frac{\gamma C\bar{p}}{G^2}\frac{\partial}{\partial\eta}\left\{\nu\frac{\partial\bar{\psi}}{\partial\eta}\frac{\partial^2\bar{\psi}}{\partial\eta^2} + \frac{1}{\mathrm{Pr}}\frac{\partial\bar{H}}{\partial\eta}\right\}x^{2\alpha-2}, \quad (4.14)$$

where the density has been eliminated using the equation of state (2.26). Self-similarity requires that

$$\bar{\psi} = \psi_0(\eta), \quad \bar{H} = H_0(\eta) \quad \text{and} \quad \bar{p} = p_0, \quad (4.15)$$

which are all independent of x. It follows using Eq. (2.47) (with $j = 0$) that the function $G(x)$ is given by:

$$G(x) = ax^{\alpha-1/2}, \quad (4.16)$$

where a is an affine transformation constant defined by:

$$a = \left\{\frac{\gamma C p_0}{\lambda(1-\alpha)}\right\}^{1/2}. \quad (4.17)$$

Substitution of Eqs. (4.15)–(4.17) into the transformed momentum and energy equations (4.13) and (4.14) yields the following system of ordinary differential equations:

$$\psi_0''' + M\psi_0\psi_0'' - (\psi_0')^2 + 2H_0 = 0, \quad (4.18)$$

$$\mathrm{Pr}^{-1}H_0'' + M\psi_0 H_0' + \nu(\psi_0'\psi_0'')' = 0, \quad (4.19)$$

where λ and ν were defined by Eqs. (2.9) and (2.28) respectively and

$$M = \frac{2\alpha - 1}{2\lambda(1-\alpha)}. \quad (4.20)$$

These equations should be solved subject to the boundary conditions:

$$\psi_0(0) = \psi_0'(0) = 0, \quad \psi_0'(\infty) = 1, \tag{4.21a}$$

$$H_0(0) = g_s, \quad H_0(\infty) = 1/2. \tag{4.21b}$$

It should also be noted that a prime is now used to denote differentiation with respect to η and that the affine transformation renders the equations independent of both r and C. An important property of the above system of equations is that the single parameter M characterizes the dependence of the solution on both α and γ. Another interesting observation is that $M = 0$ for bodies of parabolic shape (i.e. $\alpha = 1/2$), and whence the foregoing equations become:

$$\psi_0''' + \mathrm{Pr}\{1 - (\psi_0')^2\} = 0, \tag{4.22}$$

$$H_0(\eta) = \frac{1}{2}\left\{(1 - \mathrm{Pr})(\psi_0')^2 + \mathrm{Pr}\right\}. \tag{4.23}$$

It is therefore evident that the momentum equation (4.22) is reduced to an equation of second order.

In addition, the leading-order skin friction $\tau_s(x)$ and surface heat transfer rate $q_s(x)$ are given by (cf. Eqs. (3.26)–(3.28)):

$$\tau_s(x) = N\psi_0''(0)x^{\alpha-3/2}, \tag{4.24a}$$

$$q_s(x) = N\,\mathrm{Pr}^{-1}\,H_0'(0)x^{\alpha-3/2}, \tag{4.24b}$$

where

$$N = \gamma C p_0 a^{-1} = \sqrt{(1-\alpha)(1-\gamma)C p_0}. \tag{4.25}$$

The self-similar equations (4.18)–(4.21) can be easily solved numerically (using the method described in Appendix A.2) for various values of M, g_s and Pr in order to determine $\psi_0''(0)$ and $H_0'(0)$. Although this is not the main purpose of the present analysis, the numerical solution of these equations will be used to

correlate the analytical results for the upstream influence eigenvalue which will be obtained in the next sections.

It is immediately evident from Eqs. (4.1) and (4.11c) that the constant p_0 is given by:

$$p_0 = \alpha^2 r^2 \kappa(\gamma). \tag{4.26}$$

It can also be readily shown that the asymptotic expansion to the solution of Eqs. (4.18)–(4.21) near to the surface is given by:

$$\left.\begin{aligned} \psi_0 &= \tfrac{1}{2}\beta_0\eta^2 + \cdots \\ H_0 &= g_s + H'(0)\eta + \cdots \end{aligned}\right\} \quad \text{as} \quad \eta \to 0, \tag{4.27}$$

where $\beta_0 = \psi_0''(0)$. The leading-order density near to the body surface can be found using the equation of state (2.26) which yields:

$$\rho \sim \rho_s x^{2\alpha-2} \quad \text{where} \quad \rho_s = \alpha^2 r^2 \kappa(\gamma) \lambda^{-1} g_s^{-1}. \tag{4.28}$$

It can therefore be inferred that the variation of the density normal to the surface is negligible in a thin viscous near-wall sublayer. However, it should be emphasized that this sublayer is not incompressible, which is in contrast to the simpler case considered by Lighthill (1953) for the supersonic flow over a flat plate with weak viscous interaction (see also the incompressible lower-deck equations of the triple-deck structure in Sec. 5.2).

4.3 Solution in Inner Viscous Region

In order to investigate the upstream influence through the boundary layer, a new similarity variable ζ which is $O(1)$ in the thin viscous near-wall sublayer should be defined as follows:

$$\zeta = \frac{1}{bx^m} \int_0^z \rho(x, \xi)\, \mathrm{d}\xi, \tag{4.29}$$

where the exponent m must be determined using viscous-inviscid interaction theory and b is an affine-transformation constant defined by Eq. (4.37). This new variable is related to the original Dorodnitsyn variable η by:

$$\eta = ba^{-1}x^{m-\alpha+1/2}\zeta. \tag{4.30}$$

Since $\eta \ll 1$ as $x \to 0^+$ in this region, it follows that

$$\alpha - m - 1/2 < 0, \tag{4.31}$$

which will be proved to be true in due course. It can be shown that the boundary layer equations (4.3)–(4.5) can be expressed in the form (cf. Eq. (2.42)):

$$\frac{1}{bx^m}\left(\frac{\partial\psi}{\partial\zeta}\frac{\partial u}{\partial x} - \frac{\partial\psi}{\partial x}\frac{\partial u}{\partial\zeta}\right) = -\frac{\lambda(2H - u^2)}{2}\frac{1}{p}\frac{\mathrm{d}p}{\mathrm{d}x} + \frac{\gamma Cp}{b^2x^{2m}}\frac{\partial^2 u}{\partial\zeta^2}, \tag{4.32}$$

$$\left(\frac{\partial\psi}{\partial\zeta}\frac{\partial H}{\partial x} - \frac{\partial\psi}{\partial x}\frac{\partial H}{\partial\zeta}\right) = \frac{\gamma Cp}{bx^m}\frac{\partial}{\partial\zeta}\left\{\mu\left(\nu u\frac{\partial u}{\partial\zeta} + \frac{1}{\mathrm{Pr}}\frac{\partial H}{\partial\zeta}\right)\right\}. \tag{4.33}$$

It is expected that the upstream propagation of disturbances should decay exponentially as $x \to 0^+$ for the case $\alpha < 3/4$, instead of the power-law behaviour suggested by Eq. (3.11). In particular, the solution for the pressure shall be sought in the following asymptotic form:

$$p = p_0x^{2\alpha-2} + \cdots + qP\,\mathrm{e}^{-\omega x^{-n}} + \cdots \quad \text{as} \quad x \to 0^+, \tag{4.34}$$

where the *positive* constants ω and n are to be determined, and q is an arbitrary constant. The eigenvalue ω is a measure of the exponential decay of the upstream transmission of disturbances through the boundary layer. In contrast to the algebraic character of the upstream influence considered in the previous chapter, whose intensity is dependent solely upon the magnitude of the eigenvalue σ, the exponentially-decaying behaviour considered here is dependent upon the values of both the eigenvalue ω and the exponent n. Using Eqs. (4.11), (4.16), (4.27) and (4.30), it follows that the streamfunction and total enthalpy should be expressed

in the following asymptotic form as $x \to 0^+$:

$$\psi = \frac{1}{2}\beta_0 b^2 a^{-1} x^{2m-\alpha+1/2}\zeta^2 + \cdots + qc\Psi(\zeta)x^l \, \mathrm{e}^{-\omega x^{-n}} + \cdots, \tag{4.35}$$

$$H = g_s + ba^{-1}x^{m-\alpha+1/2}H'(0)\zeta \cdots + qd\Phi(\zeta)x^k \, \mathrm{e}^{-\omega x^{-n}} + \cdots, \tag{4.36}$$

where the exponents l and k are to be determined. The affine-transformation constants b, c and d are defined respectively by

$$b = \left(\frac{a\gamma C p_0}{n\sigma\beta_0}\right)^{1/3}, \quad c = \frac{aP}{\beta_0\rho_s}, \quad d = \frac{(\mathrm{Pr}-1)bc\beta_0^2}{a^2}, \tag{4.37}$$

and are introduced such that the resulting equation for Ψ and Φ can be expressed in universal canonical form. The streamwise velocity u can be obtained using the first of Eqs. (4.9) which yields:

$$\begin{aligned} u &= b^{-1}x^{-m}\frac{\partial\bar{\psi}}{\partial\zeta} \\ &= \beta_0 ba^{-1}x^{m-\alpha+1/2}\zeta + \cdots + qcb^{-1}\Psi'(\zeta)x^{l-m} \, \mathrm{e}^{-\omega x^{-n}} + \cdots. \end{aligned} \tag{4.38}$$

Upon substitution of Eqs. (4.34)–(4.38) into the transformed boundary layer equations (4.32)–(4.33), and comparing terms of comparable order of magnitude, it can be shown that Ψ and Φ satisfy the ordinary differential equations:

$$\zeta\Psi' - \Psi = -1 + \Psi''', \tag{4.39}$$

$$\mathrm{Pr}^{-1}\,\Phi'' - \zeta\Phi = (\zeta\Psi')'', \tag{4.40}$$

provided that

$$l = \frac{3}{2} - \alpha, \quad k = 2(1-\alpha), \quad 3m - n = 3\alpha - \frac{3}{2}. \tag{4.41}$$

A second equation, which shall be derived in the next section, is required for the determination of both m and n. The conditions at the body surface (4.6) imply that

$$\Psi(0) = \Psi'(0) = 0, \quad \Phi(0) = 0. \tag{4.42}$$

The arbitrary constant q, which represents the amplitude of the disturbances, formally disappears from these equations. Therefore the exponentially-decaying terms in the foregoing asymptotic expansions are unique to within a multiplicative constant (cf. Sec. 3.1). It is also evident that the equation for Ψ is independent of the higher-order enthalpy function Φ, and therefore the energy equation does not play a significant rôle in the exponentially decaying upstream influence effect. Moreover, the solution of Eq. (4.40) is not required for the subsequent analysis.

By differentiating Eq. (4.39) with respect to ζ, it follows that Ψ'' satisfies the following equation, along with the additional boundary condition (which follows from the no-slip conditions in Eq. (4.42)):

$$\zeta\Psi'' = \Psi'''', \qquad \Psi'''(0) = 1. \tag{4.43}$$

The solution of this equation can be expressed as a linear combination of Airy functions (see, for example, Abramowitz & Stegun 1965):

$$\Psi''(\zeta) = M\,\mathrm{Ai}(\zeta) + N\,\mathrm{Bi}(\zeta), \tag{4.44}$$

where M and N are constants to be determined. It is well known that Bi grows exponentially large as ζ becomes large, and thus $N = 0$. It can also be inferred from Eq. (4.43) that $M = 1/\,\mathrm{Ai}'(0)$ and therefore

$$\Psi''(\zeta) = \frac{\mathrm{Ai}(\zeta)}{\mathrm{Ai}'(0)}. \tag{4.45}$$

4.4 Displacement Effect of Inner Region

In order to determine the exponents m and n, as well as the eigenvalue ω, the displacement effect of the inner region should be considered. Firstly, the perturbation $\Delta\theta$ to the slope of the streamlines at the outer edge of the viscous sublayer is given by:

$$\Delta\theta = \lim_{\zeta\to\infty} \frac{w}{u}. \tag{4.46}$$

By making use of the definition of the streamfunction (4.9) and the transformation (4.29), it can be shown that:

$$\Delta\theta = -\frac{\psi_x}{\psi_z} = -\frac{bx^m}{\rho}\frac{\psi_x}{\psi_\zeta}. \tag{4.47}$$

The density can be eliminated using Eq. (4.28), and it follows using the expansion for the streamfunction (4.35) that

$$\Delta\theta = \Theta_2 x^{m-2\alpha+1}\zeta + \cdots + q\Theta_3 x^{l-m-n-\alpha+1/2}\,\mathrm{e}^{-\omega x^{-n}} + \cdots, \tag{4.48}$$

where[1]

$$\Theta_2 = -\frac{b}{\rho_s}\left(m - \frac{\alpha}{2} + \frac{1}{4}\right), \quad \Theta_3 = -\frac{acn\omega}{b\beta_0\rho_s}\lim_{\zeta\to\infty}\frac{\Psi}{\zeta}. \tag{4.49}$$

However, by taking into account the no-slip condition (4.42) and making use of the fact that

$$\int_0^\infty \mathrm{Ai}(\zeta)\,\mathrm{d}\zeta = \frac{1}{3}, \tag{4.50}$$

it can be deduced from the solution (4.45) that

$$\lim_{\zeta\to\infty}\frac{\Psi}{\zeta} = \frac{1}{3\,\mathrm{Ai}'(0)}. \tag{4.51}$$

Hence the coefficient Θ_3 can be expressed in the form:

$$\Theta_3 = -\frac{acn\omega\lambda g_s}{3b\beta_0\kappa r^2\alpha^2\,\mathrm{Ai}'(0)}, \tag{4.52}$$

This additional contribution to the displacement thickness determines the exponentially-decaying term in the asymptotic expansion for the pressure given by Eq. (4.34) as follows. From the tangent wedge/cone approximation (4.1),

$$\begin{aligned} p &= \kappa(\gamma)\left(r\alpha x^{\alpha-1} + \Delta\theta\right)^2 \\ &= \kappa(\gamma)\alpha^2 r^2 x^{2\alpha-2} + \cdots + 2q\kappa(\gamma)r\alpha\Theta_3 x^{l-m-n-1/2}\,\mathrm{e}^{-\omega x^{-n}} + \cdots. \end{aligned} \tag{4.53}$$

[1]The reason for the use of the subscripts '2' and '3' shall become clear in due course.

It should be noted that in deriving this formula it was assumed that

$$x^{\alpha-1} \gg x^{m-2\alpha+1}, \tag{4.54}$$

which will later be shown to be true. By comparing Eq. (4.53) with the assumed expansion for the pressure given by Eq. (4.34), it can be inferred that

$$P = 2\kappa(\gamma) r \alpha \Theta_3, \tag{4.55}$$

provided

$$l - m - n = \frac{1}{2}. \tag{4.56}$$

The solution of the third of Eqs. (4.41) and (4.56) yields

$$m = \frac{1}{2}\left(\alpha - \frac{1}{4}\right), \quad n = \frac{1}{2}\left(\frac{9}{4} - 3\alpha\right). \tag{4.57}$$

As expected, the criterion that n should be positive implies that $\alpha < 3/4$. In addition, both the assumed conditions (4.31) and (4.54) yield the same condition for α.

The upstream influence eigenvalue can now be determined by combining the second of Eqs. (4.37) with the known expressions for Θ_3 and P from Eqs. (4.52) and (4.55) respectively, yielding the result:

$$\omega = -1.5\mathrm{Ai}'(0) b \beta_0^2 \rho_s^2 a^{-2} (nr\alpha\kappa)^{-1}, \tag{4.58}$$

where

$$\mathrm{Ai}'(0) = -\{3^{1/3}\Gamma(1/3)\}^{-1} \approx -0.258819. \tag{4.59}$$

Since all quantities in this expression are positive for $\alpha < 3/4$, it follows that ω is also positive, thus proving that upstream influence does exist and that it decays exponentially as $x \to 0^+$.

4.5 Solution in Main Part of Boundary Layer

It remains to be shown whether the main part of the boundary layer contributes to the displacement thickness, and if so, whether this additional contribution alters the eigen-solution determined in the previous section. This can be accomplished by expanding the solution in the inner viscous sublayer in terms of the original Dorodnitsyn variable η, and this suggests that the asymptotic solution for $\bar{\psi}$ and $\bar{H}$ (which were defined by Eq. (4.11)) in the main part of the boundary layer can be expressed in the following asymptotic form as $x \to 0^+$:

$$\bar{\psi} = \psi_0(\eta) + \cdots + q\psi_1(\eta)x^{l-m}\,\mathrm{e}^{-\omega x^{-n}} + \cdots, \tag{4.60}$$

$$\bar{H} = H_0(\eta) + \cdots + qH_1(\eta)x^{l-m}\,\mathrm{e}^{-\omega x^{-n}} + \cdots. \tag{4.61}$$

By substituting these expansions into the transformed boundary layer equations (4.13)–(4.14), and comparing terms of comparable order of magnitude, it can be shown that

$$\psi_0'\psi_1' - \psi_1\psi_0'' = 0, \tag{4.62}$$

$$\psi_0'H_1 - \psi_1H_0' = 0. \tag{4.63}$$

In order to match with the solution in the viscous sublayer,

$$\psi_0 \to \frac{1}{2}\beta_0\eta^2, \quad \psi_1 \to \frac{c}{3b\,\mathrm{Ai}'(0)}\eta, \quad H_0 \to g_s \quad \text{as} \quad \eta \to 0. \tag{4.64}$$

It can be easily verified that the solution of Eqs. (4.62)–(4.63) satisfying the foregoing boundary conditions is given by:

$$\psi_1(\eta) = A\psi_0'(\eta), \qquad H_1(\eta) = AH_0'(\eta), \tag{4.65}$$

where

$$A = \frac{c}{3b\beta_0\,\mathrm{Ai}'(0)}. \tag{4.66}$$

This solution can now be used to compute the boundary layer thickness as follows. Firstly, it is immediately evident from the definition of η given by Eq. (4.10) that

$$\frac{\partial z}{\partial \eta} = \frac{G(x)}{\rho} = \frac{a}{\bar{\rho}} x^{3/2-\alpha}. \tag{4.67}$$

Using the equation of state (2.8), it can be shown that

$$\frac{\partial z}{\partial \eta} = B x^{3/2-\alpha} \left\{ 2\bar{H} - \left(\frac{\partial \bar{\psi}}{\partial \eta} \right)^2 \right\}, \tag{4.68}$$

where

$$B = \frac{a\lambda}{2p_0} = \frac{a\lambda}{2\kappa r^2 \alpha^2}. \tag{4.69}$$

Thus, the boundary layer thickness δ is given by

$$\delta(x) = B x^{3/2-\alpha} \int_0^\infty 2\bar{H} - \left(\frac{\partial \bar{\psi}}{\partial \eta} \right)^2 \, \mathrm{d}\eta. \tag{4.70}$$

Substitution of Eqs. (4.60)–(4.61) into this formula yields

$$\delta(x) = B J_0 x^{3/2-\alpha} + \cdots + q B J_1 x^{l-m-\alpha+3/2} \, \mathrm{e}^{-\omega x^{-n}} + \cdots, \tag{4.71}$$

where

$$J_0 = \int_0^\infty 2H_0 - (\psi_0')^2 \, \mathrm{d}\eta, \quad J_1 = 2 \int_0^\infty H_1 - \psi_0' \psi_1' \, \mathrm{d}\eta. \tag{4.72}$$

The integral J_0 can be calculated from a numerical solution of the self-similar equations (4.18)–(4.21). The quantity J_1 can be determined analytically with the help of Eq. (4.65) and by taking into consideration the boundary conditions (4.21) yielding

$$J_1 = -2A g_s. \tag{4.73}$$

The slope of the streamlines at the outer edge of the boundary layer can now be determined as:

$$\Delta\theta = \frac{\mathrm{d}\delta}{\mathrm{d}x} = \Theta_1 x^{1/2-\alpha} + \cdots + q\Theta_3 x^{l-m-n-\alpha+1/2} \, \mathrm{e}^{-\omega x^{-n}} + \cdots, \tag{4.74}$$

where the coefficients Θ_1 and Θ_3 are obtained using Eqs. (4.69) and (4.73) giving:

$$\Theta_1 = \left(\frac{3}{2} - \alpha\right) BJ_0, \quad \Theta_3 = n\omega BJ_1 = -2n\omega g_s AB. \tag{4.75}$$

By substituting the known expressions for A and B from Eqs. (4.66) and (4.69), it follows that Θ_3 can be expressed in the form:

$$\Theta_3 = -\frac{acn\omega\lambda g_s}{3b\beta_0\kappa r^2\alpha^2\,\mathrm{Ai}'(0)}, \tag{4.76}$$

which is identically equal to the previously obtained expression given by Eq. (4.52).

Therefore, the leading-order term of $O(x^{1/2-\alpha})$ in Eq. (4.74) is much larger in magnitude than the corresponding term of $O(x^{m-2\alpha+1})$ in Eq. (4.48) if $\alpha < 3/4$. This implies that the slope of the streamlines does change across the main part of the boundary layer. However, the coefficient Θ_3 of the eigen-term in both solutions is identical, which means that the solution for the eigenvalue derived in the previous section remains unaltered. Thus although viscous effects are important throughout the entire boundary layer, its effects on the upstream influence induced by the viscous-inviscid interaction are negligible in the main part of the boundary layer. This fact is also evident from the observation that Eqs. (4.62)–(4.63) are locally inviscid.

4.6 Eigenvalue Results & Discussion

The formula for the eigenvalue ω may be expressed in a more useful form by substituting the known expressions for a, b and ρ_s from Eqs. (4.17), (4.28) and (4.37) respectively into Eq. (4.58), and after some algebraic manipulation it can be shown that

$$\omega = (|\mathrm{Ai}'(0)|)^{3/4} r^{3/2} C^{-3/8} \nu, \tag{4.77}$$

where

$$\nu = \gamma^{-3/8}\lambda^{-7/8}\kappa^{3/8}\alpha^{3/2}(1-\alpha)^{5/8} n^{-1} g_s^{-3/2}\beta_0^{5/4}. \tag{4.78}$$

In these equations, λ and n are defined respectively by:

$$\lambda = \frac{\gamma - 1}{\gamma}, \quad n = \frac{1}{2}\left(\frac{9}{4} - 3\alpha\right), \tag{4.79}$$

and $\kappa(\gamma)$ is the coefficient in the tangent wedge/cone formula which was defined by Eq. (2.35). It should be emphasized that the intensity of the exponentially-decaying upstream influence is dependent upon the values of both the eigenvalue ω and the exponent n (which depends only on α).

The above formula for ω yields a wealth of information regarding the nature of the exponentially decaying upstream influence. Firstly, it is immediately clear that ω increases as the slenderness ratio r increases. This behaviour implies a lesser degree of upstream influence for larger slenderness ratios, which is reminiscent of the numerical results of the previous chapter. As $\alpha \to 3/4$, it follows from the second of Eqs. (4.79) that $n \to 0$. This implies that ν becomes infinitely large and thus the character of the upstream influence develops an algebraic form (cf. Eq. (3.11)), rather than the exponential behaviour considered here. It is also clear from Eq. (4.30) that in this situation, the thickness of the viscous sublayer grows and ultimately merges with the main part of the boundary layer in the limit as $\alpha \to 3/4$.

Since the quantity $\kappa(\gamma)$ is smaller for AXI flows (cf. Eq. (2.35)), it follows from Eq. (4.78) that the intensity of the exponentially-decaying upstream influence is slightly greater for the flow over AXI bodies. This result is entirely due to the fact that axially-symmetric curvature effects are only prevalent within the inviscid flow outside the boundary layer, which is in contrast to the analysis for three-quarter power-law bodies, for which transverse curvature effects must be fully taken into account. It can also be inferred from Eq. (4.78) that $\nu \to \infty$ as $\gamma \to 1$ or $g_s \to 0$, which again are in accord with the results of Chapter 3.

These findings are presented in Figs. 4.1 (a)–(d), which show the effect of varying one of the following reference conditions upon the value of ν (which is

proportional to ω):

$$\alpha = 0.5, \quad g_s = 0.5, \quad \gamma = 1.4, \quad \mathrm{Pr} = 0.725. \tag{4.80}$$

The quantity $\beta_0 = \psi_0''(0)$ has been computed from the numerical solution of the self-similar equations (4.18)–(4.21), which were solved simultaneously using the global finite-difference method described in Appendix A.2. A uniform mesh consisting of $N = 1000$ grid points was employed, where the maximum value of η was taken as 10 and the tolerance level $\epsilon = 10^{-7}$. All the results presented here appear to show the expected behaviour. In particular, the results for bodies of parabolic shape (i.e. $\alpha = 1/2$), which are presented in Figs. 4.1 (b)–(d), appear to show the same qualitative behaviour to those shown in Figs. 3.6 (b)–(d) for the algebraic eigenvalue σ for the flow over three-quarter power-law bodies.

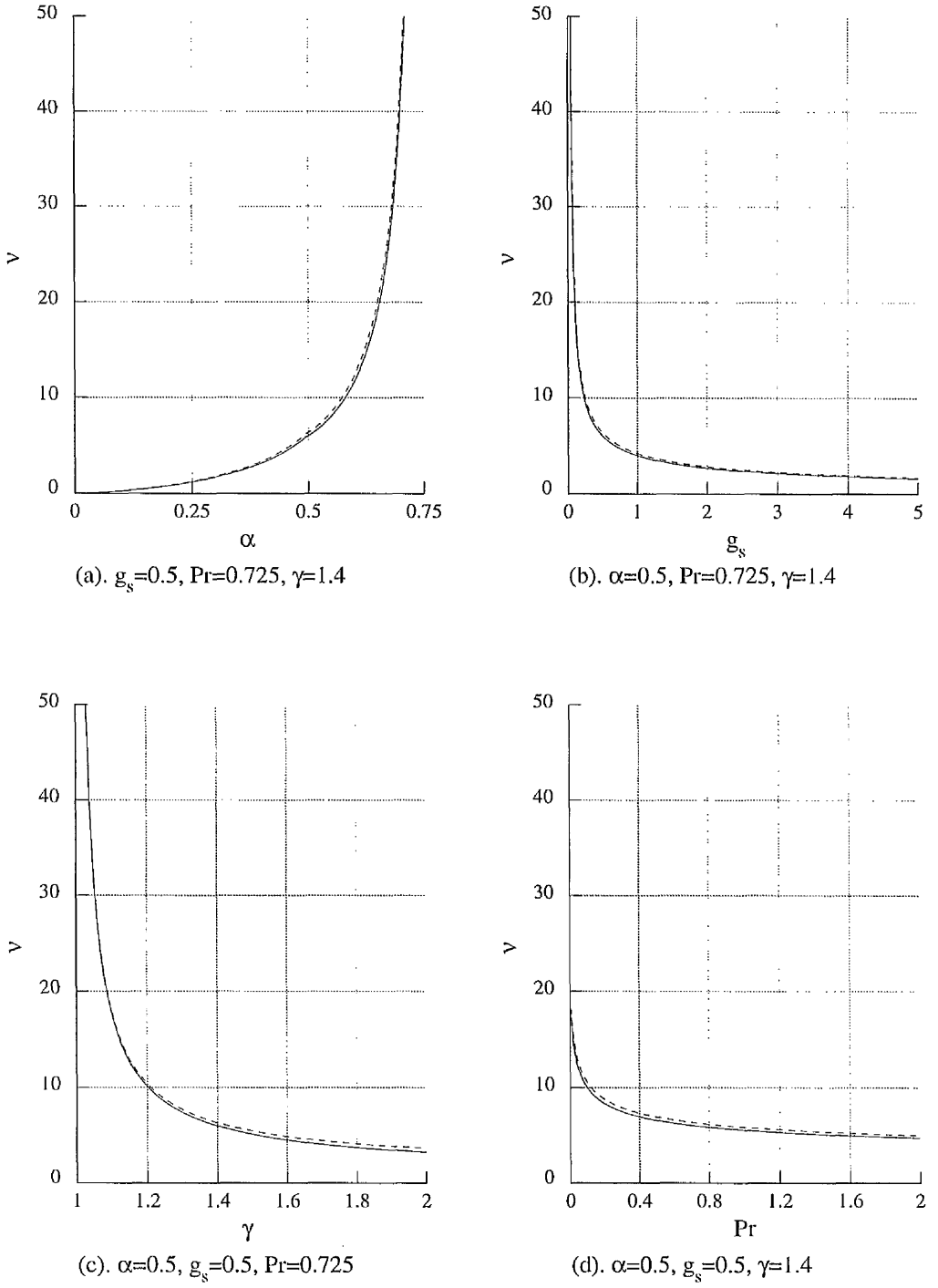

(a). g_s=0.5, Pr=0.725, γ=1.4

(b). α=0.5, Pr=0.725, γ=1.4

(c). α=0.5, g_s=0.5, Pr=0.725

(d). α=0.5, g_s=0.5, γ=1.4

Figure 4.1: Effect of varying one of the reference conditions (4.80) on the upstream influence eigenvalue ν (for legend see page 55).

Part II

Hypersonic Flow with Weak Viscous Interaction and Strong Wall Cooling

Chapter 5

Hypersonic Triple-Deck with Wall Cooling

5.1 Introduction

Consider the flow over a cold compression or expansion corner having an asymptotically small ramp angle, with the upstream flat surface oriented parallel to the oncoming freestream flow (see Fig. 5.1). If the ramp occurs in a region of weak global viscous interaction, i.e. $\chi \ll 1$, then the flow develops a so-called *triple-deck structure*, as shown in Fig. 5.1 (see also Sec. 1.5). The effects of wall cooling are particularly important for hypersonic flows in order to combat the high temperatures generated near to the surface (see Townend 1991 and Walberg 1991 for further details). The two-dimensional hypersonic triple-deck formulation with significant wall cooling was first considered by Neiland (1973), and later by Brown *et al.* (1990) and Kerimbekov *et al.* (1994). Wall cooling brings about numerous changes to the flow structure, the most important of which are listed below:

1. An overall reduction in the length scales of the interaction region.

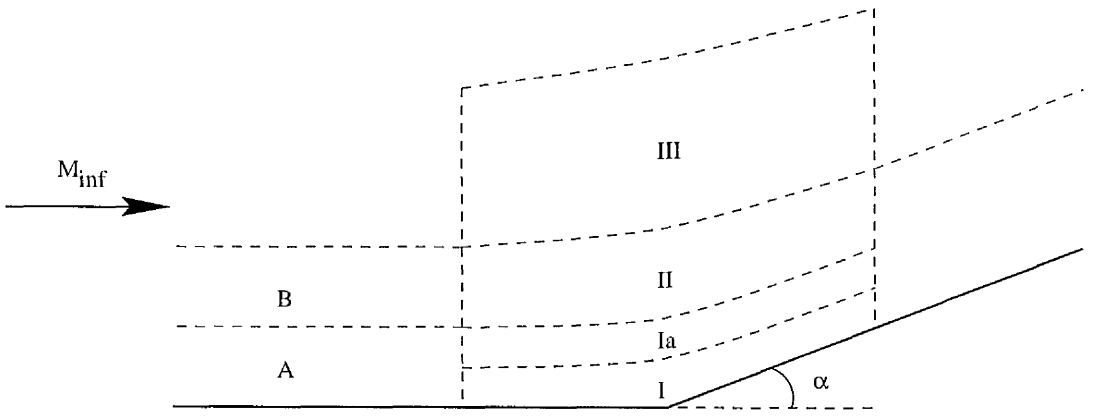

Figure 5.1: Schematic of the triple-deck structure for the hypersonic flow over a cold compression ramp (not to scale).

2. The upstream boundary layer bifurcates into two regions, since a near-wall sublayer (labelled region A in Fig. 5.1) is required to adjust the relatively high boundary layer temperatures to that of the cold surface.

3. The main part of the boundary layer (region II) does contribute into the displacement effect, and an additional intermediate layer (region Ia) in the interaction region is required to match the solutions in regions I and II. This is in sharp contrast to the original supersonic triple-deck theory of Neiland (1969) and Stewartson & Williams (1969) without wall cooling.

4. The location and extent of any recirculating region is affected by wall cooling, and sufficient cooling can ultimately inhibit separation altogether.

Region I is a layer in which changes to the pressure gradient provoke a nonlinear response to the flow, and in particular may result in separation. Regions Ia and II are effectively continuations of regions A and B into the interaction region, and the flow in region III is inviscid and governed by the Euler Equations. The nature of the solution in each of these regions has been described in detail by

Kerimbekov *et al.* (1994); the subsequent analysis shall extend this study, with a minimum of detail, to include axially-symmetric effects.

The spatial lengths, velocity, pressure, density, enthalpy and absolute viscosity are made non-dimensional with respect to L, u_∞, p_∞, ρ_∞, u_∞^2 and μ_0 respectively. Here, μ_0 denotes the viscosity evaluated at a reference enthalpy of u_∞^2, and L is the length of the upstream flat surface from the leading edge. The viscosity is assumed to depend upon the static enthalpy according to the power law:

$$\hat{\mu} = (\hat{h})^n, \tag{5.1}$$

where n is a positive constant. In this chapter, the superscript '^' will be used to denote unscaled non-dimensional variables. In order to be consistent with the notation of Kerimbekov *et al.* (1994), the subsequent analysis is presented in terms of the Reynolds number Re_0, which is defined by

$$\mathrm{Re}_0 = \frac{\rho_\infty u_\infty L}{\mu_0}. \tag{5.2}$$

For the special case of a linear temperature-viscosity law (i.e. $n = 1$), it follows from Eq. (2.15) that $\mu_0 \sim M_\infty^2 \mu_\infty$ and therefore $\mathrm{Re}_0 \sim M_\infty^{-2}\mathrm{Re}_\infty$. Moreover, the hypersonic viscous interaction parameter χ_0 and small perturbation parameter ϵ_0 are defined by

$$\chi_0 = M_\infty^2 \mathrm{Re}_0^{-1/2}, \quad \epsilon_0 = \mathrm{Re}_0^{-1/4}, \tag{5.3}$$

both of which are assumed to be small. For $n = 1$, these two parameters are equivalent to the classical definitions given by Eqs. (1.3) and (1.5) (apart from the factor of $C^{1/2}$).

In order to keep the present analysis general for various body shapes, the surface $\hat{y}_s$ is chosen as

$$\hat{y}_s = \hat{r} + \hat{f}(\hat{x}), \tag{5.4}$$

where $\hat{r}$ is the characteristic body radius. For a true compression ramp

$$\hat{f}(\hat{x}) = \begin{cases} 0, & \hat{x} \leq 0, \\ \hat{\alpha}\hat{x}, & \hat{x} > 0. \end{cases} \tag{5.5}$$

where $\hat{\alpha}$ is the ramp angle. It should be emphasized that the triple-deck formulation is only valid if the ramp angle $\hat{\alpha} \sim \epsilon_0$.

5.2 Viscous Lower Deck

In the lower viscous sublayer (region I), a new transverse boundary layer coordinate $\hat{Y}$ is defined such that the ramp geometry is represented by $\hat{Y} = \hat{f}(\hat{x})$. Using an order-of-magnitude analysis similar to that employed in Sec. 2.2, it can be shown that the solution in this region depends upon the following scaled variables:

$$\hat{x} = 1 + (\gamma - 1)^{1/2}\lambda^{-5/4}\chi_0^{3/4} g_s^{n+1/2} x, \tag{5.6a}$$

$$\hat{Y} = (\gamma - 1)^{1/2}\lambda^{-3/4}\epsilon_0\chi_0^{3/4} g_s^{n+1/2}\{y + f(x)\}, \tag{5.6b}$$

$$\hat{u} = (\gamma - 1)^{1/2}\lambda^{1/4}\chi_0^{1/4} g_s^{1/2} u, \tag{5.6c}$$

$$\hat{v} = (\gamma - 1)^{1/2}\lambda^{3/4}\epsilon_0\chi_0^{1/4} g_s^{1/2}\{v + uf'(x)\}, \tag{5.6d}$$

$$\hat{p} = 1 + \gamma\lambda^{1/2}\chi_0^{1/2} p, \quad \hat{\rho} = M_\infty^{-2} g_s^{-1}\rho, \tag{5.6e}$$

$$\hat{h} = g_s h, \quad \hat{\mu} = g_s^n \mu, \tag{5.6f}$$

where $g_s = h_s/u_\infty^2$ is the temperature factor and λ is an $O(1)$ constant which can be determined from a global solution of the upstream boundary layer flow. In addition, the body contour and ramp angle must also be scaled according to:

$$\hat{f}(\hat{x}) = (\gamma - 1)^{1/2}\lambda^{-3/4}\epsilon_0\chi_0^{3/4} g_s^{n+1/2} f(x), \tag{5.7a}$$

$$\hat{\alpha} = \lambda^{1/2}\epsilon_0\alpha. \tag{5.7b}$$

It should be noted that an affine transformation and a Prandtl transposition has been incorporated into Eqs. (5.6)–(5.7), so that the ramp surface is represented by $y = 0$.

Upon substitution of the transformations (5.6)–(5.7) into the Navier-Stokes equations, it follows that the flow in the lower deck is incompressible to leading-order with density $\rho = 1/(\gamma - 1)$ and $h = \mu = 1$. Furthermore, it can be inferred from the transverse momentum equation that $p = p(x)$ in region I. The remaining dependent variables in the viscous sublayer satisfy the generic triple-deck problem:

$$u\frac{\partial u}{\partial x} + v\frac{\partial u}{\partial y} = -\frac{\mathrm{d}p}{\mathrm{d}x} + \frac{\partial^2 u}{\partial y^2}, \tag{5.8}$$

$$\frac{\partial u}{\partial x} + \frac{\partial v}{\partial y} = 0, \tag{5.9}$$

subject to the boundary conditions:

$$u = v = 0 \quad \text{at} \quad y = 0, \tag{5.10a}$$

$$u \to y + \cdots \quad \text{as} \quad x \to -\infty, \tag{5.10b}$$

$$u \to y + A(x) + \cdots \quad \text{as} \quad y \to \infty, \tag{5.10c}$$

where $A(x)$ is the displacement function. It can also be inferred from the above equations that

$$v \to -\{y + A(x)\}\frac{\mathrm{d}A}{\mathrm{d}x} - \frac{\mathrm{d}p}{\mathrm{d}x} \quad \text{as} \quad y \to \infty. \tag{5.11}$$

Using this result, it can be inferred from Eqs. (5.6c–d) that the slope $\hat{\theta}$ of the streamlines at the outer edge of region I is given by:

$$\hat{\theta} = \lim_{y\to\infty}\left(\frac{\hat{v}}{\hat{u}}\right) = \lambda^{1/2}\epsilon_0\left\{-\frac{\mathrm{d}A}{\mathrm{d}x} + \frac{\mathrm{d}f}{\mathrm{d}x}\right\}. \tag{5.12}$$

5.3 Main Part of Boundary Layer

The nature of the solution in the intermediate layer (regions Ia) and the main part of the boundary layer (region II) was determined by Kerimbekov *et al.* (1994). In particular, it was shown that the slope $\hat{\theta}$ of the streamlines remains invariant across regions I and Ia, and that at the outer edge of region II:

$$\hat{\theta} = \lambda^{1/2}\epsilon_0 \left\{ -\frac{\mathrm{d}A}{\mathrm{d}x} + \frac{\mathrm{d}f}{\mathrm{d}x} + S\mathcal{L}\frac{\mathrm{d}p}{\mathrm{d}x} \right\}, \tag{5.13}$$

where $A(x)$ is the displacement function given by Eq. (5.10c). The parameters S and $\mathcal{L}$ are defined by:

$$S = (\gamma - 1)^{-1/2}\lambda^{5/4}\chi_0^{1/4}g_s^{-n-1/2}, \tag{5.14}$$

$$\mathcal{L} = \int_0^{\delta_0} \{M(Y)\}^{-2} - 1 \, \mathrm{d}Y, \tag{5.15}$$

where δ_0 and $M(Y)$ are the thickness and Mach number distribution of the upstream boundary layer. The first two terms on the right-hand side of Eq. (5.13) represent the conventional displacement effect associated with region I (cf. Eq. (5.12)), while the third term is the contribution due to the main part of the boundary layer (region II).

It should be noted that if $\mathcal{L} > 0$, an adverse pressure gradient results in an increase of the displacement thickness $A(x)$ of region II. A similar kind of behaviour occurs in subsonic flows, and therefore this case shall be referred to as *subcritical*. On the other hand, if $\mathcal{L} < 0$, a pressure rise leads to a decrease in the displacement thickness, just as for a supersonic flow. Consequently, this case is called *supercritical*. In addition, the temperature factor g_s enters into the interaction problem only via the parameter S which is $O(1)$ if the wall is relatively cold, i.e. $g_s \ll 1$. This implies that the surface temperature T_s is small in comparison to the stagnation temperature of the external inviscid flow, but *not* necessarily that T_s is much less than the mainstream static temperature T_∞.

5.4 Inviscid Upper Deck

Following the analysis of Kerimbekov *et al.* (1994) for 2D flows, the solution in the inviscid upper deck (region III) depends upon the following scaled variables, suitably extended for AXI flows:

$$\hat{x} = 1 + (\gamma - 1)^{1/2}\lambda^{-5/4}\chi_0^{3/4} g_s^{n+1/2} x, \tag{5.16a}$$

$$\hat{y} = (\gamma - 1)^{1/2}\lambda^{-5/4} M_\infty^{-1}\chi_0^{3/4} g_s^{n+1/2}\{z + r\}, \tag{5.16b}$$

$$\hat{u} = 1 + \lambda^{1/2}\epsilon_0 M_\infty^{-1}\bar{u}, \quad \hat{v} = \lambda^{1/2}\epsilon_0\bar{v}, \tag{5.16c}$$

$$\hat{p} = 1 + \gamma\lambda^{1/2}\chi_0^{1/2} q, \quad \hat{\rho} = 1 + \lambda^{1/2}\chi_0^{1/2}\bar{\rho}, \tag{5.16d}$$

$$\hat{h} = h_\infty u_\infty^{-2} + \lambda^{1/2}\epsilon_0 M_\infty^{-1}\bar{h}. \tag{5.16e}$$

Furthermore, the radius $\hat{r}$ of the body is assumed to be of the same order-of-magnitude as the thickness of region III, and must therefore be scaled according to:

$$\hat{r} = (\gamma - 1)^{1/2}\lambda^{-5/4} M_\infty^{-1}\chi_0^{3/4} g_s^{n+1/2} r. \tag{5.17}$$

It can be shown using Eqs. (5.16b), (5.17) and (5.7a) that the body contour defined by Eq. (5.4) can be expressed in the form $z = (\lambda\chi_0)^{1/2} f(x)$. Since $\chi_0 \ll 1$, it follows that to leading-order the body surface is represented by $z = 0$. However, the function $f(x)$ does enter into the interaction problem by matching with the solution in region II, as will be discussed later. In addition, the ratio $\hat{\Omega}$ of the body thickness to that of the boundary layer is given by

$$\hat{\Omega} = \frac{\hat{r}}{\hat{\delta}} \sim (\lambda\chi_0)^{-1/2}\frac{r}{\delta}, \tag{5.18}$$

which is therefore much greater than unity. Consequently, axially-symmetric transverse effects *within regions I–II* can be neglected to leading-order (cf. Sec. 4.2). Nevertheless, transverse effects are important in the inviscid region III.

Substitution of Eqs. (5.16a–e) into the Euler Equations yields the following linear system of equations:

$$\frac{\partial \bar{u}}{\partial x} = -\frac{\partial q}{\partial x}, \quad \frac{\partial \bar{v}}{\partial x} = -\frac{\partial q}{\partial z}, \tag{5.19a}$$

$$\frac{\partial \bar{\rho}}{\partial x} = -\frac{1}{(z+r)^j}\frac{\partial}{\partial z}\{(z+r)^j \bar{v}\}, \quad \frac{\partial \bar{h}}{\partial x} = \frac{\partial q}{\partial x}, \tag{5.19b}$$

$$(\gamma - 1)\bar{h} = \gamma q - \bar{\rho}, \tag{5.19c}$$

where $j = 0$ or 1 corresponds to 2D or AXI flows respectively. It follows from these equations that the pressure $q(x, z)$ in the upper deck is governed by a *wave equation* of the form:

$$\frac{\partial^2 q}{\partial x^2} - \frac{\partial^2 q}{\partial z^2} - \frac{j}{z+r}\frac{\partial q}{\partial z} = 0. \tag{5.20}$$

The condition that the flow be undisturbed far upstream of the ramp corner and also as $z \to \infty$ requires that

$$q = 0 \quad \text{as} \quad x \to -\infty, \; z \to \infty. \tag{5.21}$$

Equation (5.20) also requires a boundary condition at the body surface $z = 0$, which will be derived later in this section by matching the solutions in the viscous and inviscid layers. For flows with subcritical wall cooling, the following additional boundary condition is required in order to take the upstream influence effect into account:

$$\partial q/\partial x = 0 \quad \text{as} \quad x \to \infty. \tag{5.22}$$

This condition is frequently used in the computation of inviscid hypersonic flows (see, for example, Guardino 1995); however Eq. (5.22) can not be applied for supercritical flows, since there are no upstream influence effects for this case.

From Eqs. (5.16c), the slope $\hat{\theta}$ of the streamlines as $z \to 0$ is given by

$$\hat{\theta} = \frac{\hat{v}}{\hat{u}} = \lambda^{1/2}\epsilon_0 \bar{v} + \cdots \quad \text{as} \quad z \to 0. \tag{5.23}$$

Since this quantity must match with the value of $\hat{\theta}$ at the outer edge of region II (cf. Eq. (5.13)), it follows that

$$\bar{v}(x,0) = -\frac{\mathrm{d}A}{\mathrm{d}x} + \frac{\mathrm{d}f}{\mathrm{d}x} + S\mathcal{L}\frac{\mathrm{d}p}{\mathrm{d}x}. \tag{5.24}$$

With the help of Eq. (5.19a), this condition can also be expressed in the form:

$$\left(\frac{\partial q}{\partial z}\right)_{z=0} = \frac{\mathrm{d}^2 A}{\mathrm{d}x^2} - \frac{\mathrm{d}^2 f}{\mathrm{d}x^2} - S\mathcal{L}\frac{\mathrm{d}^2 p}{\mathrm{d}x^2}, \tag{5.25}$$

which is just the required boundary condition for Eq. (5.20).

5.5 Surface Temperature Regimes

It is convenient to introduce the *Neiland number* Ne, which is defined by:

$$\mathrm{Ne} = |S\mathcal{L}|^{4/3}. \tag{5.26}$$

This parameter represents the ratio of the contributions to the displacement thickness due to the main deck (region II) and viscous sublayer (region I). Furthermore, there exist three temperature regimes which will now be described.

1. $\mathrm{Ne} \ll 1$, corresponding to moderate or high surface temperatures, i.e. $g_s \gg \chi_0^{-2(2n+1)}$. In this case, the contribution of the main deck to the displacement thickness is negligible, and the problem reduces to the classical supersonic triple-deck formulation first developed by Neiland (1969) and Stewartson & Williams (1969). Numerical solutions for this regime in the 2D case have been obtained by numerous authors, most recently by Bos (1998) and Cassel *et al.* (1995). These results generally show that a separation zone develops near the corner for ramp angles greater than a certain critical value.

2. $\mathrm{Ne} = O(1)$, corresponding to moderate wall cooling, i.e. $g_s \sim \chi_0^{-2(2n+1)}$. Numerical solutions for the 2D case have been obtained by Brown *et al.* (1990),

and more recently by Cassel *et al.* (1996) who showed that wall cooling acts to inhibit separation. Moreover, it was shown that wall cooling has a strong de-stabilizing effect for subcritical flows, while for the supercritical case, it has a strong stabilizing effect.

3. $\mathrm{Ne} \gg 1$, corresponding to strong wall cooling, i.e. $g_s \ll \chi_0^{-2(2n+1)}$. In this case, the contribution of the lower deck to the displacement thickness is negligible. This regime, which is of interest in the present study, was first considered for 2D flows by Zhikharev (1993) for the case of marginal separation from a cold wall with strong subcritical wall cooling, and also by Kerimbekov *et al.* (1994) for supercritical flows. The purpose of the present work is to extend these seminal studies to the case of AXI flows over both compression and expansion corners (see Chapter 6), and also to investigate the separation and reattachment process in the vicinity of the ramp corner for subcritical flows, where a Goldstein (1948) singularity is expected immediately upstream of the separation point (see Chapter 7).

5.6 Formulation for Strong Wall Cooling Case

Following the analysis of Kerimbekov *et al.* (1994) for 2D flows, the following scaled variables are indicated for the viscous sublayer in the cold wall limit as $\mathrm{Ne} \to \infty$:

$$x = \mathrm{Ne}^{3/4}\,\hat{x}, \quad y = \mathrm{Ne}^{1/4}\,\hat{y}, \tag{5.27a}$$

$$u = \mathrm{Ne}^{1/4}\,\hat{u}, \quad v = \mathrm{Ne}^{-1/4}\,\hat{v}, \quad p = \mathrm{Ne}^{1/2}\,\hat{p}, \tag{5.27b}$$

$$A = \mathrm{Ne}^{1/4}\,\hat{A}, \quad f = \mathrm{Ne}^{5/4}\,\hat{f}, \quad \alpha = \mathrm{Ne}^{1/2}\,\beta. \tag{5.27c}$$

The corresponding variables for the inviscid upper deck are given by:

$$z = \mathrm{Ne}^{3/4}\,\hat{z}, \quad q = \mathrm{Ne}^{1/2}\,\hat{q}, \quad r = \mathrm{Ne}^{3/4}\,\hat{r}. \tag{5.28}$$

Upon substitution of these transformations into the interaction problem defined by Eqs. (5.8)–(5.10) and Eqs. (5.20)–(5.22), it can be verified that the governing equations remain invariant. However, the matching condition given by Eq. (5.25) becomes:

$$\left(\frac{\partial \hat{q}}{\partial \hat{z}}\right)_{\hat{z}=0} = \frac{1}{\mathrm{Ne}}\frac{\mathrm{d}^2\hat{A}}{\mathrm{d}\hat{x}^2} - \frac{\mathrm{d}^2\hat{f}}{\mathrm{d}\hat{x}^2} - \mathrm{sgn}(\mathcal{L})\frac{\mathrm{d}^2\hat{p}}{\mathrm{d}\hat{x}^2}. \tag{5.29}$$

Therefore, the first term on the right-hand-side of this equation, which represents the contribution of region I to the displacement thickness, can be neglected for large values of the Neiland number Ne. This implies that the pressure distribution $\hat{q}(\hat{x}, \hat{z})$ in the inviscid layer can be determined independently of the flow in the viscous sublayer. In addition, the ramp geometry is given by:

$$\hat{f}(\hat{x}) = \begin{cases} 0, & \hat{x} \leq 0, \\ \beta\hat{x}, & \hat{x} > 0, \end{cases} \tag{5.30}$$

where β is the scaled ramp angle defined by the third of Eqs. (5.27c). For convenience, **the superscript '^' will be dropped and the equations considered to be scaled with respect to the Neiland number for the rest of this thesis.**

The form of equation (5.29) suggests the use of the following asymptotic expansion for large Neiland number Ne:

$$\phi = \phi_0 + \mathrm{Ne}^{-1}\,\phi_1 + \mathrm{Ne}^{-4/3}\,\phi_2 + \cdots, \tag{5.31}$$

where ϕ represents u, v, ψ, p or A. The form for the third term is suggested from the asymptotic analysis of Chapter 7 (see also Kerimbekov *et al.* 1994). Moreover, the scaled ramp angle β should also be expanded in the form:

$$\beta = \beta_0^* + \mathrm{Ne}^{-4/3}\,\beta_2 + \cdots \tag{5.32}$$

in order to consider small perturbations about the critical ramp angle β_0^* for which separation first occurs. Upon substitution of these expansions into Eqs. (5.8)–(5.9), it can be easily verified that the problem for the leading-order streamfunction ψ_0 is given by:

$$\frac{\partial\psi_0}{\partial y}\frac{\partial^2\psi_0}{\partial x\partial y} - \frac{\partial\psi_0}{\partial x}\frac{\partial^2\psi_0}{\partial y^2} = -\frac{\mathrm{d}p_0}{\mathrm{d}x} + \frac{\partial^3\psi_0}{\partial y^3}. \tag{5.33}$$

where

$$u_0 = \frac{\partial\psi_0}{\partial y}, \quad v_0 = -\frac{\partial\psi_0}{\partial x}. \tag{5.34}$$

In addition, the boundary conditions (5.10) become

$$\psi_0 = \frac{\partial\psi_0}{\partial y} = 0 \quad \text{at} \quad y = 0, \tag{5.35a}$$

$$\psi_0 \to \frac{1}{2}y^2 + \cdots \quad \text{as} \quad x \to -\infty, \tag{5.35b}$$

$$\psi_0 \to \frac{1}{2}y^2 + A_0(x)y + \cdots \quad \text{as} \quad y \to \infty. \tag{5.35c}$$

It can also be shown that the interaction problem for the higher-order terms ϕ_i (for $i = 1$ and 2) is given by:

$$\frac{\partial\psi_0}{\partial y}\frac{\partial^2\psi_i}{\partial x\partial y} + \frac{\partial^2\psi_0}{\partial x\partial y}\frac{\partial\psi_i}{\partial y} - \frac{\partial\psi_0}{\partial x}\frac{\partial^2\psi_i}{\partial y^2} - \frac{\partial^2\psi_0}{\partial y^2}\frac{\partial\psi_i}{\partial x} = -\frac{\mathrm{d}p_i}{\mathrm{d}x} + \frac{\partial^3\psi_i}{\partial y^3}, \tag{5.36}$$

subject to the boundary conditions:

$$\psi_i = \frac{\partial\psi_i}{\partial y} = 0 \quad \text{at} \quad y = 0, \tag{5.37a}$$

$$\psi_i \to 0 \quad \text{as} \quad x \to -\infty, \tag{5.37b}$$

$$\psi_i \to A_i(x)y + \cdots \quad \text{as} \quad y \to \infty. \tag{5.37c}$$

5.7 Pressure Distribution for 2D Flows

For the 2D case (i.e. $j = 0$), the solution of Eq. (5.20) can be expressed in *D'Alembert's* form:

$$q(x, z) = g(x + z) + h(x - z), \tag{5.38}$$

where g and h are arbitrary functions. Since only outgoing waves are important for hypersonic flows, it follows that $g \equiv 0$. It can therefore be inferred from Eq. (5.29) that

$$p = -\frac{\mathrm{d}A}{\mathrm{d}x} + \frac{\mathrm{d}f}{\mathrm{d}x} + S\mathcal{L}\frac{\mathrm{d}p}{\mathrm{d}x}. \tag{5.39}$$

The parameter $S \ll 1$ for moderate or hot surface temperatures, and in this case the foregoing equation reduces to the conventional *Ackeret Law* (1.18) for supersonic flows.

Substitution of the scaled variables defined by Eqs. (5.27) into the above equation, and omitting the '^', yields the interaction law:

$$p = -\frac{1}{\mathrm{Ne}}\frac{\mathrm{d}A}{\mathrm{d}x} + \frac{\mathrm{d}f}{\mathrm{d}x} + \mathrm{sgn}(\mathcal{L})\frac{\mathrm{d}p}{\mathrm{d}x}. \tag{5.40}$$

In the cold-wall limit $\mathrm{Ne} \to \infty$, the first term on the right-hand-side of this equation becomes negligibly small. Furthermore, if the ramp geometry is given by Eq. (5.30), then to leading-order Eq. (5.40) yields the following ordinary differential equation for $p_0(x)$:

$$p_0 = \mathrm{sgn}(\mathcal{L})\frac{\mathrm{d}p_0}{\mathrm{d}x} + \beta_0 H(x), \tag{5.41}$$

where $H(x)$ is the Heaviside function. For the subcritical case, i.e. $\mathcal{L} > 0$, the solution of this equation satisfying the condition that the flow be undisturbed far upstream of the corner (i.e. $p \to 0$ as $x \to -\infty$) is given by:

$$p_0(x) = \begin{cases} \beta_0\,\mathrm{e}^x, & x \le 0, \\ \beta_0, & x > 0. \end{cases} \tag{5.42}$$

The corresponding solution for the supercritical case, i.e. $\mathcal{L} < 0$ is given by:

$$p_0(x) = \begin{cases} 0, & x \le 0, \\ \beta_0(1 - \mathrm{e}^{-x}), & x > 0. \end{cases} \tag{5.43}$$

Chapter 6

Numerical Results for the Strong Wall Cooling Case

6.1 Introduction

In this chapter, numerical solutions of the leading-order inviscid upper deck problem given by Eqs. (5.20)–(5.22) shall be obtained for both 2D and AXI hypersonic flows with strong wall cooling. As discussed in Sec. 5.6, the displacement function $A(x)$ formally disappears from the boundary condition (5.29) in the cold wall limit $\mathrm{Ne} \to \infty$. Thus, to leading-order, Eq. (5.29) can be expressed in the form:

$$\frac{\partial q}{\partial z} = -\frac{\mathrm{d}^2 f}{\mathrm{d}x^2} - \mathrm{sgn}(\mathcal{L})\frac{\mathrm{d}^2 p}{\mathrm{d}x^2} \quad \text{at} \quad z = 0, \tag{6.1}$$

where the surface pressure $p(x) = q(x, 0)$, and the '^' has been omitted for convenience. Consequently, the solution in the inviscid region III can be obtained independently of the flow in the viscous sublayer (region I). As soon as the surface pressure distribution has been computed, the solution in the viscous sublayer can be found by solving the boundary layer equations (5.8)–(5.10) with prescribed pressure gradient, as in the classical theory of Prandtl (1904). It should be noted that the solution for the pressure can also be expressed in terms of an integral

involving source and sink distribution functions (see Ashley & Landahl 1965 and Kluwick *et al.* 1984), but the boundary condition (6.1) renders this approach impractical.

A uniform mesh defined by

$$x_i = x_{\min} + (i-1)\Delta x, \quad 1 \le i \le I, \tag{6.2}$$

$$z_k = (k-1)\Delta z, \quad 1 \le k \le K, \tag{6.3}$$

shall be employed for the inviscid calculations, and quantities such as $q_{i,k}$ will be used to denote approximations to $q(x_i, z_k)$. In addition, an asterisk shall be used to refer to the known solution from the previous iteration, i.e. $q^*_{i,k}$. Using the computed surface pressure $p(x) = q(x, 0)$ from the inviscid calculation, the solution in the viscous sublayer shall be obtained using a uniform grid defined by:

$$x_i = x_{\min} + (i-1)\Delta x, \quad 1 \le i \le I, \tag{6.4}$$

$$y_j = (j-1)\Delta y, \quad 1 \le j \le J. \tag{6.5}$$

6.2 Numerical Algorithm for Inviscid Upper Deck

6.2.1 Subcritical flows ($\mathcal{L} > 0$)

Since subcritical flows do permit the upstream propagation of disturbances, the x-derivative in Eq. (6.1) should be approximated using a second-order accurate *central* difference quotient as follows:

$$\frac{-3q_{i,1} + 4q_{i,2} - q_{i,3}}{2\Delta z} = -\left(\frac{\mathrm{d}^2 f}{\mathrm{d}x^2}\right)_i - \frac{p_{i+1} - 2p_i + p_{i-1}}{(\Delta x)^2} \tag{6.6}$$

Notice the use of a second-order accurate forward difference approximation for the normal derivative of the wall pressure. Since the surface pressure $p_i = q_{i,1}$,

the foregoing equation yields the following linear tridiagonal system of equations for p_i:

$$a_i p_{i-1} + b_i p_i + c_i p_{i+1} = d_i, \qquad 2 \leq i \leq I-1 \tag{6.7}$$

where

$$a_i = c_i = \frac{1}{(\Delta x)^2}, \tag{6.8a}$$

$$b_i = \frac{3}{2\Delta z} + \frac{2}{(\Delta x)^2}, \tag{6.8b}$$

$$d_i = W_i^* + \left(\frac{\mathrm{d}^2 f}{\mathrm{d}x^2}\right)_i, \tag{6.8c}$$

and

$$W_i^* = \frac{4q_{i,2}^* - q_{i,3}^*}{2\Delta z}. \tag{6.9}$$

The quantity W_i^* involves the solution in the interior of the computational domain, and is assumed known from the previous iteration. Methods for calculating W_i^* will be discussed in Secs. 6.2.3 and 6.2.4. The upstream boundary condition (5.21) requires that $p_1 = 0$. The boundary condition far downstream of the ramp corner given by Eq. (5.22) was approximated by:

$$\left(\frac{\mathrm{d}p}{\mathrm{d}x}\right)_{x\to\infty} = 0 \approx \frac{p_{I-2} - 4p_{I-1} + 3p_I}{2\Delta x}. \tag{6.10}$$

The above system of equations can be expressed in the form:

$$\begin{pmatrix} 1 & 0 & & & & & \\ a_2 & b_2 & c_2 & & & & \\ & \ddots & \ddots & \ddots & & & \\ & & \ddots & \ddots & \ddots & & \\ & & & \ddots & \ddots & \ddots & \\ & & & & a_{I-1} & b_{I-1} & c_{I-1} \\ & & & & 1 & -4 & 3 \end{pmatrix} \begin{pmatrix} p_1 \\ p_2 \\ \cdot \\ \cdot \\ \cdot \\ p_{I-1} \\ p_I \end{pmatrix} = \begin{pmatrix} 0 \\ d_2 \\ \cdot \\ \cdot \\ \cdot \\ d_{I-1} \\ 0 \end{pmatrix}. \tag{6.11}$$

Unless otherwise specified, all the other elements in the coefficient matrix are zero. The I-th row of the system can be expressed in tri-diagonal form using the $(I-1)$-th row as follows:

$$-(4a_{I-1}+b_{I-1})p_{I-1}+(3a_{I-1}-c_{I-1})p_I=-d_{I-1}. \tag{6.12}$$

The solution thus proceeds as follows. First compute the solution $q_{i,k}$ in the interior of the computational domain using either of the methods described in Secs. 6.2.3 or 6.2.4, from which W_i^* can be determined. Then solve the above tri-diagonal system using Gaussian Elimination to compute a new distribution for the wall pressure p_i. Next, recalculate the solution throughout the entire computational domain, and continue in this fashion until the maximum change in p_i is less than a specified tolerance level ϵ, which was taken as 10^{-7} in the present study.

6.2.2 Supercritical flows ($\mathcal{L}<0$)

In contrast to the subcritical case, supercritical flows do not permit the upstream propagation of disturbances, and therefore the solution can be computed using a downstream marching technique. Moreover, since the flow is undisturbed upstream of the compression ramp, the numerical integration may be initiated from $x=0$.[1] Equation (6.1) is discretised as follows:

$$\frac{-3q_{i,1}+4q_{i,2}-q_{i,3}}{2\Delta z}=-\left(\frac{\mathrm{d}^2 f}{\mathrm{d}x^2}\right)_i+\frac{-p_{i-3}+4p_{i-2}-5p_{i-1}+2p_i}{(\Delta x)^2}, \tag{6.13}$$

where a second-order accurate *backward* difference is used to approximate $\mathrm{d}^2p/\mathrm{d}x^2$, since the solution at any point depends solely on the flow immediately upstream. Since $p_i=q_{i,1}$, this equation yields the following numerical scheme for $2\le i\le I$:

$$Mp_i=W_i-\frac{-p_{i-3}+4p_{i-2}-5p_{i-1}}{(\Delta x)^2}+\left(\frac{\mathrm{d}^2 f}{\mathrm{d}x^2}\right)_i, \tag{6.14}$$

[1] Due to the slight rounding of the ramp (cf. Eq. (6.36)), $x_{\min}$ was taken as -2.

where W_i was defined by Eq. (6.9) and

$$M = \frac{3}{2\Delta z} + \frac{2}{(\Delta x)^2}. \tag{6.15}$$

This method allows the computation of the wall pressure p_i using the known solution at the grid points $i-1$, $i-2$ and $i-3$. In order to start the marching procedure, the values p_{-1}, p_0 and p_1 are set equal to zero. It should be noted that no global iterations are required for this case, and that no boundary condition can be applied far downstream at $i = I$.

6.2.3 Method of Characteristics

The *Method of Characteristics* has been frequently employed in the computation of inviscid supersonic or hypersonic flows, since it permits the solution to be computed downstream along the characteristics. This reflects the real physical aspect that disturbances in a supersonic flow are propagated along these curves. Moreover, the two-dimensional Euler Equations reduce to ordinary differential equations (sometimes known as the *compatibility equations*) along the characteristics, which are more readily solved than the original partial differential equation.

The wave equation (5.20) is particularly suited for solution using the Method of Characteristics since the characteristics are straight lines with gradient ± 1. By defining

$$s = \frac{\partial q}{\partial x} \quad \text{and} \quad t = \frac{\partial q}{\partial y}, \tag{6.16}$$

it can be shown that the compatibility equations along the characteristics with gradient ± 1 are given by (see Appendix B):

$$\frac{\mathrm{d}s}{\mathrm{d}x} \mp \frac{\mathrm{d}t}{\mathrm{d}x} = \frac{jt}{z+r}. \tag{6.17}$$

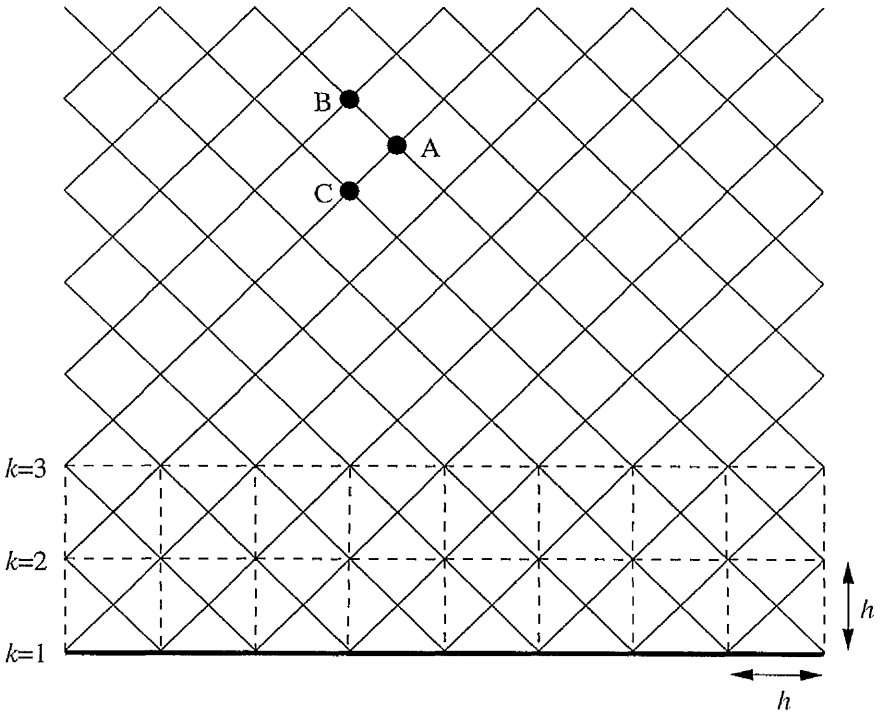

Figure 6.1: Grid for the Method of Characteristics showing three typical points; mesh points intersecting the dashed lines are used for computing W_i.

This equation can be used to compute the solution locally, as shown in Fig. 6.1, where the solution at any given point A depends solely on information propagated from two neighbouring points B and C. If these points are chosen close enough together, it follows that Eq. (6.17) can be approximated along the characteristic from B to A by the difference equation:

$$\frac{s_A - s_B}{h/2} - \frac{t_A - t_B}{h/2} = \frac{j(t_A + t_B)}{z_A + z_B + 2r}. \tag{6.18}$$

where $h = \Delta x = \Delta z$. Notice the use of average values on the right-hand-side of this equation. Similarly, the solution along the characteristic from C to A can be approximated by:

$$\frac{s_A - s_C}{h/2} + \frac{t_A - t_C}{h/2} = \frac{j(t_A + t_C)}{z_A + z_C + 2r}. \tag{6.19}$$

The solution of this pair of linear equations is given by:

$$s_A = \frac{(1-b_C)a_B + (1-b_B)a_C}{2+b_B-b_C}, \quad t_A = \frac{a_C - a_B}{2+b_B-b_C}, \tag{6.20}$$

where

$$b_B = \frac{jh}{4(z_A - r) - h)}, \quad b_C = \frac{jh}{4(z_A + r) + h)}, \tag{6.21}$$

$$a_B = s_S + (b_B - 1)t_B, \quad a_C = s_C + (b_C + 1)t_C. \tag{6.22}$$

Finally, since

$$dq = sdx + tdy, \tag{6.23}$$

the solution at point A is given by

$$q_A = q_B + \frac{h}{4}(s_A + s_B + t_A + t_B). \tag{6.24}$$

The boundary conditions given by Eq. (5.21) require that:

$$q_{1,k} = 0, \quad 1 \le k \le K, \tag{6.25}$$

$$q_{i,K} = 0, \quad 1 \le i \le I, \quad \text{if} \quad z_{\max} \ge x_{\max} - x_{\min}. \tag{6.26}$$

For $k = 2$, this algorithm requires knowledge of the wall pressure $p_i = q_{i,1}$. For subcritical flows, this is assumed known from the previous iteration, whilst for the supercritical case p_i is to be computed at the current streamwise location x_i. Due to the geometry of the characteristic mesh, there is some difficulty associated with the implementation of the matching condition (6.1). However, this problem was resolved by evaluating the quantity W_i (which was defined by Eq. (6.9)) using only the mesh points which coincide with an effective finite-difference grid, as shown by the dashed lines in Fig. 6.1.

6.2.4 Finite-difference method

An alternative method considered here for the numerical solution of Eq. (5.20) was an explicit finite-difference scheme, and the equation was discretised using second-order accurate central differences as follows:

$$\frac{q_{i+1,k} - 2q_{i,k} + q_{i-1,k}}{(\Delta x)^2} - \frac{q_{i,k+1} - 2q_{i,k} + q_{i,k-1}}{(\Delta z)^2} = \frac{j(q_{i,k+1} - q_{i,k-1})}{2\Delta z(z_k + r)}. \qquad (6.27)$$

This equation yields the following explicit scheme for $2 \leq i \leq I$ and $2 \leq k \leq K - 1$:

$$q_{i+1,k} = 2(1 - \lambda^2)q_{i,k} + \left\{\lambda^2 + \frac{j(\Delta x)^2}{2\Delta z(z_k + r)}\right\}(q_{i,k+1} - q_{i,k+1}) - q_{i-1,k}, \qquad (6.28)$$

where $\lambda = \Delta x/\Delta z$, and $\lambda < 1$ in order to ensure stability of the numerical algorithm (see, for example, Burden & Faires 1993). This scheme, which is also known as the *Leap-frog method*, enables the solution to be computed everywhere, starting from the initial conditions $q_{0,k} = q_{1,k} = 0$.

It was observed that this scheme generated spurious oscillations in the solution if $\lambda < 1$, which are visible in the result for the pressure distribution $q(x, z)$ shown in Fig. 6.13 (which was obtained using $I = 200$ and $K = 100$ which gives $\lambda = 0.5$). It is believed that these oscillations appear because the finite-difference grid does not properly match with the physical characteristics (unless $\lambda = 1$, in which case the stability criterion would be violated). In fact, the appearance of oscillations in the numerical solution of hyperbolic equations is not uncommon using explicit second-order accurate schemes (see, for example, Guardino 1995). By comparison, the Method of Characteristics yields an oscillation-free solution (cf. Fig. 6.12, where a mesh consisting of 200×200 points was employed). Moreover, the finite-difference method requires the solution to be known at two previous streamwise locations, whilst the Method of Characteristics only requires the upstream solution at two adjacent points on the characteristics mesh.

6.3 Numerical Algorithm for Viscous Sublayer

Equations (5.8)–(5.10) represent a conventional boundary layer problem with prescribed pressure gradient, and can be solved using a downstream marching technique, provided that the flow does not separate from the body surface. The following second-order accurate difference equation was used to approximate the momentum equation (5.8):

$$u^*_{i,j}\left(\frac{u_{i-2,j}-4u_{i-1,j}+3u_{i,j}}{2\Delta x}\right)+v^*_{i,j}\left(\frac{u_{i,j+1}-u_{i,j-1}}{2\Delta y}\right)= -\left(\frac{\mathrm{d}p}{\mathrm{d}x}\right)_i+\frac{u_{i,j+1}-2u_{i,j}+u_{i,j-1}}{(\Delta y)^2}, \quad (6.29)$$

This equation defines the following tri-diagonal problem for $u_{i,j}$, $2 \le i \le I$:

$$a_j u_{i,j-1} + b_j u_{i,j} + c_j u_{i,j+1} = d_j, \qquad 2 \le j \le J-1, \quad (6.30)$$

where

$$a_j = \frac{1}{(\Delta y)^2} + \frac{v^*_{i,j}}{2\Delta y}, \quad (6.31a)$$

$$b_j = -\frac{2}{(\Delta y)^2} - \frac{3u^*_{i,j}}{2\Delta x}, \quad (6.31b)$$

$$c_j = \frac{2}{(\Delta y)^2} - a_j, \quad (6.31c)$$

$$d_j = \frac{u^*_{i,j}}{2\Delta x}(u_{i-2,j}-4u_{i-1,j}) + \left(\frac{\mathrm{d}p}{\mathrm{d}x}\right)_i. \quad (6.31d)$$

The no-slip conditions at the body surface require $u_{i,1} = v_{i,1} = 0$. At the outer edge of the viscous sublayer, the condition Eq. (5.10c) was approximated by:

$$\left(\frac{\partial u}{\partial y}\right)_{y\to\infty} = 1 \approx \frac{u_{i,J-2}-4u_{i,J-1}+3u_{i,J}}{2\Delta y}. \quad (6.32)$$

The above tri-diagonal system of equations was solved using Gaussian Elimination. It should be noted that the condition (6.32) requires that the J-th row of the system be expressed in tri-diagonal form using the $(J-1)$-th row in a manner similar to that used for the I-th row of Eq. (6.11):

$$-(4a_{J-1}+b_{J-1})u_{i,J-1} + (3a_{J-1}-c_{J-1})u_{i,J} = 2\Delta y\, a_{J-1} - d_{J-1}. \quad (6.33)$$

The continuity equation (5.9) was approximated using:

$$\frac{1}{2}\left(\frac{u_{i-2,j}-4u_{i-1,j}+3u_{i,j}}{2\Delta x}+\frac{u_{i-2,j-1}-4u_{i-1,j-1}+3u_{i,j-1}}{2\Delta x}\right) + \frac{v_{i,j}-v_{i,j-1}}{2\Delta y}=0, \quad (6.34)$$

which yields the following iterative scheme for $v_{i,j}$, $2 \leq j \leq J$:

$$v_{i,j}=v_{i,j-1}+\frac{\Delta y}{4\Delta x}\left(u_{i-2,j}-4u_{i-1,j}+3u_{i,j}+u_{i-2,j-1}-4u_{i-1,j-1}+3u_{i,j-1}\right). \quad (6.35)$$

Starting from the upstream solution given by Eq. (5.10b), the above system of equations were solved iteratively to determine the solution at the current streamwise location, using the computed solution from the previous location as the initial distribution. The solution was marched downstream to $x = x_{\max}$, or until the flow separates.

Since second-order accurate *backward* differences have been employed for the x-derivatives in Eqs. (6.29) and (6.34), the resulting method is sometimes referred to as a three-level fully implicit scheme. This scheme was found to be robust and unconditionally stable (in the Von Neumann sense). The Crank-Nicolson scheme (see, for example, Burden & Faires 1993) was also utilised for the solution of the present problem, but this method required a relatively large number of mesh points (as compared to the three-level scheme) in order to preclude the occurrence of numerical oscillations. In addition, the three-level fully-implicit method is more stable to short harmonic oscillations. For this reason the three-level scheme was preferred and all of the solutions shown here were obtained using this method.

6.4 Results & Discussion

Numerical results have been obtained by the author for various ramp angles and body radii for both subcritical and supercritical cases. Unless otherwise specified, the pressure distribution $q(x,z)$ in the inviscid layer was computed using the Method of Characteristics with $I = K = 500$ and $x_{\max} = 10$. For subcritical flows $x_{\min} = -10$, whilst for the supercritical case $x_{\min} = -2$. In order to avoid problems associated with the discontinuous derivative of the body contour $f(x)$ at $x = 0$, the ramp corner was rounded slightly so that $f''(x)$ is a smooth function everywhere. In the present study, $f(x)$ was defined by:

$$f(x) = \frac{\beta}{2}\left\{x + \sqrt{x^2 + R^2}\right\}, \tag{6.36}$$

where the *rounding parameter* R was taken as 0.05. Using the computed surface pressure $p(x) = q(x,0)$ from the inviscid calculation, the solution in the viscous sublayer was computed using the fully-implicit three-level scheme with $I = 500$, $J = 250$ and $y_{\max} = 10$. Results are presented for the pressure $p(x)$ and skin friction $\tau_s(x)$ defined by:

$$\tau_s(x) = \left(\frac{\partial u}{\partial y}\right)_{y=0}. \tag{6.37}$$

The solution in the viscous sublayer was computed up to $x = x_{\max}$, or until the flow separates in which case $\tau_s(x_s) = 0$, where x_s is the location of the separation point. Solutions were also obtained using various other mesh sizes, and the results are believed to be globally grid independent.

6.4.1 Two-dimensional compression corners

Results for the 2D flow over a true compression corner (i.e. with no rounding of the ramp corner) are shown in Figs. 6.3 and 6.4. In this case, the surface pressure distribution is given analytically either by Eq. (5.42) or (5.43). Furthermore, the

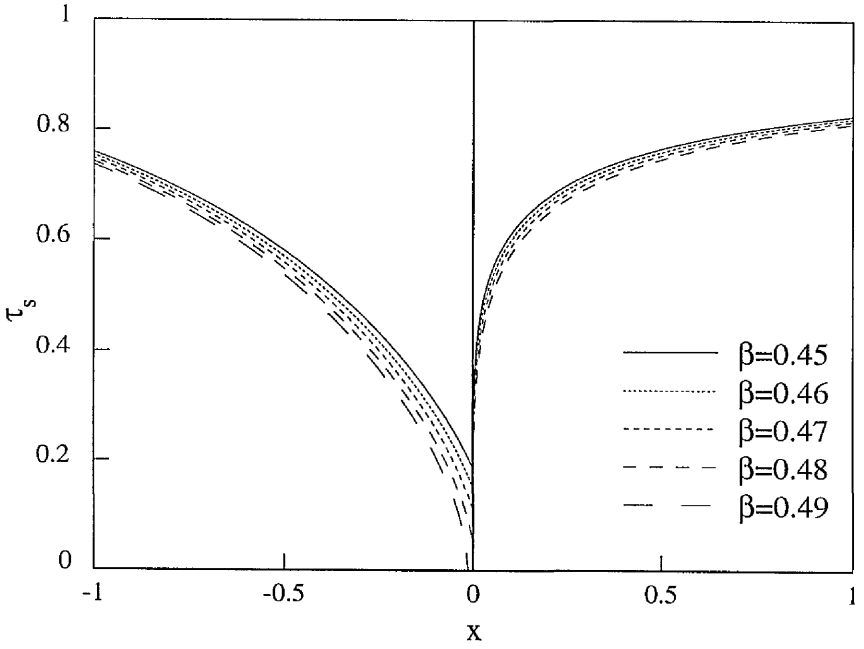

Figure 6.2: Skin friction τ_s distributions for various ramp angles β close to the critical value $\beta^* \approx 0.48$ for 2D subcritical flows.

solution for the supercritical case was initiated from the ramp corner, since the flow is unperturbed upstream (i.e. $p = 0$ and $\tau_s = 1$ for $x < 0$ and $\mathcal{L} < 0$). As expected, the minimum τ_0 in the skin friction distribution decreases as the ramp angle β is increased, and eventually reaches zero at a certain critical value β^* at a streamwise location $x = x_s$. This phenomenon is also known as *incipient separation*. It is evident from Fig. 6.2 that for subcritical flows $x_s = 0$ and $\beta^* \approx 0.48$. An important feature of this case is the occurrence of a Goldstein (1948) singularity upstream of the separation point, and the sharp behaviour of the skin friction immediately downstream of the ramp corner. It should also be observed that the flow separates just upstream of the ramp corner for the case $\beta = 0.49$, and therefore this particular solution could not be continued downstream of x_s

using the current downstream marching technique. However, it will be shown in the next chapter that the flow in the separation region can be described by considering a multi-layer structure near to the wall, and using the method of matched asymptotic expansions to determine the solution in each region to form a coherent description of the separation and reattachment process.

For the supercritical case, it was observed that $x_s = 0.5$ and $\beta^* \approx 0.75$, which are in good agreement with the numerical results of Kerimbekov *et al.* (1994). In contrast to the subcritical case, the skin friction vanishes linearly at the separation point, and this phenomenon is known as *marginal separation* (see Appendix C). It can also be observed that for both subcritical and supercritical 2D flows,

$$p \to \beta, \quad \tau_s \to 1 \qquad \text{as} \quad x \to \infty. \tag{6.38}$$

6.4.2 Axially-symmetric compression corners

Results for the AXI case are shown in Figs. 6.5–6.15. It is evident from these solutions that AXI effects have a major influence on the flow properties, especially for comparatively small body radii. In particular, the wall pressure reaches a maximum value at a certain streamwise location[2] , after which it decreases further downstream. This results in a favourable pressure gradient which accelerates the flow and may cause the skin friction to exceed unity downstream of the ramp corner, particularly for small radii. A similar kind of behaviour can be seen in the results of Kluwick *et al.* (1984) for supersonic flows, although their results did not take wall cooling into consideration. A rather surprising result is that, for a fixed radius r, the skin friction becomes greater than unity at almost the same streamwise location, regardless of the ramp angle (see Figs. 6.5 and 6.7).

It can be observed from Figs. 6.6 and 6.8 that the minimum τ_0 in the skin

[2]For subcritical flows, this maximum in the pressure distribution occurs in the vicinity of, but not exactly at, the corner $x = 0$ due to the slight rounding of the ramp.

friction distribution increases with decreasing radius r *for fixed ramp angle.* Consequently, the critical ramp angle β_0^* at which separation first occurs is greater for AXI flows, and increases as r decreases. In the limit as $r \to \infty$, the results for AXI flows approach those for the corresponding 2D case, as shown by the dashed curves in Figs. 6.6 and 6.8[3] . In this case, the AXI wave equation (5.20) reduces to the corresponding 2D case.

Figure 6.11 (a) shows a comparison of the exact solution given by Eq. (5.42) for the 2D subcritical case with the result obtained using the Method of Characteristics. Figure 6.11 (b) shows the result for the corresponding AXI case obtained using both the Method of Characteristics and the finite difference method. Very good agreement is obtained in both cases, and this is despite the presence of numerical oscillations in the interior solution obtained using the finite-difference method (see Fig. 6.13).

The pressure distribution $q(x, z)$ in the inviscid region is shown in Figs. 6.14 and 6.15, which were obtained using a mesh consisting of 200×200 points, and the rounding parameter R was taken as 0.2. It is clear that the pressure decays at large distances from the body surface, which is in sharp contrast to the 2D case for which the pressure remains constant along the characteristic lines with gradient unity, as shown in Figs. 6.12 and 6.13.

6.4.3 Expansion corners

Although the present study has so far been devoted exclusively to flows over compression ramps, the governing equations can be equally applied to expansion corners by merely requiring the ramp angle to be negative. For the 2D case, the pressure $p(x)$ decreases monotonically, thus resulting in a favourable pressure gradient which accelerates the flow as it passes over the expansion corner. However,

[3]The pressure $p(x)$ for these 2D cases were obtained by solving the full inviscid upper-deck equations with $j = 0$ in order to take into account the slight rounding of the ramp corner.

for AXI flows there is expected to be a region of unfavourable pressure gradient, which may result in flow separation and reversal.

Solutions for various body radii are shown in Figs. 6.9 and 6.10, where the ramp angle was kept fixed. It is evident that the flow separates if the radius is smaller than a certain critical value r^*, which is itself dependent on the ramp angle. Since the flow separates downstream of the expansion corner, the singularity encountered at the separation point appears to be weak and can be described using marginal separation theory (see Appendix C). In addition, no separation phenomenon was observed for the 2D flow over expansion corners, regardless of the ramp angle. It is surprising to observe that the skin friction distribution shown in Fig. 6.9 for the 2D hypersonic flow with subcritical wall cooling is qualitatively similar to that obtained by Rizzetta *et al.* (1978) for supersonic flows without wall cooling.

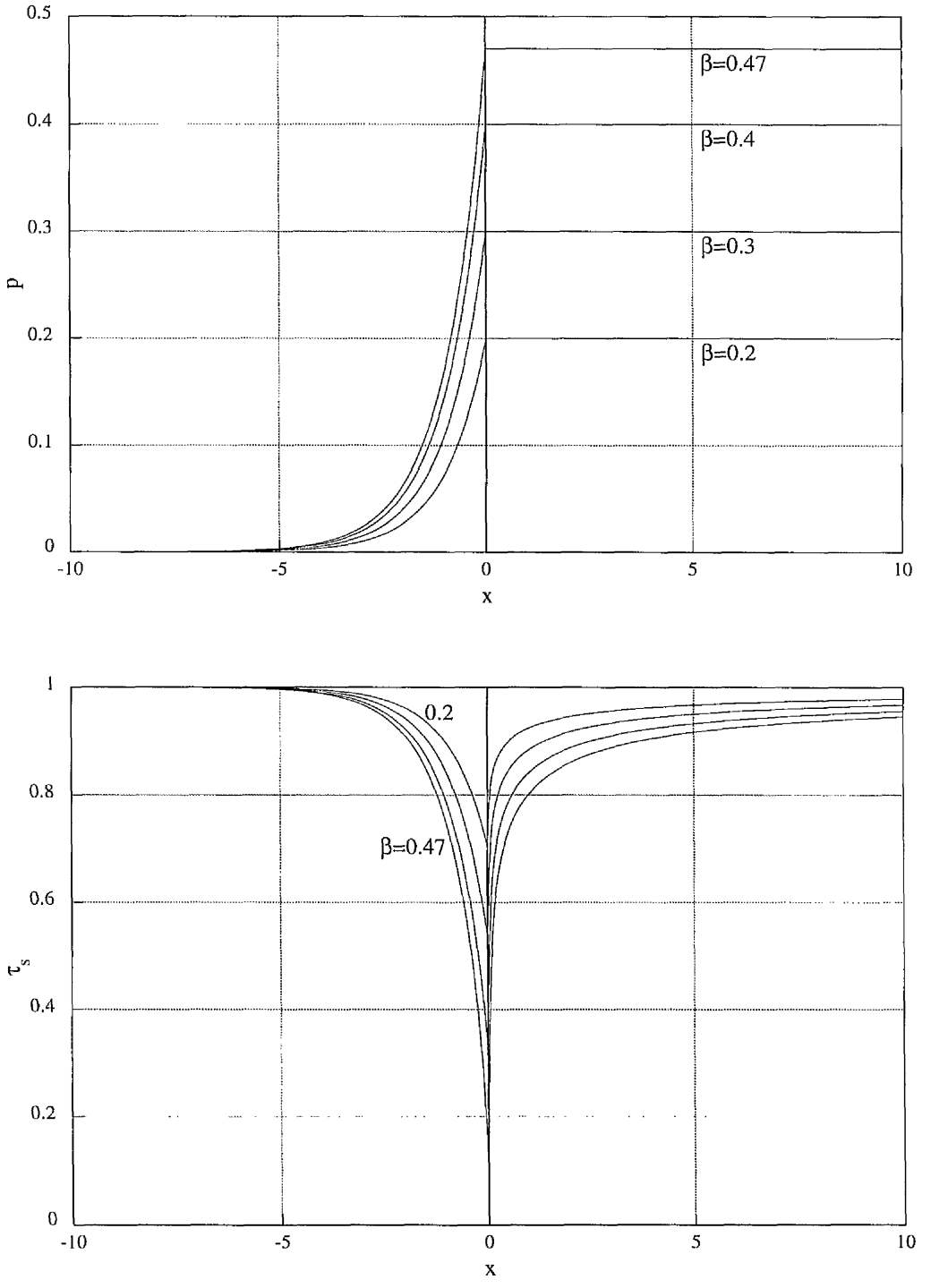

Figure 6.3: Pressure p and skin friction τ_s distributions for various ramp angles β (2D, subcritical case).

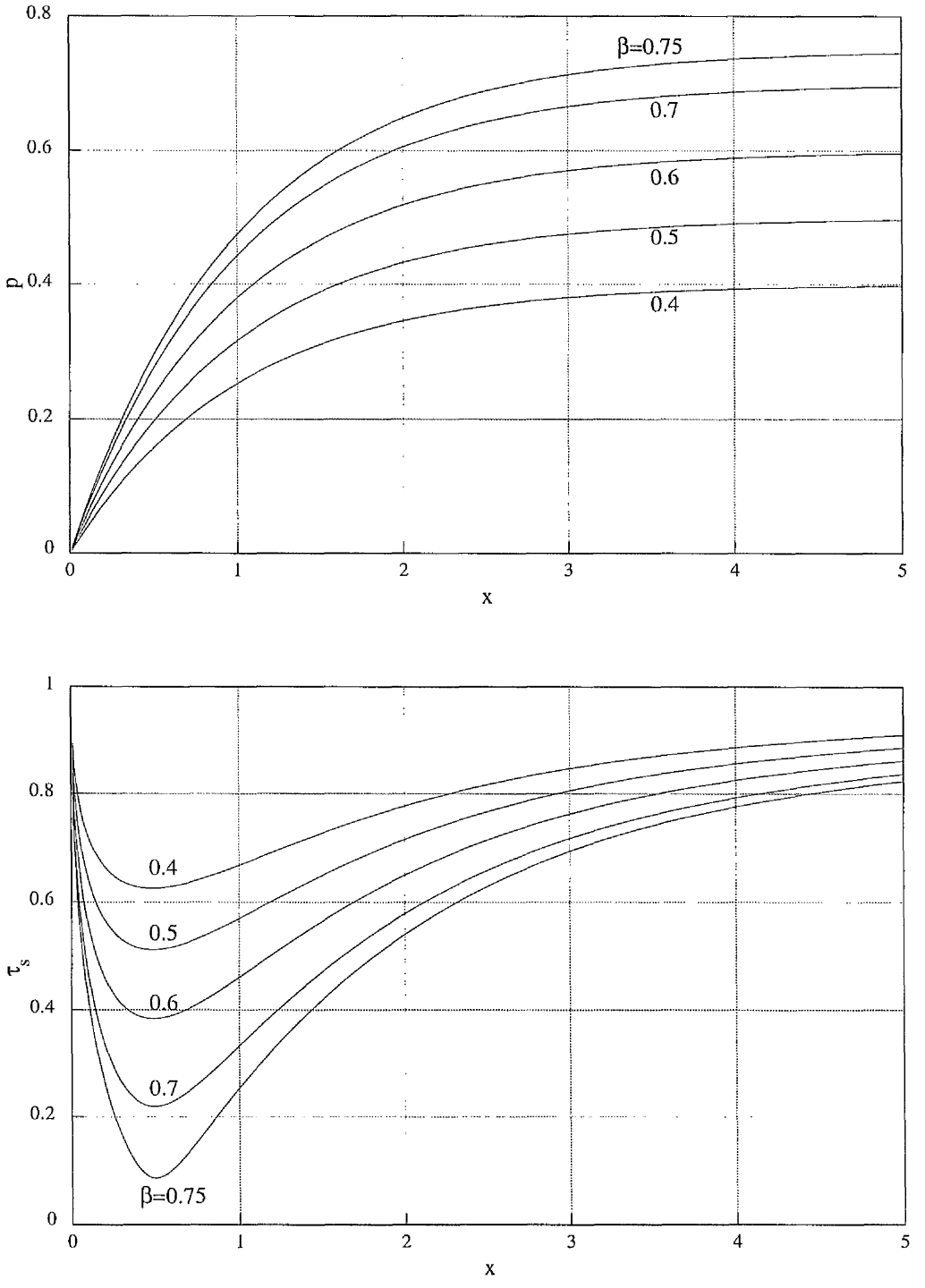

Figure 6.4: Pressure p and skin friction τ_s distributions for various ramp angles β (2D, supercritical case).

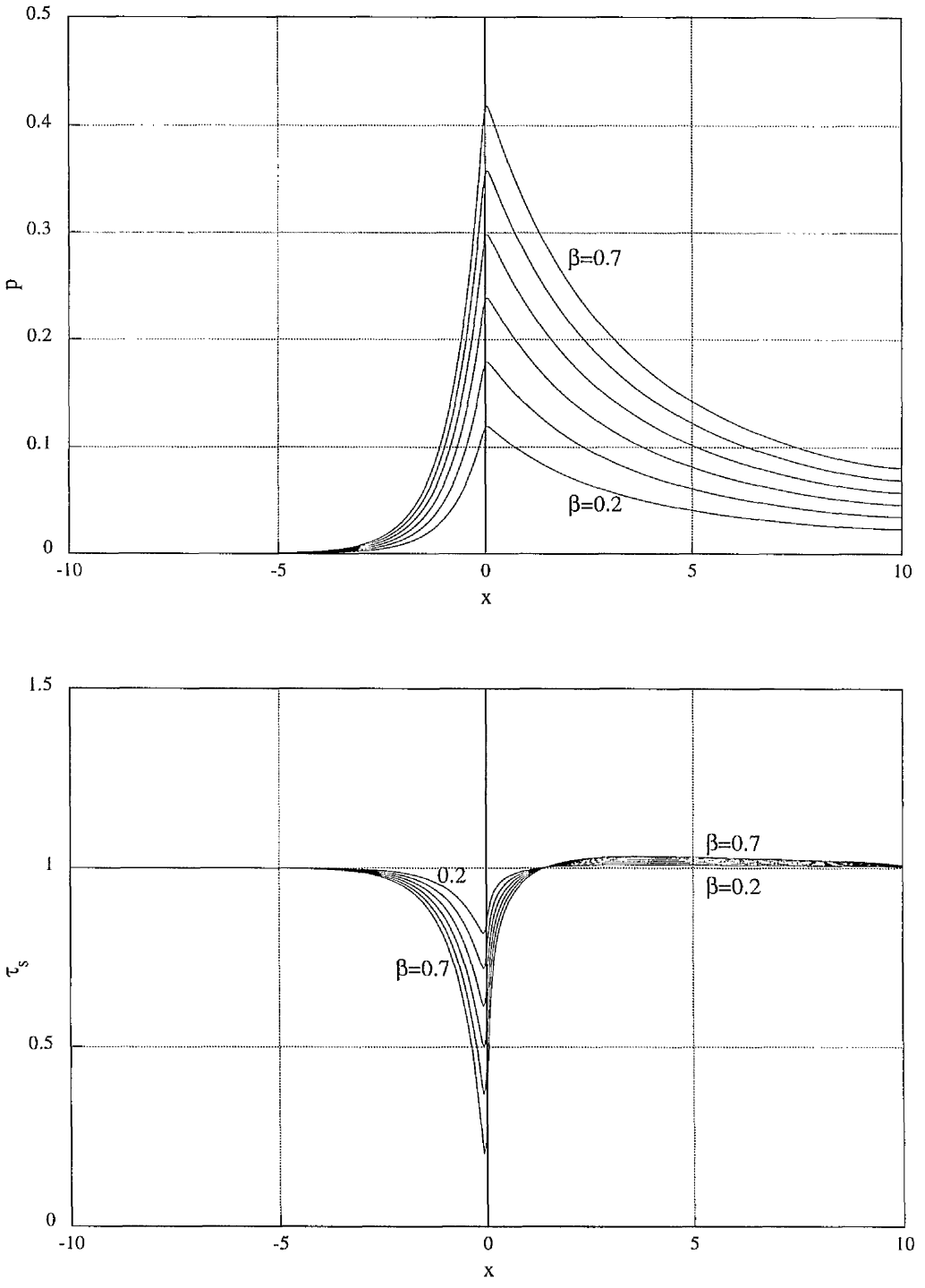

Figure 6.5: Pressure p and skin friction τ_s distributions for various ramp angles $\beta = 0.2, \ldots, 0.7$ with increment $\Delta\beta = 0.1$ (AXI, subcritical case, radius r=1).

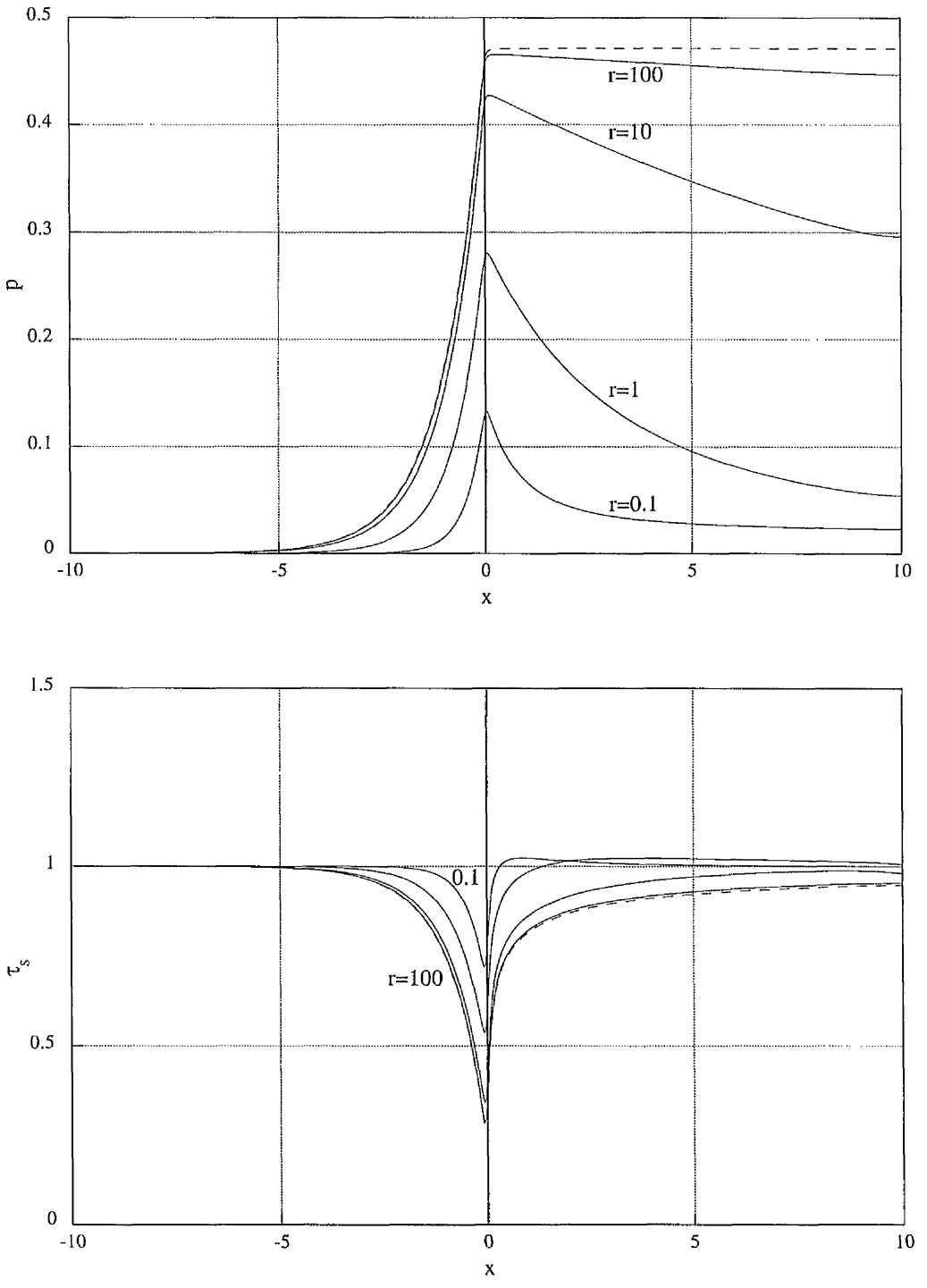

Figure 6.6: Pressure p and skin friction τ_s distributions for various body radii r (AXI, subcritical case, β=0.47). Dashed curve (- - -) represents the 2D case (i.e. $r = \infty$).

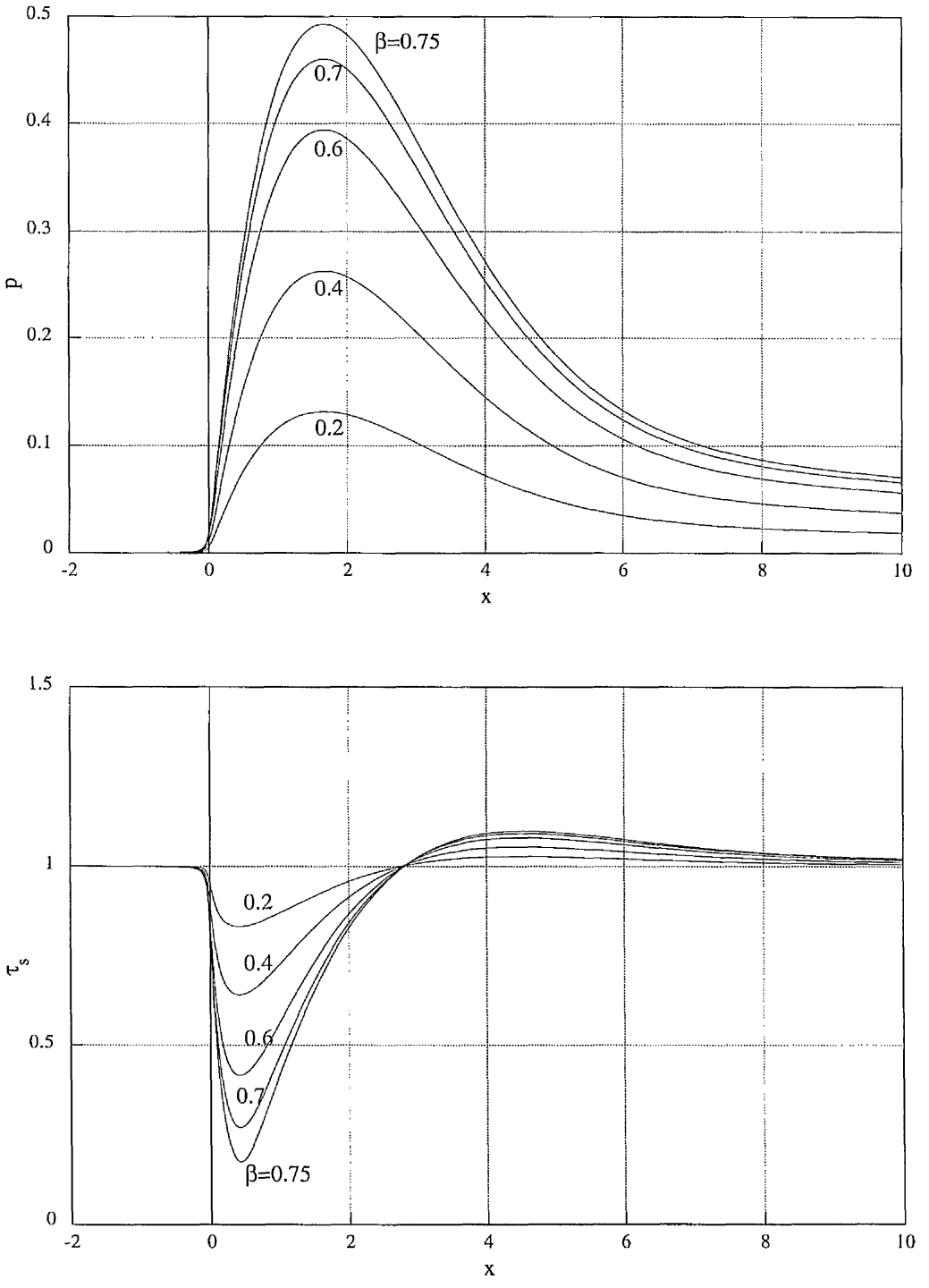

Figure 6.7: Pressure p and skin friction τ_s distributions for various ramp angles β (AXI, supercritical case, radius r=1).

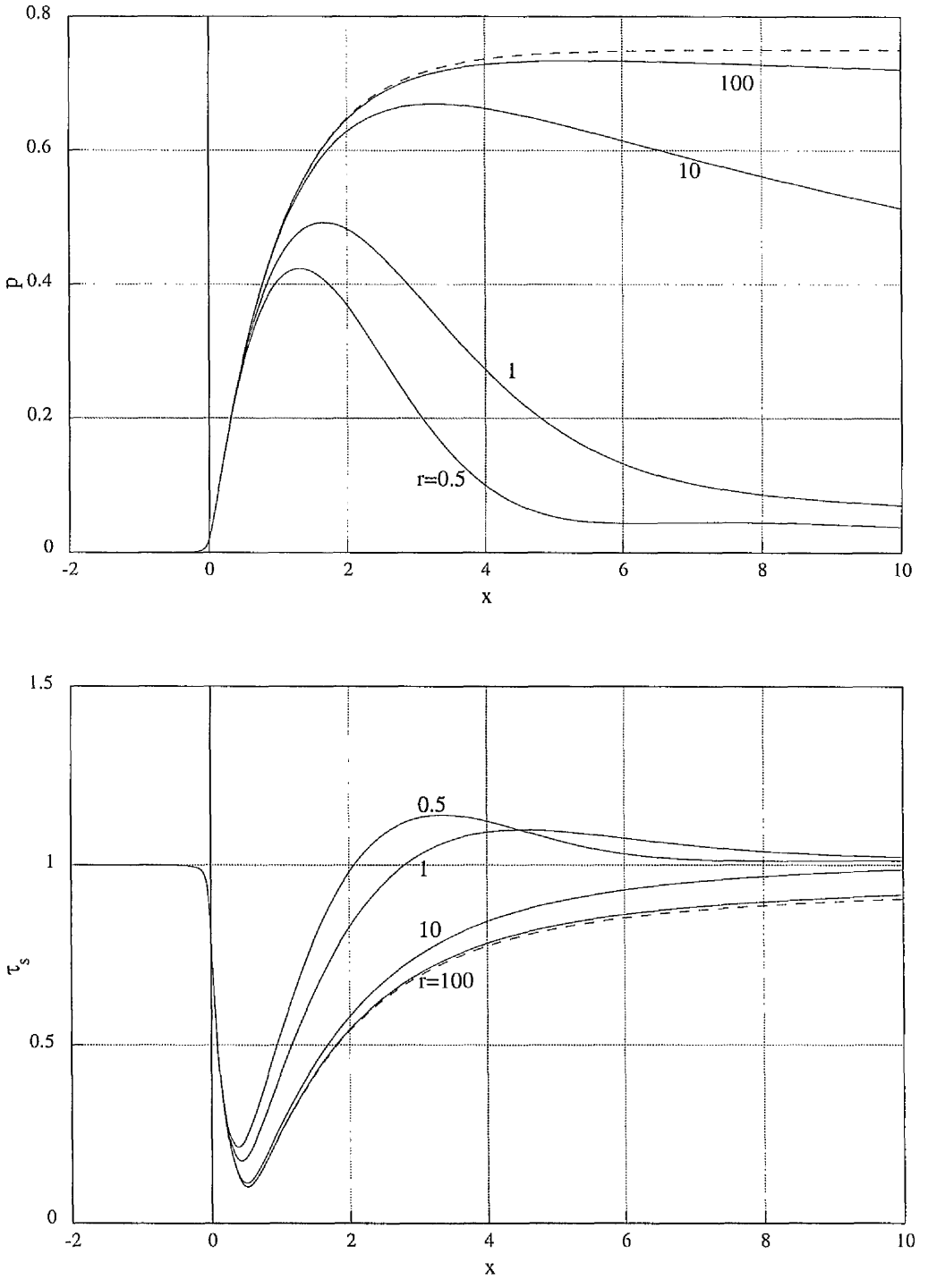

Figure 6.8: Pressure p and skin friction τ_s distributions for various body radii r (AXI, supercritical case, β=0.75). Dashed curve (- - -) represents the 2D case (i.e. $r = \infty$).

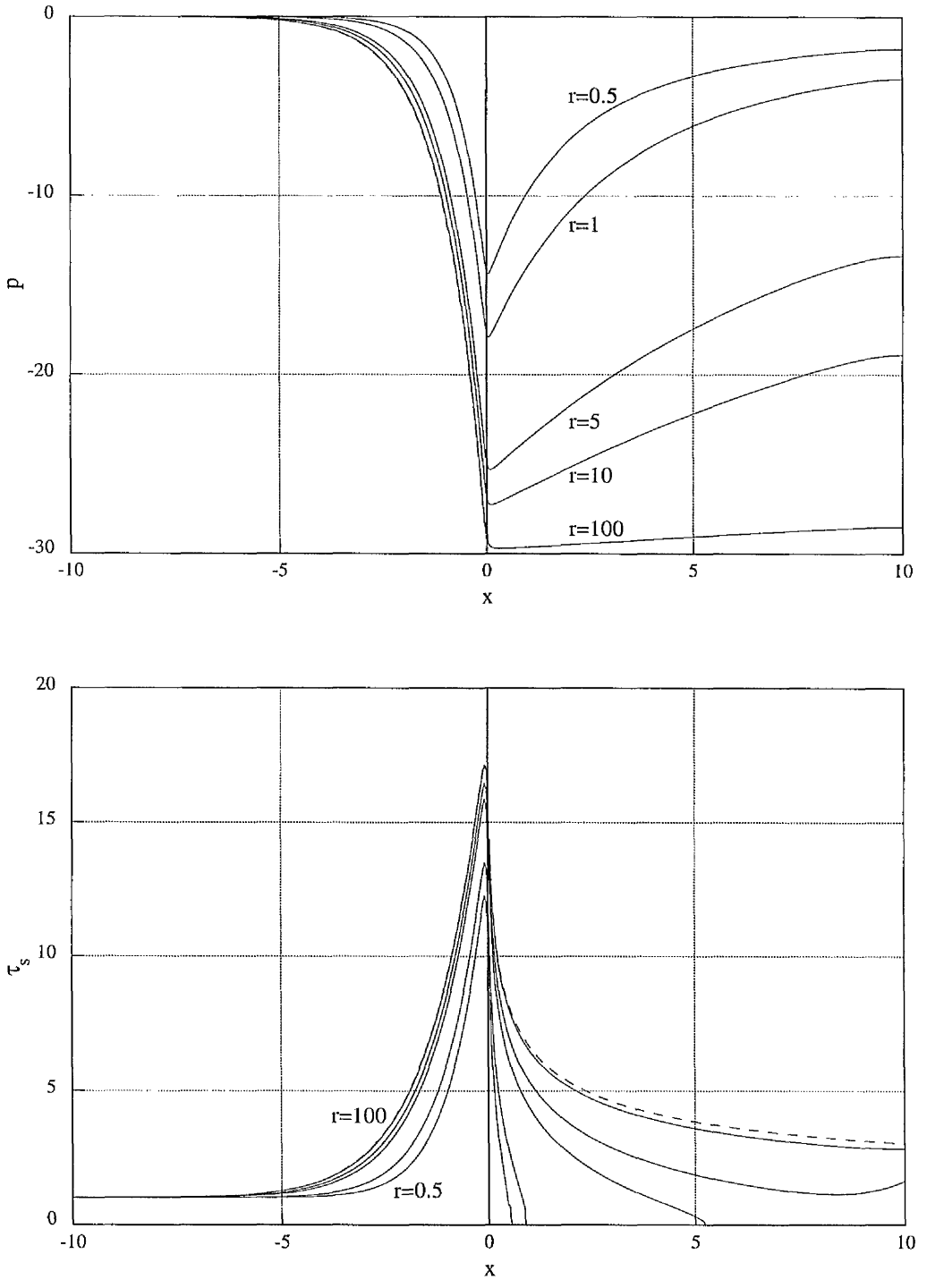

Figure 6.9: Pressure p and skin friction τ_s distributions for various body radii r (AXI, subcritical case, $\beta = -30$). Dashed curve (- - -) represents the 2D case (i.e. $r = \infty$).

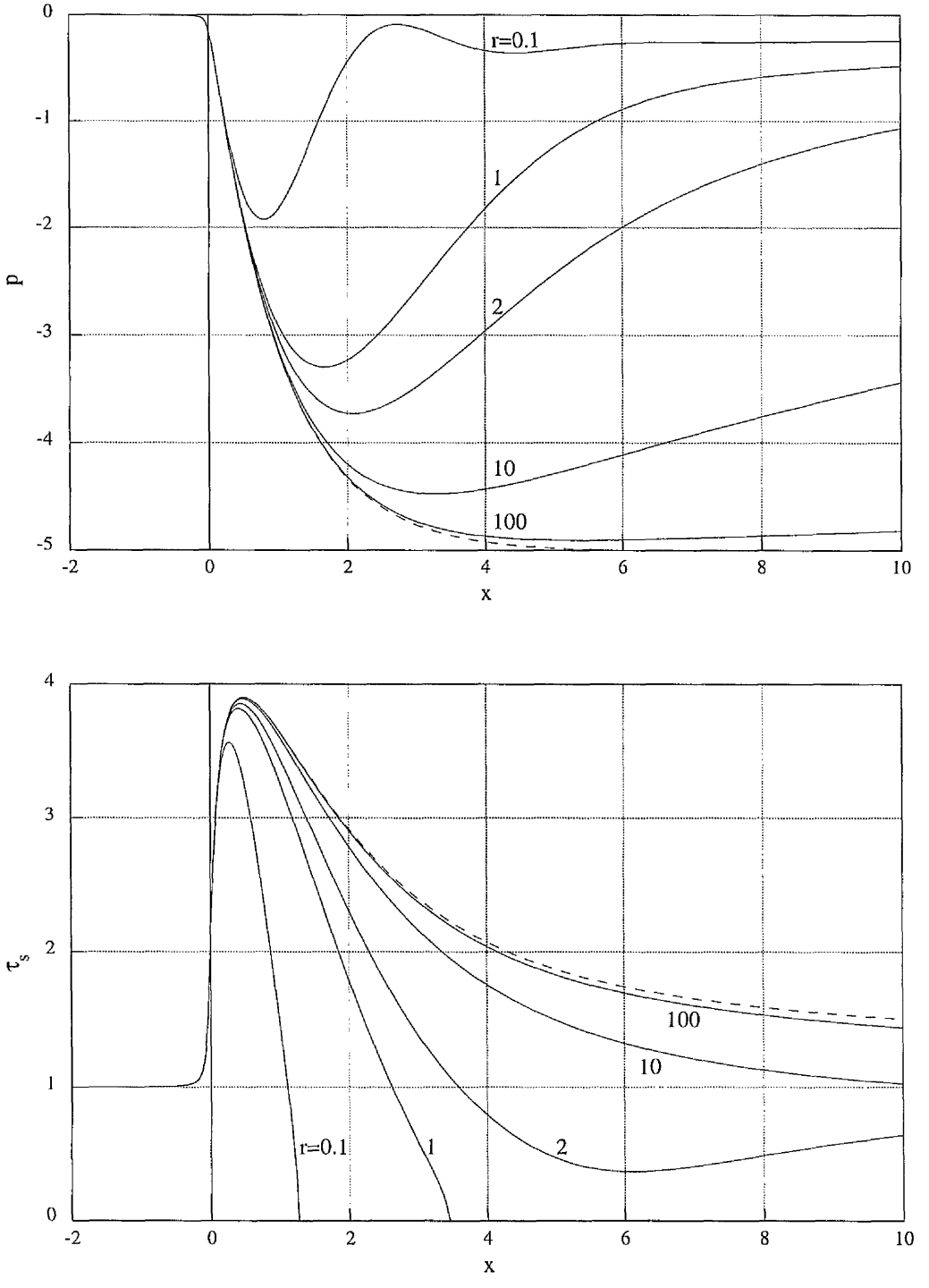

Figure 6.10: Pressure p and skin friction τ_s distributions for various body radii r (AXI, supercritical case, $\beta = -5$). Dashed curve (- - -) represents the 2D case (i.e. $r = \infty$).

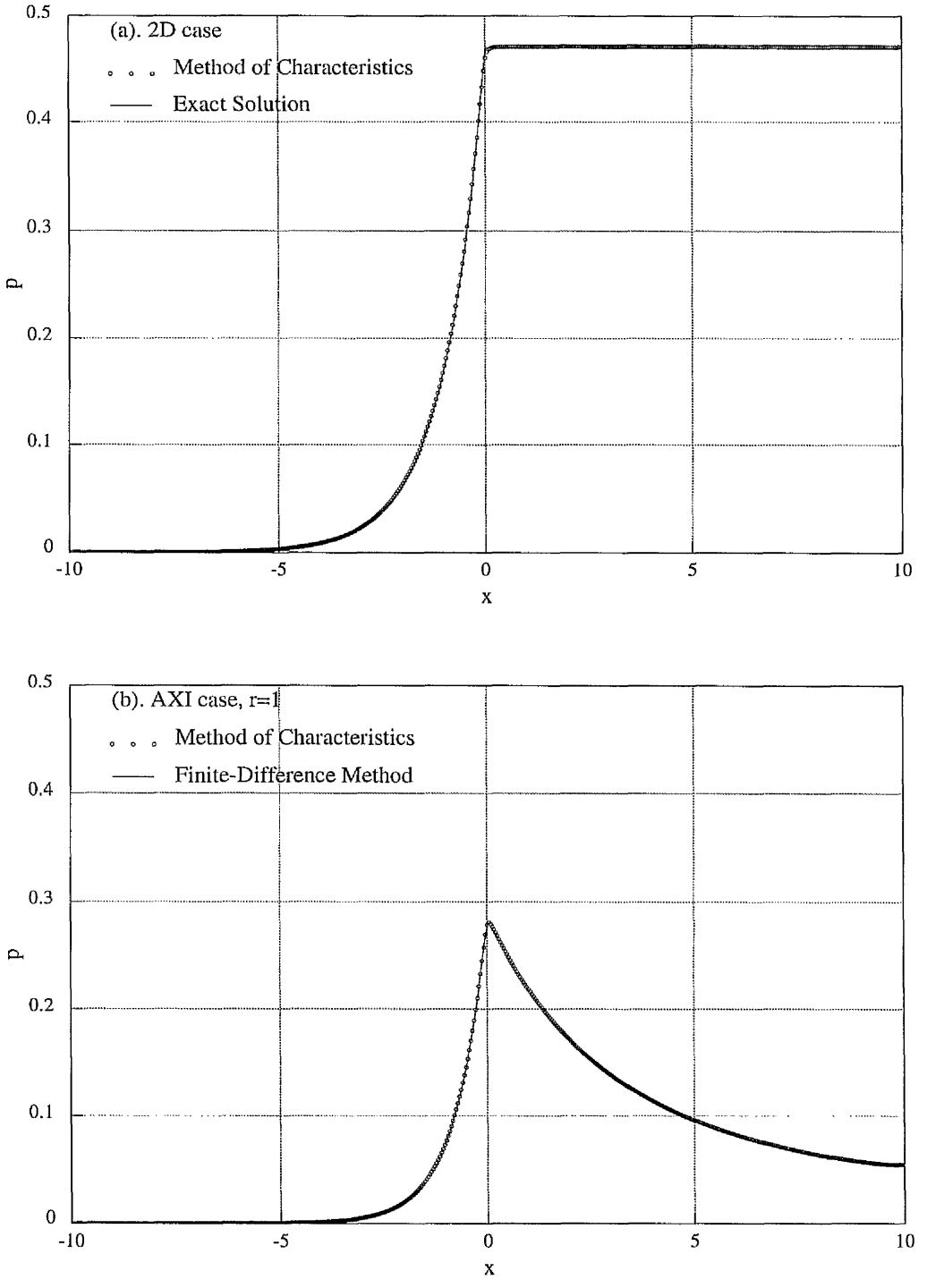

Figure 6.11: Comparison of the pressure distribution for the subcritical case with $\beta = 0.47$ obtained using the Method of Characteristics with: (a). the exact result (2D case); (b). result obtained using the finite-difference method (AXI case).

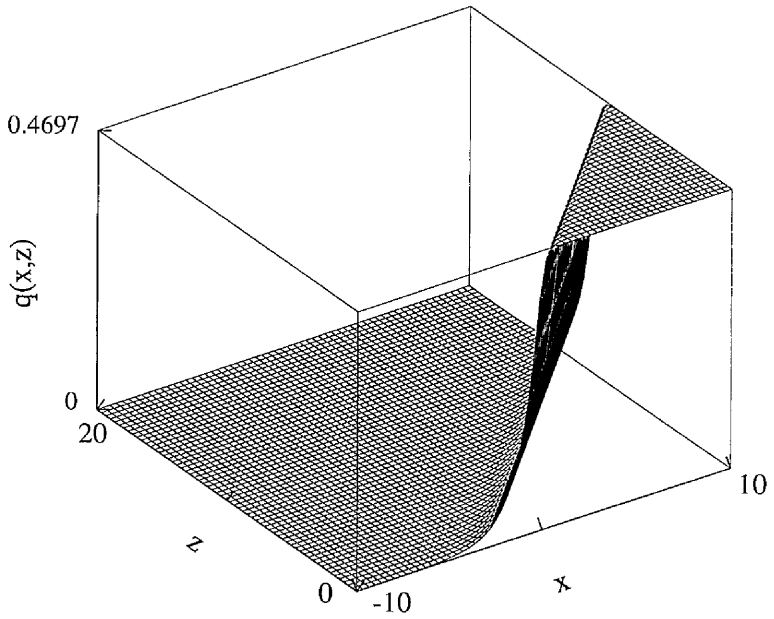

Figure 6.12: Pressure $q(x, z)$ obtained using the Method of Characteristics for the 2D subcritical flow with $\beta = 0.47$.

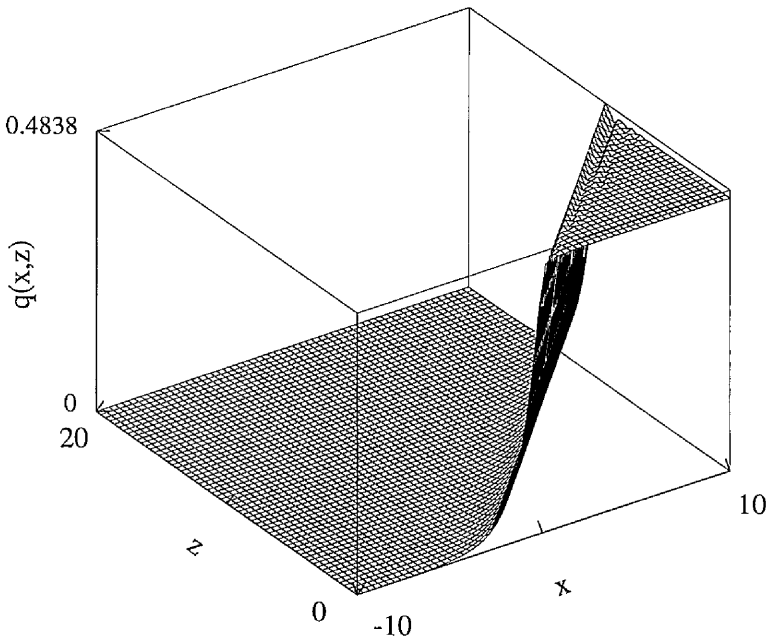

Figure 6.13: Pressure $q(x, z)$ obtained using the Finite-Difference method for the 2D subcritical flow with $\beta = 0.47$.

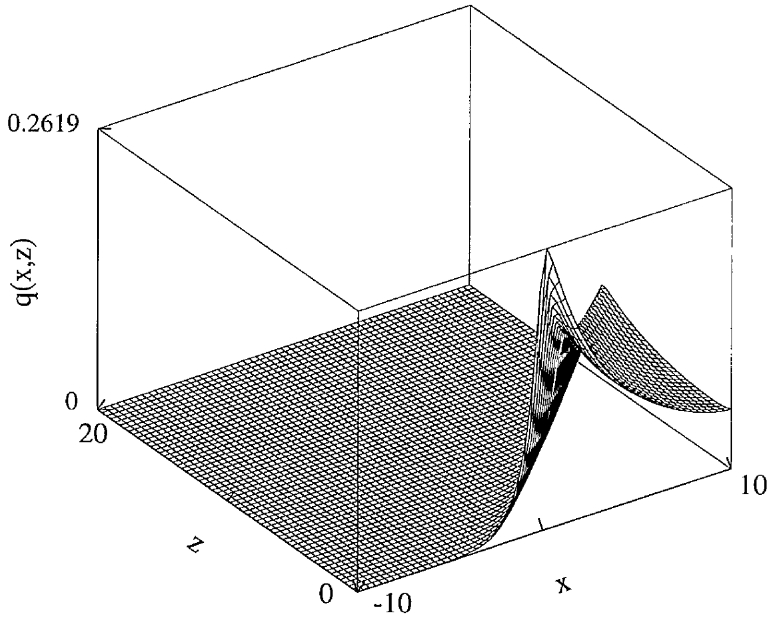

Figure 6.14: Pressure $q(x, z)$ obtained using the Method of Characteristics for the AXI subcritical flow with $\beta = 0.47$ and $r = 1$.

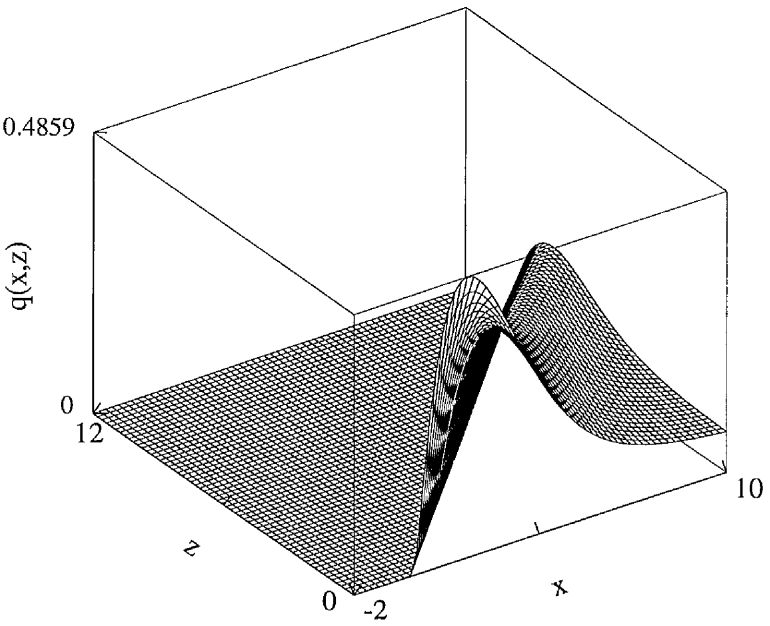

Figure 6.15: Pressure $q(x, z)$ obtained using the Method of Characteristics for the AXI supercritical flow with $\beta = 0.75$ and $r = 1$.

6.5 Asymptotic Solution for Subcritical Flows

6.5.1 Upstream solution

It can be easily shown using the momentum equation (5.33) that the solution for the streamfunction near to the surface can be expressed in the form of a Taylor series expansion as follows:

$$\psi_0(x,y) = \frac{1}{2}\tau_s(x)y^2 + \frac{1}{6}\frac{\mathrm{d}p_0}{\mathrm{d}x}y^3 + \cdots, \tag{6.39}$$

where $\tau_s(x)$ is the skin friction distribution defined by Eq. (6.37). Furthermore, by defining

$$\lambda_0 = \left(\frac{\mathrm{d}p_0}{\mathrm{d}x}\right)_{x\to 0-}, \quad \nu_0 = \left(\frac{\mathrm{d}p_0}{\mathrm{d}x}\right)_{x\to 0+}, \tag{6.40}$$

the asymptotic solution immediately upstream of the corner can be written in the form

$$\psi_0 = \frac{1}{2}\tau_0 y^2 + \frac{1}{6}\lambda_0 y^3 + \cdots \quad \text{as} \quad x \to 0^-, \tag{6.41}$$

where $\tau_0 = \tau_s(0)$. For 2D flows with subcritical wall cooling, it follows from Eq. (5.42) that $\lambda_0 = \beta_0$ and $\nu_0 = 0$. This appears to suggest a discontinuous behaviour of the streamfunction at $x = 0$, which is clearly a physical impossibility. This paradox can be explained by seeking a solution downstream of the ramp corner in the form of an eigen-function, as will now be described.

6.5.2 Downstream solution for non-separated cases

If the minimum τ_0 in the wall shear stress is $O(1)$, it follows from Eq. (6.41) that the longitudinal velocity $u_0 = \partial\psi_0/\partial y$ is approximately linear as y becomes small. Consequently it can be inferred from the momentum equation that a new near wall sublayer of thickness $y \sim x^{1/3}$ should be considered. This suggests that

the solution for ψ_0 immediately downstream has the following asymptotic form:

$$\psi_0(x,y) = \frac{1}{2}\tau_0^{1/3}\eta^2 x^{2/3} + \lambda_0\tau_0^{-1}xh(\eta) + \cdots \quad \text{as} \quad x \to 0^+, \tag{6.42}$$

where η is an $O(1)$ similarity variable in the near-wall sublayer defined by

$$\eta = \tau_0^{1/3}\frac{y}{x^{1/3}}. \tag{6.43}$$

An affine transformation has been incorporated into these equations such that the resulting equation for $h(\eta)$ is independent of λ_0, ν_0 and τ_0. Upon substitution of the above equations into the leading-order momentum equation (5.33), and taking the limit as $x \to 0^+$, the following ordinary differential equation can be derived:

$$h''' + \frac{1}{3}\eta^2 h'' - \eta h' + h = \omega. \tag{6.44}$$

The parameter ω characterizes the intensity of the axially-symmetric effects and is defined by

$$\omega = \frac{\nu_0}{\lambda_0}. \tag{6.45}$$

It should be noted from Eq. (5.42) that the pressure gradient immediately downstream of the corner $\nu_0 = 0$ for 2D flows with subcritical wall cooling, which implies that $\omega = 0$. However, it is clear from the numerical results shown in Figs. 6.5 and 6.6 that ν_0 is non-zero for the AXI case. The appropriate boundary conditions are given by:

$$h(0) = h'(0) = 0, \quad h'''(\infty) = 1. \tag{6.46}$$

The latter condition follows from the upstream asymptotic solution given by Eq. (6.41), and also from the condition that the streamfunction ψ_0 should be continuous at $x = 0$. It follows from Eq. (6.42) that the wall shear stress distribution immediately downstream of the corner point is given by:

$$\tau_s(x) = \tau_0 + \lambda_0\tau_0^{-1/3}h''(0)x^{1/3} + \cdots \quad \text{as} \quad x \to 0^+. \tag{6.47}$$

The quantity $h''(0)$ can be determined from a numerical solution of Eqs. (6.44)–(6.46), which were solved using the global finite-difference method described in Appendix A.2. The condition $h'''(\infty) = 1$ was approximated using a second-order accurate backward difference quotient, i.e.

$$\left(\frac{\mathrm{d}^2 k}{\mathrm{d}\eta^2}\right)_{\eta\to\infty} = 1 \approx \frac{-k_{N-3} + 4k_{N-2} - 5k_{N-1} + 2k_N}{(\Delta\eta)^2}, \tag{6.48}$$

where $k = h'$ and N is the number of mesh points. It should be noted that this requires two preliminary Gaussian eliminations to eliminate the two extra off-diagonal elements in the Jacobian matrix (see Appendix A.2).

A uniform grid defined by $\eta_i = (i-1)\Delta\eta$ was employed, where $\Delta\eta$ was taken as 0.01. The maximum value of η was taken as 20 and the tolerance level $\epsilon = 10^{-7}$. The numerical solution for the 2D case (i.e. $\omega = 0$) yields $h''(0) = 1.536$ (accurate to three decimal places).

6.5.3 Downstream solution for incipient separation

If the ramp angle is close to the critical value β_0^* for which separation first occurs (which is also referred to as *incipient* separation), it follows from Eq. (6.41) that the asymptotic behaviour of the streamfunction immediately upstream of the corner point is given by:

$$\psi_0 = \frac{1}{6}\lambda_0 y^3 + \cdots \quad \text{as} \quad x \to 0^-. \tag{6.49}$$

Using this result, it follows from the momentum equation that the thickness of the near-wall sublayer $y \sim x^{1/4}$. This suggests that the solution immediately downstream should be expressed in the form

$$\psi_0(x,y) = \lambda_0^{1/4} x^{3/4} g(\zeta) + \cdots \quad \text{as} \quad x \to 0^+, \tag{6.50}$$

where ζ is an $O(1)$ similarity variable in the near-wall sublayer defined by:

$$\zeta = \lambda_0^{1/4} \frac{y}{x^{1/4}}, \tag{6.51}$$

and once again an affine transformation has been incorporated. Following a procedure similar to that used above, it can be shown that $g(\zeta)$ satisfies the following nonlinear differential equation:

$$4g''' - 2(g')^2 + 3gg'' = 4\omega, \tag{6.52}$$

along with the boundary conditions

$$g(0) = g'(0) = 0, \quad g'''(\infty) = 1. \tag{6.53}$$

This nonlinear equation was solved using the same numerical procedure used before, and the solution for $\omega = 0$ yields $g''(0) = 2.009$ (correct to three decimal places). Furthermore, the wall shear stress distribution immediately downstream of the corner point is given by

$$\tau_s(x) = \lambda_0^{3/4} g''(0) x^{1/4} + \cdots \quad \text{as} \quad x \to 0^+. \tag{6.54}$$

Figure 6.16 compares the skin friction for 2D flows obtained using the three-level finite-difference method described in Sec. 6.3 with the asymptotic results given by Eqs. (6.47) and (6.54). It is evident that the numerical solution exhibits the correct asymptotic behaviour as $x \to 0^+$, thus confirming the sharp behaviour of τ_s immediately downstream of the ramp.

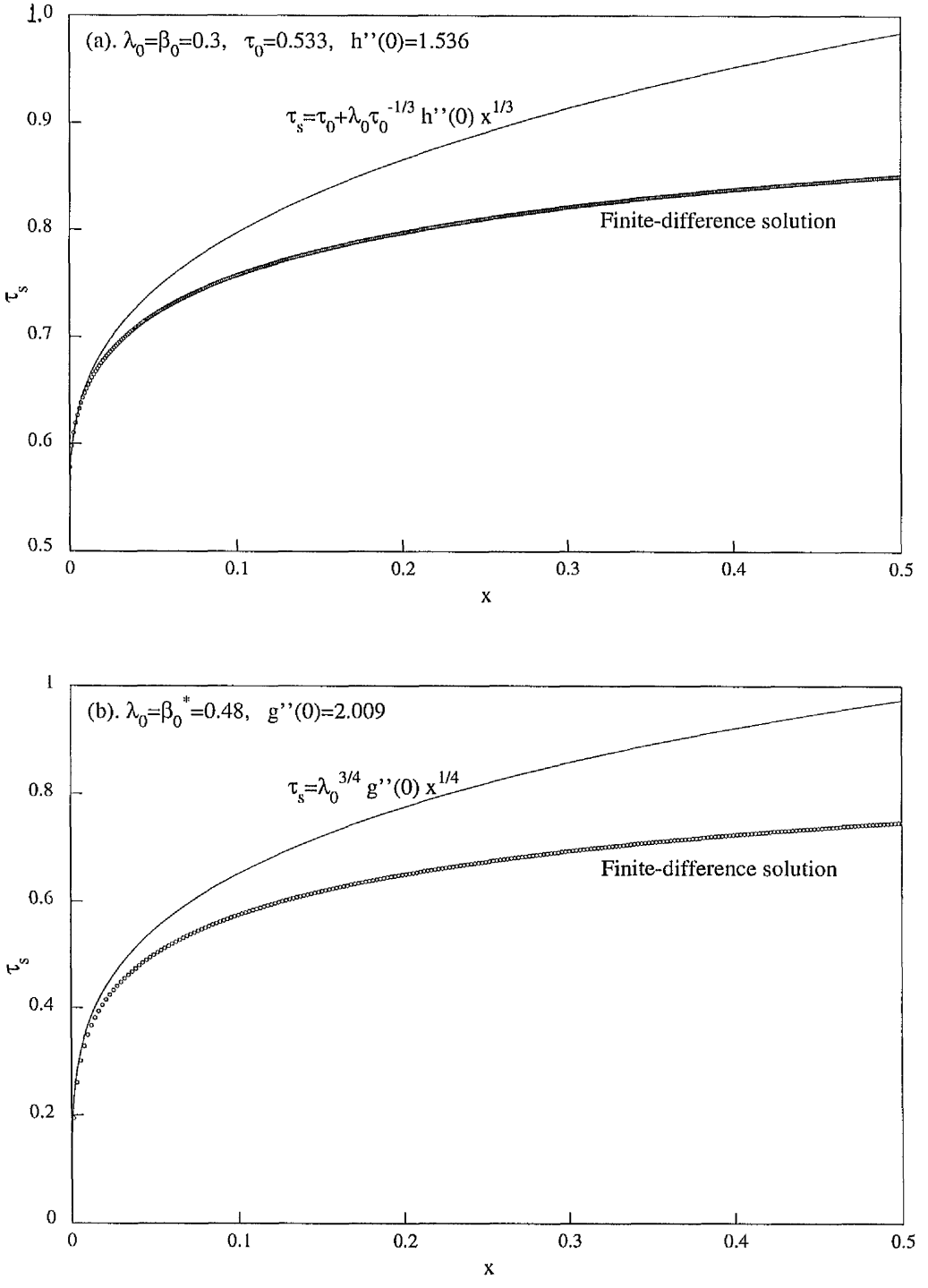

Figure 6.16: Asymptotic behaviour of the skin friction τ_s immediately downstream of the ramp (2D, subcritical case).

Chapter 7

Subcritical Flows with Separation

7.1 Introduction

It is clear from the results of the previous chapter that flow separation occurs once the scaled ramp angle exceeds a certain critical value β_0^*, which is itself dependent on the body radius. Solutions exhibiting comparatively large regions of reversed flow have been obtained by Brown *et al.* (1990) and Cassel *et al.* (1996) for 2D flows with moderate supercritical wall cooling (i.e. Ne $\sim$ 1 and $\mathcal{L} < 0$). These results indicate that the size of the separation region becomes smaller as the temperature factor decreases – or equivalently as the Neiland number increases – and that strong wall cooling can ultimately inhibit separation altogether.

This chapter will primarily focus on the separation phenomenon occurring in 2D hypersonic flows over compression ramps with strong subcritical wall cooling. It is rather surprising that no solutions of the triple-deck equations (5.8)–(5.10) and (5.39) containing reversed flow regions have so far been obtained for this case, which is believed to be due to the de-stabilizing effect of subcritical wall cooling (see Cassel *et al.* 1996).

The present problem for the lower viscous sublayer is similar to that considered by Smith & Daniels (1981) in their study of the incompressible boundary

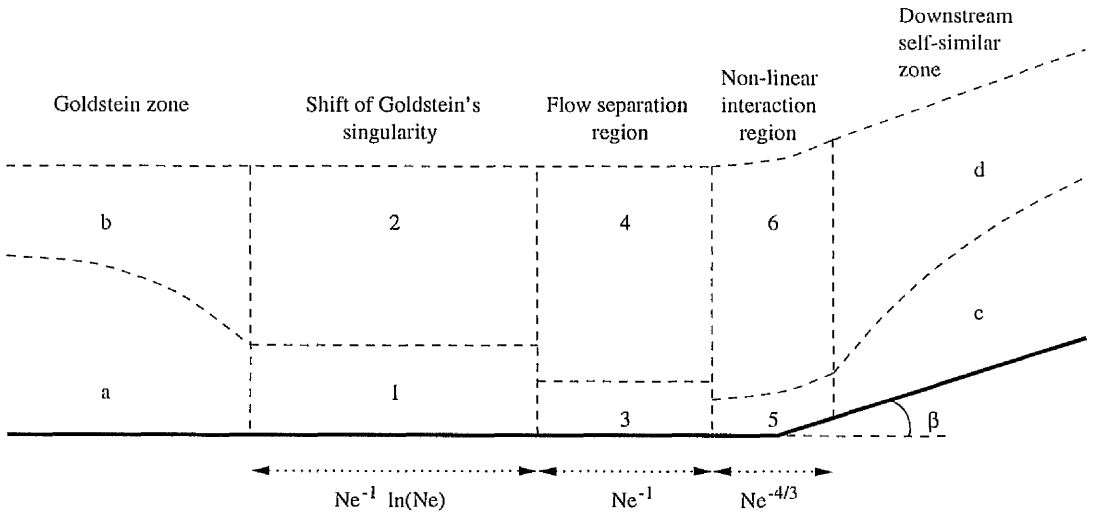

Figure 7.1: Schematic of the multi-layer structure in the sublayer near the ramp corner where the flow separates (not to scale).

layer flow over a small hump on a wall. In particular, it was shown that the Goldstein (1948) singularity, which shall be described in Sec. 7.2, can be removed through consideration of a series of regions having successively shorter streamwise length-scales, thereby permitting a smooth transition into a separated region downstream of the hump (see Fig. 7.1).

Regions 1 and 2 simply serve to shift the singularity downstream to a certain streamwise location $\tilde{X}_0$. The flow within regions 3 and 4 is governed by an integro-differential equation, and its numerical solution shows that the flow can pass smoothly through separation. However the solution then terminates at a subsequent location $\bar{X}_0$, where a more severe singularity develops. This behaviour indicates a strengthening of the reversed flow, and that another nonlinear region (labelled regions 5 and 6 in Fig. 7.1), centered on $\bar{X}_0$, is required to remove the singularity.

The scalings and nature of the solution in regions 1–4 have been described in

detail by Smith & Daniels (1981) for the incompressible case, and later by Kerimbekov *et al.* (1994) for subcritical hypersonic flows with separation well upstream of the ramp corner. The purpose of the present study is to extend this work to consider the flow separation and reattachment regions near the compression corner for ramp angles close to the critical value β_0^* for which separation first occurs, i.e.

$$\beta = \beta_0^* + \mathrm{Ne}^{-4/3}\,\beta_2 + \cdots . \tag{7.1}$$

The numerical results of Chapter 6 suggest that $\beta_0^* = 0.48$ for 2D flows with subcritical wall cooling, and that this critical value increases as the radius decreases for the AXI case.

In Sec. 7.3, the equations governing the flow in the inner interaction regions 5 and 6 shall be derived, and their subsequent numerical solution and asymptotic behaviours shall be obtained in Secs. 7.3–7.7. The asymptotic solution in regions c and d downstream of the ramp corner shall also be determined in Sec. 7.5, and it shall be deduced that the reattachment point lies well within the nonlinear region 5. It will also be shown in Sec. 7.8 that the separation process on AXI bodies within the inner interaction region 5 reduces to the 2D case. A similar situation occurs for AXI flows with marginal separation, as will be shown in Appendix C.

7.2 Goldstein's Singularity

7.2.1 Leading-order terms

The structure of the solution ahead of a point of zero skin friction x_s, where separation first occurs, was first investigated by Landau & Lifschitz (1944) and Goldstein (1948). Immediately upstream of x_s, it was shown that the boundary layer splits into two parts (labelled regions a and b in Fig. 7.1). It can be inferred from the momentum equation that the transverse coordinate y which is

$O((-s)^{1/4})$ in region a, where $s = x - x_s$. In addition, the asymptotic expansion in Eq. (6.49) can be continued in the following form (see, for example, Sychev *et al.* 1998):

$$\psi_0(x,y) = \frac{1}{6}\lambda_0(-s)^{3/4}\eta^3 + \frac{1}{2}a_0(-s)\eta^2 + \frac{1}{2}(-s)^{5/4}\left(a_1\eta^2 - \frac{a_0^2\eta^5}{120}\right) + \cdots \quad \text{as} \quad s \to 0^-, \quad (7.2)$$

where the constant λ_0 is the pressure gradient upstream of the separation point, and η is an $O(1)$ similarity variable in this region defined by:

$$\eta = \frac{y}{(-s)^{1/4}}. \quad (7.3)$$

The constants a_0 and a_1 can, in principle, be found through a numerical solution of the full leading-order problem given by Eqs. (5.33)–(5.35). It follows from this solution that the skin friction distribution immediately upstream of x_s develops a parabolic profile as given by Eq. (1.19). An important consequence of this singular behaviour is that the solution cannot be continued downstream of x_s if the pressure gradient is prescribed in advance.

It can be inferred from the foregoing equations that the asymptotic solution as $s \to 0^-$ in the quasi-inviscid region b can be expressed in the following form (see also Kerimbekov *et al.* 1994):

$$\psi_0(x,y) = \Phi_0(y) + a_0\lambda_0^{-1}(-s)^{1/2}\Phi_0'(y) + a_1\lambda_0^{-1}(-s)^{3/4}\Phi_0'(y) + \cdots \quad \text{as} \quad s \to 0^-. \quad (7.4)$$

The leading-order streamfunction $\Phi_0(y)$ must satisfy

$$\Phi_0(y) = \frac{1}{6}\lambda_0 y^3 - \frac{a_0^2}{240}y^5 + \cdots, \quad \text{as} \quad y \to 0 \quad (7.5)$$

in order to match with the solution (7.2) in region a. Matching at the outer edge of region b also requires that

$$\Phi_0(y) \to \frac{1}{2}y^2 + A_0(x_s)y + \cdots \quad \text{as} \quad y \to \infty, \quad (7.6)$$

where $A_0(x_s)$ can, in principle, be found from a global numerical solution.

The displacement function upstream of x_s can be determined by a comparison of Eqs. (5.35c), (7.4) and (7.6), from which it can be shown that:

$$A_0(x) = A_0(x_s) + a_0\lambda_0^{-1}(-s)^{1/2} + a_1\lambda_0^{-1}(-s)^{3/4} + \cdots \quad \text{as} \quad s \to 0^-. \tag{7.7}$$

This implies that the slope of the streamlines θ_0 at the external edge of the viscous sublayer is given by:

$$\theta_0(x) = -\frac{\mathrm{d}A_0}{\mathrm{d}s} = -\frac{a_0}{2}\lambda_0^{-1}(-s)^{-1/2} - \frac{3a_1}{4}\lambda_0^{-1}(-s)^{-1/4} + \cdots \quad \text{as} \quad s \to 0^-. \tag{7.8}$$

Hence as $s \to 0^-$, the slope of streamlines becomes very large in magnitude. This provokes the formation of an additional inner interaction region centred on $x = x_s$, where the contribution of the sublayer to the displacement thickness can not be neglected. A preliminary estimate of the streamwise extent Δx of this inner region can be obtained by a comparison of the $\mathrm{Ne}^{-1}\,A'(x)$ term in the original interaction law given by Eq. (5.40) with the pressure term on the left-hand side yielding

$$\Delta x \sim \mathrm{Ne}^{-2}, \tag{7.9}$$

which is very small indeed for large Neiland numbers. However, it will later be shown in Sec. 7.5 that Eq. (7.9) underestimates the true extent of the inner interaction region (cf. Eq. (7.73)), since it does not take into consideration the solution downstream of the separation point.

7.2.2 Higher-order terms

It follows from Eq. (5.31) and the 2D interaction law given by Eq. (5.40) that p_1 satisfies the equation:

$$p_1 = \frac{\mathrm{d}p_1}{\mathrm{d}x} - \frac{\mathrm{d}A_0}{\mathrm{d}x}. \tag{7.10}$$

Since the distribution of $A_0(x)$ immediately upstream of x_s is given by Eq. (7.7), Eq. (7.10) can be solved yielding the following asymptotic behaviour for p_1:

$$p_1(x) = p_1(x_s) - a_0\lambda_0^{-1}(-s)^{1/2} + \cdots, \quad \text{as} \quad s \to 0^-. \tag{7.11}$$

The asymptotic solution for the next-order term ψ_1 was given by Smith & Daniels (1981):

$$\psi_1(x,y) = \ln(-s)^{1/4}h_1(\eta) + h_2(\eta) + (-s)^{1/4}\ln(-s)^{1/4}h_3(\eta) + (-s)^{1/4}h_4(\eta) + \cdots \quad \text{as} \quad s \to 0^-, \tag{7.12}$$

where the functions $h_i(\eta)$ satisfy the boundary conditions:

$$h_i(0) = h_i'(0) = 0 \quad \text{for} \quad i = 1, \ldots, 4. \tag{7.13}$$

The solutions for h_1, h_2 and h_3 are given by:

$$h_i(\eta) = \frac{1}{2}b_i\eta^2 \quad \text{for} \quad i = 1,\ 2,\ 3, \tag{7.14}$$

where b_i are constants. The equation for $h_4(\eta)$ is given by:

$$h_4''' - \frac{1}{8}\lambda_0\eta^3 h_4'' + \frac{1}{4}\lambda_0\eta^2 h_4' - \frac{1}{4}\lambda_0\eta h_4 = -\frac{a_0}{2\lambda_0} - \frac{a_0\, b_1}{8}\eta^2. \tag{7.15}$$

By making the substitution $k = \eta h_4$, Smith & Daniels (1981) were able to obtain an analytic solution of this equation which is not exponentially large as $\eta \to \infty$ provided that

$$b_1 = \mu\lambda_0^{-1/2}, \tag{7.16}$$

where

$$\mu = -\frac{1}{\sqrt{2}}\frac{\Gamma(3/4)}{\Gamma(5/4)} \approx -0.9560. \tag{7.17}$$

Equation (7.12) suggests that in region b

$$\psi_1(x,y) = \left\{\frac{b_1}{4}\ln(-s) + b_2 + \frac{b_3}{4}(-s)^{1/4}\ln(-s) + b_4(-s)^{1/4}\right\} \times \lambda_0^{-1}(-s)^{-1/2}\Phi_0'(y) + \cdots \quad \text{as} \quad s \to 0^-. \tag{7.18}$$

It can be inferred from Eqs. (5.31) and (5.40) that for 2D subcritical flows, p_2 is given by:

$$p_2(x) = \begin{cases} \beta_2 \, \mathrm{e}^x, & x \leq 0, \\ \beta_2, & x > 0. \end{cases} \tag{7.19}$$

The solution for ψ_2 in region a was sought in the following asymptotic form:

$$\psi_2(x,y) = (-s)^m f_1(\eta) + (-s)^{m+1/4} f_2(\eta) + \cdots \quad \text{as} \quad s \to 0^-, \tag{7.20}$$

where m is an unknown constant to be determined as part of the solution and the functions f_i satisfy $f_i(0) = f_i'(0) = 0$ for $i = 1$ and 2. Upon substitution of this expansion into Eq. (5.36), it can be shown that the only non-trivial solution which does not exhibit exponential growth as $\eta \to \infty$ occurs when $m = 0$, in which case

$$f_i(\eta) = \frac{1}{2} c_i \eta^2 \quad \text{for} \quad i = 1, \ 2, \tag{7.21}$$

where c_i are arbitrary constants. Hence the solution for ψ_2 in region a can be expressed as

$$\psi_2(x,y) = \frac{1}{2}\eta^2 \left\{ c_1 + c_2(-s)^{1/4} \right\} + \cdots \quad \text{as} \quad s \to 0^-. \tag{7.22}$$

This solution suggests the following expansion in region b:

$$\psi_2(x,y) = \Phi_2(y)(-s)^{-1/2} + \cdots \quad \text{as} \quad s \to 0^-, \tag{7.23}$$

where

$$\Phi_2(y) \to \frac{1}{2} c_1 y^2 + \cdots \quad \text{as} \quad y \to 0. \tag{7.24}$$

By making use of Eqs. (5.42), (7.11) and (7.19), the asymptotic behaviour of the pressure immediately upstream of x_s is given by:

$$p(x) = \lambda_0 + \lambda_0 s + \mathrm{Ne}^{-1} \left\{ p_1(x_s) - a_0 \lambda_0^{-1} (-s)^{1/2} \right\} + \mathrm{Ne}^{-4/3} \left\{ \beta_2 + \beta_2 s \right\} + \cdots, \quad \text{as} \quad s \to 0^-. \tag{7.25}$$

7.3 The Inner Interaction Region

7.3.1 Upper region 6

It can be shown that the solution for the pressure, displacement and streamfunction in the upper region 6 can be expressed in the following asymptotic form:

$$\begin{aligned} p(x) =& p_0(x_s) + (\mathrm{Ne}^{-1}\ln \mathrm{Ne})\lambda_0 \tilde{X}_0 \\ &+ \mathrm{Ne}^{-1}\{p_1(x_s) + \lambda_0 \bar{X}_0\} + \mathrm{Ne}^{-4/3}\,\lambda_0^{-2/3} P(X) + \cdots, \end{aligned} \tag{7.26a}$$

$$A(x) = A_0(x_s) + \mathrm{Ne}^{-1/3}\,\lambda_0^{-2/3} B(X) + \cdots, \tag{7.26b}$$

$$\psi(x,y) = \Phi_0(y) + \lambda_0^{-2/3}\,\mathrm{Ne}^{-1/3}\,B(X)\Phi_0'(y) + \cdots, \tag{7.26c}$$

where X is a new streamwise variable defined by:

$$x = x_s + (\mathrm{Ne}^{-1}\ln \mathrm{Ne})\tilde{X}_0 + \mathrm{Ne}^{-1}\,\bar{X}_0 + \lambda_0^{-5/3}\,\mathrm{Ne}^{-4/3}\,X. \tag{7.27}$$

Matching with the solution in region 4 obtained by Kerimbekov *et al.* (1994) requires that:

$$\left.\begin{aligned} P(X) &\to X + \mu(-X)^{-1/2} + \cdots \\ B(X) &\to \mu(-X)^{-1/2} + \cdots \end{aligned}\right\} \quad \text{as} \quad X \to -\infty, \tag{7.28}$$

where the constant μ was defined by Eq. (7.17).

Upon substitution of Eqs. (7.26a–b) into the pressure-displacement relation given by Eq. (5.40), and making use of the above upstream boundary conditions, it follows that the interaction law in the inner region takes the following form:

$$\frac{\mathrm{d}P}{\mathrm{d}X} = \frac{\mathrm{d}B}{\mathrm{d}X} - \frac{\mathrm{d}F}{\mathrm{d}X} + 1. \tag{7.29}$$

Since $\lambda_0 = \beta_0$ (to leading-order) in the interaction region, the scaled surface geometry $f(x) = \mathrm{Ne}^{-4/3}\,\lambda_0^{-4/3} F(X)$ is given by

$$F(X) = \begin{cases} 0, & X \le 0, \\ X, & X > 0. \end{cases} \tag{7.30}$$

JOHN RYLANDS
UNIVERSITY
LIBRARY OF
MANCHESTER

In addition, it can be inferred that the slope of the streamlines θ at the external edge of region 6 is given by:

$$\theta(x) = -\frac{\mathrm{d}A}{\mathrm{d}x} = -\lambda_0 \,\mathrm{Ne}\, \frac{\mathrm{d}B}{\mathrm{d}X}. \tag{7.31}$$

This result can also be determined from the fact that

$$\theta(x) = \frac{v}{u} = -\frac{\psi_x}{\psi_y}, \tag{7.32}$$

and it can be easily verified that the slope of the streamlines throughout region 6 remains constant and equal to that given by Eq. (7.31).

7.3.2 Lower region 5

The solution in the nonlinear reattachment region 5 can be expressed in the following form:

$$\psi(x,y) = \lambda_0^{-1}\,\mathrm{Ne}^{-1}\,\Psi(X,Y), \tag{7.33}$$

where Y is a scaled transverse variable defined by:

$$y = \lambda_0^{-2/3}\,\mathrm{Ne}^{-1/3}\,Y. \tag{7.34}$$

Hence, it follows that the inner interaction problem is now defined by:

$$\frac{\partial\Psi}{\partial Y}\frac{\partial^2\Psi}{\partial X\partial Y} - \frac{\partial\Psi}{\partial X}\frac{\partial^2\Psi}{\partial Y^2} = -\frac{\mathrm{d}P}{\mathrm{d}X} + \frac{\partial^3\Psi}{\partial Y^3}, \tag{7.35}$$

along with the no-slip conditions at the body surface:

$$\Psi = \frac{\partial\Psi}{\partial Y} = 0 \quad \text{at} \quad Y = 0. \tag{7.36}$$

The upstream boundary condition for Ψ is determined by asymptotically matching with the solution in region 3 obtained by Kerimbekov *et al.* (1994) yielding:[1]

$$\Psi \to \frac{1}{6}Y^3 + \frac{1}{2}\mu(-X)^{-1/2}Y^2 + \cdots \quad \text{as} \quad X \to -\infty. \tag{7.37}$$

[1]Eqs. (7.28) and (7.37) correct mathematical errors in Kerimbekov *et al.* (1994).

It should be noted that in view of Eqs. (5.31) and (7.33), the third-order term given by Eq. (7.22) does not influence the solution in the inner interaction region. Matching with the solution (7.26c) in region 6 yields the following condition:

$$\Psi \to \frac{1}{6}Y^3 + \frac{1}{2}B(X)Y^2 + \cdots \quad \text{as} \quad Y \to \infty. \tag{7.38}$$

Furthermore, it can be shown using Eq. (7.32) that the distribution of θ in region 5 is given by:

$$\theta(x) = -\lambda_0 \,\mathrm{Ne}\, \frac{\Psi_X}{\Psi_Y}. \tag{7.39}$$

Matching with Eq. (7.31), which is valid at the outer edge of region 5, shows that

$$\frac{\partial \Psi}{\partial X} = \frac{\mathrm{d}B}{\mathrm{d}X}\frac{\partial \Psi}{\partial Y} \quad \text{as} \quad Y \to \infty, \tag{7.40}$$

and it can be confirmed that this expression is consistent with the boundary condition (7.38) for large Y. It should be emphasized that the affine transformations employed in this chapter render the inner interaction problem completely independent of both the critical ramp angle β_0^* and the pressure gradient λ_0 immediately upstream of the ramp corner.

Smith & Daniels (1981) obtained a numerical solution of a similar inner interaction problem for the incompressible boundary layer flow over a small hump on a wall, and found that a smooth solution exists for all X. However, their steady-state code eventually proved to be divergent at a certain streamwise location. Zhikharev (1993) obtained solutions of another interaction problem with marginal separation far upstream of the ramp corner where $F(X) \equiv 0$ (see also Appendix C). However, it should be emphasized that both of these solutions were obtained using boundary conditions different from those employed in the present study.

Before discussing the unsteady numerical algorithm for the solution of Eqs. (7.35)–(7.38), along with the interaction law (7.29), the asymptotic behaviour of this system of equations far upstream and downstream of the ramp corner shall first be determined.

7.4 Upstream Asymptotic Solution

7.4.1 Leading-order terms

The solution of the nonlinear inner interaction problem was sought in the following asymptotic form in the limit as $X \to -\infty$:

$$\Psi = \frac{1}{6}(-X)^{3/4}\eta^3 + (-X)^{\alpha} f_1(\eta) + (-X)^{2\alpha-3/4} f_2(\eta) + \cdots, \tag{7.41a}$$

$$P = X + c(-X)^{\gamma} + \cdots, \tag{7.41b}$$

$$B = c(-X)^{\gamma} + \cdots, \tag{7.41c}$$

where α, γ and c are constants to be determined and

$$\eta = \frac{Y}{(-X)^{1/4}} \tag{7.42}$$

is $O(1)$ in the inner interaction region. From the no-slip conditions (7.36) on the body surface, the required boundary conditions for f_1 are given by:

$$f_1(0) = f_1'(0) = 0. \tag{7.43}$$

Upon substitution of Eqs. (7.41a–c) into the system of Eqs. (7.29) and (7.35)–(7.38), it can be easily verified that the only non-trivial solution for f_1 satisfying the required boundary conditions is given by

$$f_1(\eta) = \frac{1}{2}a_1\eta^2, \tag{7.44}$$

where a_1 is an arbitrary constant. It should be noted that this solution is valid for any value of α. Moreover, since the pressure gradient is of the same order of magnitude as the convective and viscous terms, it can be inferred from the interaction law and Eq. (7.38) that

$$\gamma = \alpha - 1/2 \quad \text{and} \quad c = a_1. \tag{7.45}$$

7.4.2 Higher-order terms

It can be shown that f_2 satisfies the following equation:

$$f_2''' - \frac{1}{8}\eta^3 f_2'' + \left(\alpha - \frac{1}{4}\right)\eta^2 f_2' - \left(2\alpha - \frac{3}{4}\right)\eta f_2 = \frac{1}{4}(1-2\alpha)a_1^2\eta^2 + \frac{1}{2}a_1, \quad (7.46)$$

along with the no-slip boundary conditions:

$$f_2(0) = f_2'(0) = 0. \quad (7.47)$$

It is evident from Eqs. (7.41a–c) and (7.44) that in order to be consistent with the upstream boundary condition given by Eq. (7.37), it is required that

$$\alpha = 0 \quad \text{and} \quad a_1 = \mu \approx -0.9560, \quad (7.48)$$

where μ was defined by Eq. (7.17). The solution of Eqs. (7.46) and (7.47) for the case $\alpha = 0$, which has never been obtained before, is unique under the additional condition of absence of exponentially growing terms in the asymptotic expansion of the function $f_2(\eta)$ as $\eta \to \infty$. This condition occurs only if the second of the matching conditions (7.48) is satisfied.

In the present study, a novel technique shall be employed in order to solve Eqs. (7.46) and (7.47) with $\alpha = 0$ for both $f_2(\eta)$ and the constant a_1 (which will be assumed unknown), and in so doing it will be verified that $a_1 = \mu$. Therefore, this analysis will produce the required solution for f_2, and it will also confirm the validity of the upstream boundary condition (7.37), both of which are required for the subsequent numerical solution of the inner interaction problem.

The function f_2 was expressed in the form:

$$f_2(\eta) = \frac{1}{2}a_1\{a_1 s_1(\eta) + s_2(\eta)\}, \quad (7.49)$$

where the linearly independent solutions s_1 and s_2 satisfy the following equations:

$$s_1''' - \frac{1}{8}\eta^3 s_1'' - \frac{1}{4}\eta^2 s_1' + \frac{3}{4}\eta s_1 = \frac{1}{2}\eta^2, \quad (7.50)$$

$$s_2''' - \frac{1}{8}\eta^3 s_2'' - \frac{1}{4}\eta^2 s_2' + \frac{3}{4}\eta s_2 = 1, \quad (7.51)$$

subject to the initial conditions:

$$s_i(0) = 0, \quad s_i'(0) = \kappa_i, \quad s_i''(0) = 0 \qquad i = 1,\ 2. \tag{7.52}$$

The third condition follows from the observation that an arbitrary term of $O(\eta^2)$ can be added to any solution of Eqs. (7.50)–(7.51). The value of κ_i is determined from the requirement that the resulting solution for s_i must not exhibit exponential growth as $\eta \to \infty$.

From inspection, it can be deduced that the solution for the case $i = 1$ is given by:

$$s_1 = \eta \quad \text{and} \quad \kappa_1 = 1. \tag{7.53}$$

The solution for $s_2(\eta)$ was obtained numerically by integrating Eq. (7.51) using the predictor-corrector method described in Appendix A.1, starting from the initial conditions (7.52). In order to determine the value of κ_2 which does not result in exponential growth in s_2 as $\eta \to \infty$, it is important to consider first the asymptotic behaviour of Eq. (7.51) for large η. It can be verified that to leading-order:

$$s_2 \sim \frac{1}{2} b_2 \eta^2 + \frac{4}{3\eta} + \cdots \quad \text{as} \quad \eta \to \infty, \tag{7.54}$$

where the constant b_2 is to be determined. This suggests that κ_2 can be computed as a root of the equation:

$$\phi(\kappa_2) = s_2'''(\infty; \kappa_2) = 0, \tag{7.55}$$

which can be solved using either the Newton-Secant or Bisection method. The numerical solution for s_2 – which is shown in Fig. 7.2 – yields:

$$\kappa_2 \approx 0.9560 \quad \text{and} \quad b_2 \approx 1.312. \tag{7.56}$$

It is also evident that this solution exhibits the correct asymptotic behaviour for large η given by Eq. (7.54).

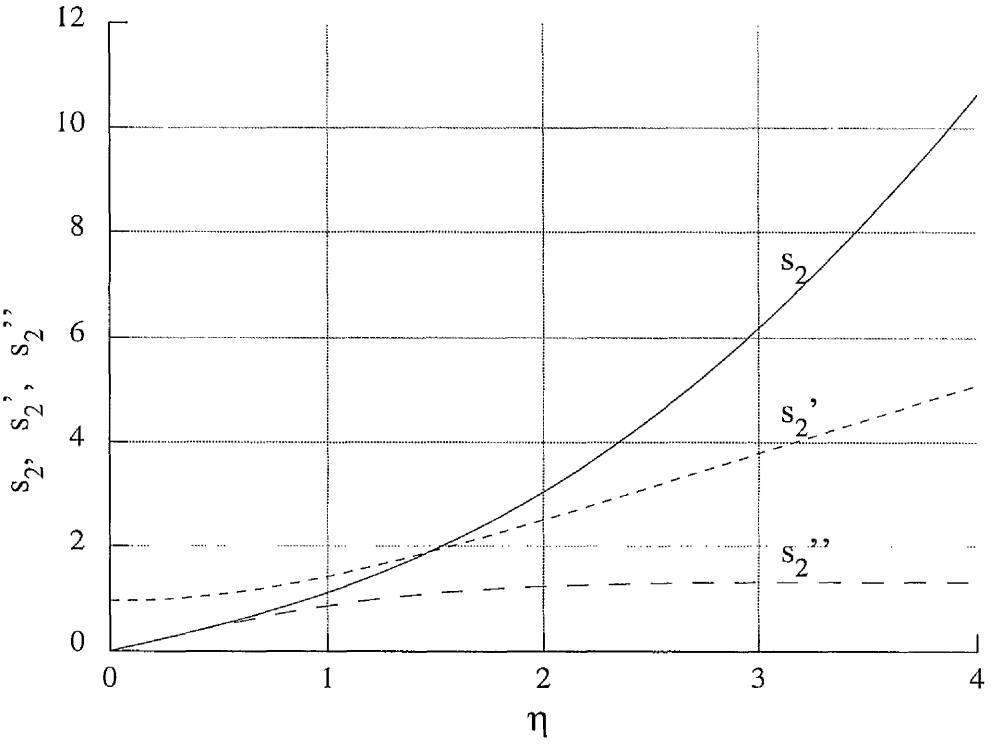

Figure 7.2: Numerical solution for $s_2(\eta)$, $s_2'(\eta)$ and $s_2''(\eta)$.

In addition, since $f_2'(0) = 0$, it follows from Eqs. (7.49), (7.53) and (7.56) that

$$a_1 = -\frac{s_2'(0)}{s_1'(0)} = -\frac{\kappa_2}{\kappa_1} \approx -0.9560, \tag{7.57}$$

which is in very good agreement with the expected result that a_1 must be equal to μ (cf. Eq. (7.48)). This confirms the analysis of Smith & Daniels (1981) for the higher-order streamfunction ψ_1 (see also Sec. 7.2.2). The numerical scheme employed here can also be used to solve Eq. (7.50), and the resulting numerical solution strongly confirms the analytic solution given by Eq. (7.53).

The above analysis yields the following asymptotic expansion for the stream-function as $X \to -\infty$:

$$\Psi = \frac{1}{6}\eta^3(-X)^{3/4} + \frac{1}{2}\mu\eta^2 + \frac{1}{2}\mu(-X)^{-3/4}\{\mu\eta + s_2(\eta)\} + \cdots . \tag{7.58}$$

By substituting Eqs. (7.53) and (7.54) into Eq. (7.58), and making the replacement $\eta = Y(-X)^{-1/4}$, it can be shown that:

$$\Psi = \frac{1}{6}Y^3 + \frac{1}{2}\mu\frac{Y^2}{(-X)^{1/2}} + \frac{1}{2}\mu(-X)^{-3/4}\left\{\mu\frac{Y}{(-X)^{1/4}} + \frac{1}{2}b_2\frac{Y^2}{(-X)^{1/2}}\right\} + \cdots . \tag{7.59}$$

This result can now be used to determine the asymptotic behaviour of the displacement function $B(X)$ upstream of the ramp corner by comparing with Eq. (7.38) which yields:

$$B(X) = \mu(-X)^{-1/2} + \frac{1}{2}b_2(-X)^{-5/4} + \cdots \quad \text{as} \quad X \to -\infty. \tag{7.60}$$

Finally, the pressure $P(X)$ can be determined using Eq. (7.29), and making use of the fact that $F(X) = 0$ upstream of the ramp corner:

$$P(X) = X + \mu(-X)^{-1/2} + \frac{1}{2}b_2(-X)^{-5/4} + \kappa + \cdots \quad \text{as} \quad X \to -\infty, \tag{7.61}$$

where κ is defined by

$$\kappa = \lambda_0^{2/3}\beta_2. \tag{7.62}$$

7.5 Downstream Asymptotic Solution

7.5.1 Leading-order terms

Using an argument analogous to that used in Sec. 7.2, it can be inferred that the boundary layer downstream of the interaction regions 5 and 6 remains split into two parts (labelled regions 'c' and 'd' in Fig. 7.1). From Eq. (6.50), the leading-order solution in the lower viscous sublayer c is given by

$$\psi_0(x,y) = \lambda_0^{1/4}\bar{x}^{3/4}g(\zeta) + \cdots \quad \text{as} \quad \bar{x} \to 0^+, \tag{7.63}$$

where $g(\zeta)$ is the solution of Eqs. (6.52)–(6.53) and $\bar{x}$ denotes the streamwise distance from the ramp corner which is given by (cf. Eq. (7.27)):

$$\bar{x} = x - x_s - (\mathrm{Ne}^{-1}\ln \mathrm{Ne})\tilde{X}_0 - \mathrm{Ne}^{-1}\bar{X}_0 = \lambda_0^{-5/3}\,\mathrm{Ne}^{-4/3}\,X. \tag{7.64}$$

The similarity variable ζ was defined by Eq. (6.51), and can be expressed in terms of the inner variables as follows:

$$\zeta = \lambda_0^{1/4}\frac{y}{\bar{x}^{1/4}} = \frac{Y}{X^{1/4}}. \tag{7.65}$$

In order to determine the solution in the upper region d where the viscous term is negligible in comparison to the convective terms, the asymptotic behaviour of Eqs. (6.52)–(6.53) for large ζ should be considered, and it can be verified that:

$$g \sim \frac{1}{6}\zeta^3 + \frac{1}{2}c_0\zeta^2 - \frac{3}{2}c_0^2\zeta + \cdots \quad \text{as} \quad \zeta \to \infty. \tag{7.66}$$

The constant c_0 can, in principle, be found through a numerical solution of Eqs. (6.52)–(6.53). Equations (7.63)–(7.66) suggest that the solution in the quasi-inviscid region d can be expressed in the following asymptotic form:

$$\psi_0(x,y) = \Phi_0(y) + \bar{x}^{1/4}\Phi_1(y) + \cdots \quad \text{as} \quad \bar{x} \to 0^+, \tag{7.67}$$

where $\Phi_0(y)$ is the streamfunction in the vicinity of the ramp corner (cf. Eqs. (7.4)–(7.6)). In order to match with the solution (7.63) in region c, the functions $\Phi_i(y)$ must satisfy the following boundary conditions:

$$\Phi_0(y) = \frac{1}{6}\lambda_0 y^3 + \cdots, \quad \Phi_1(y) = \frac{1}{2}\lambda_0^{3/4} c_0 y^2 + \cdots \quad \text{as} \quad y \to 0. \tag{7.68}$$

Upon substitution of Eq. (7.67) into the momentum equation (5.33), it can be verified that

$$\Phi_1(y) = \sigma \frac{\mathrm{d}\Phi_0}{\mathrm{d}y}. \tag{7.69}$$

The constant σ can be determined using the boundary conditions given by Eq. (7.68), and it follows that

$$\sigma = c_0 \lambda_0^{-1/4}. \tag{7.70}$$

It can also be inferred using Eqs. (5.35c), (7.6) and (7.67) that the asymptotic solution for the displacement function $A(x)$ in regions c and d is given by:

$$A_0(x) = A_0(x_s) + \sigma \bar{x}^{1/4} + \cdots \quad \text{as} \quad \bar{x} \to 0^+. \tag{7.71}$$

Therefore, the slope of the streamlines at the outer edge of region d is given by:

$$\theta_0(\bar{x}) = -\frac{\mathrm{d}A_0}{\mathrm{d}\bar{x}} = \frac{\sigma}{4}\bar{x}^{-3/4} + \cdots \quad \text{as} \quad \bar{x} \to 0^+, \tag{7.72}$$

which can become very large as $\bar{x} \to 0^+$. Using this result, it can be inferred from the interaction law (5.40) that the streamwise extent of the nonlinear interaction region is given by

$$\Delta x \sim \mathrm{Ne}^{-4/3}, \tag{7.73}$$

which is much larger than the previous estimate given by Eq. (7.9). Moreover, this estimate is of the same order of magnitude as that of the inner interaction regions 5 and 6, thus confirming the expectation that the reattachment point lies within this region.

Although not required for the subsequent analysis, the solution in regions c and d for the case in which $\tau_0 = O(1)$ can also be obtained using a method similar to that employed above. From Sec. 6.5, the solution in region c is given by:

$$\psi_0(x,y) = \frac{1}{2}\tau_0^{1/3}\eta^2\bar{x}^{2/3} + \lambda_0\tau_0^{-1}\bar{x}h(\eta) + \cdots \quad \text{as} \quad \bar{x} \to 0^+, \tag{7.74}$$

where

$$\eta = \tau_0^{1/3}\frac{y}{\bar{x}^{1/3}}. \tag{7.75}$$

It can be verified that the asymptotic behaviour of the function $h(\eta)$ for large η is given by:

$$h \sim \frac{1}{6}\eta^3 + d_0\eta + \cdots \quad \text{as} \quad \eta \to \infty. \tag{7.76}$$

The numerical solution of Eqs. (6.44)–(6.46), which was obtained in Sec. 6.5, shows that $d_0 = 1.427$. Using these results, it can be shown that the asymptotic solution in region d is given by:

$$\psi_0(x,y) = \Omega_0(y) + d_0\lambda_0\tau_0^{-5/3}\bar{x}^{2/3}\Omega_0'(y) + \cdots \quad \text{as} \quad \bar{x} \to 0^+, \tag{7.77}$$

where

$$\Omega_0(y) = \frac{1}{2}\tau_0 y^2 + \frac{1}{6}\lambda_0 y^3 + \cdots \quad \text{as} \quad y \to 0, \tag{7.78}$$

$$\Omega_0(y) \to \frac{1}{2}y^2 + A_0(x_s)y + \cdots \quad \text{as} \quad y \to \infty. \tag{7.79}$$

It follows using the above boundary condition that

$$A_0(x) = A_0(x_s) + d_0\lambda_0\tau_0^{-5/3}\bar{x}^{2/3} + \cdots \quad \text{as} \quad \bar{x} \to 0^+. \tag{7.80}$$

7.5.2 Higher-order terms

By making use of Eq. (7.71), the asymptotic behaviour of p_1 can be found by solving Eq. (7.10) which yields:

$$p_1(x) = p_1(x_s) + \sigma \bar{x}^{1/4} + \cdots \quad \text{as} \quad \bar{x} \to 0^+. \tag{7.81}$$

The solutions in region c for the higher-order streamfunction terms ψ_1 and ψ_2 in the asymptotic expansion (5.31) were sought in the following form:

$$\psi_i(x, y) = \sigma \bar{x}^n k_i(\zeta) + \cdots \quad \text{as} \quad \bar{x} \to 0^+ \quad (i = 1 \text{ or } 2), \tag{7.82}$$

where σ was defined by Eq. (7.70) and n is to be determined. Substitution of Eqs. (7.63) and (7.82) into Eqs. (5.36)–(5.37) yields the following linear equation for k_i:

$$k_i''' + \frac{3}{4} g k_i'' - \left(n + \frac{1}{4}\right) g' k_i' + n g'' k_i = \begin{cases} \frac{1}{4}, & i = 1, \\ 0, & i = 2, \end{cases} \tag{7.83}$$

subject to the no-slip boundary conditions $k_i(0) = k_i'(0) = 0$. The third required boundary condition shall be discussed later in this section. The forcing term on the right-hand side for the case $i = 1$, which enters into the equation for k_1 if $n = 0$, is due to the second-order pressure term given by Eq. (7.81). The appropriate value of n for the case $i = 2$ was determined by considering a small streamwise perturbation of the form $\bar{x} = x_0 + \Delta x$, where x_0 is a characteristic streamwise distance downstream of the inner interaction region. It follows from Eq. (7.65) that the similarity variable ζ can be expressed in the form:

$$\zeta = \zeta_0 - \frac{\zeta_0}{4x_0} \Delta x, \quad \text{where} \quad \zeta_0 = \lambda_0^{1/4} \frac{y}{x_0^{1/4}}. \tag{7.84}$$

Using this result, it follows from Eqs. (5.31), (7.63) and (7.82) that

$$\begin{aligned} \psi = {} & \lambda_0^{1/4} x_0^{3/4} g(\zeta_0) + \sigma k_1(\zeta_0)\, \mathrm{Ne}^{-1} \\ & + \lambda_0^{1/4} x_0^{-1/4} \Delta x \left\{ \frac{3}{4} g(\zeta_0) - \frac{1}{4} \zeta_0 g'(\zeta_0) \right\} + \sigma x_0^n k_2(\zeta_0)\, \mathrm{Ne}^{-4/3} + \cdots . \end{aligned} \tag{7.85}$$

If the streamwise disturbances are confined within the length-scale of the inner interaction region (i.e. $\Delta x \sim \mathrm{Ne}^{-4/3}$ from Eq. (7.73)), it can be inferred by comparing the third and fourth terms of the above expansion that $n = -1/4$. Moreover, it follows that

$$k_2(\zeta) \sim 3g - \zeta g', \tag{7.86}$$

which can be verified by direct substitution into Eq. (7.83) with $n = -1/4$.

The higher-order terms for the solution in region d can be obtained using an argument similar to that used in Sec. 7.5.1 for the leading-order terms. For $n = 0$ or $-1/4$, it follows from Eqs. (7.66) and (7.83) that to leading-order:

$$k_i \sim \frac{1}{2} d_i \zeta^2 + \cdots \quad \text{as} \quad \zeta \to \infty, \quad (i = 1 \text{ or } 2), \tag{7.87}$$

where d_i are constants. Upon substitution of this result into Eq. (7.82), and making the replacement $\zeta = \lambda_0^{1/4} y \bar{x}^{-1/4}$, it follows that the solution in region d can be expressed in the form:

$$\left.\begin{aligned} \psi_1(x,y) &= \Upsilon_1(y)\bar{x}^{-1/2} + \cdots \\ \psi_2(x,y) &= \Upsilon_2(y)\bar{x}^{-3/4} + \cdots \end{aligned}\right\} \quad \text{as} \quad \bar{x} \to 0^+, \tag{7.88}$$

where the functions $\Upsilon_i(y)$ satisfy the boundary conditions (for $i = 1$ or 2):

$$\Upsilon_i(y) \to \frac{1}{2}\sigma d_i \lambda_0^{1/2} y^2 + \cdots \quad \text{as} \quad y \to 0. \tag{7.89}$$

Upon substitution of Eqs. (7.67) and (7.88) into the higher-order momentum equation (5.36), and making use of the boundary condition given by Eq. (7.89), it can be verified that

$$\Upsilon_i(y) = \frac{\sigma d_i}{\lambda_0^{1/2}} \frac{\mathrm{d}\Phi_0}{\mathrm{d}y}. \tag{7.90}$$

Since $\psi_i \to A_i(x) y$ as $y \to \infty$, it follows that

$$\left.\begin{aligned} A_1(x) &= A_1(x_s)\bar{x}^{-1/2} + \cdots \\ A_2(x) &= A_2(x_s)\bar{x}^{-3/4} + \cdots \end{aligned}\right\} \quad \text{as} \quad \bar{x} \to 0^+. \tag{7.91}$$

In addition, since $\Upsilon_i \to A_i(x_s)y$ as $y \to \infty$, it can be inferred from Eqs. (7.6) and (7.90) that

$$d_i = \sigma^{-1}\lambda_0^{1/2}A_i(x_s). \tag{7.92}$$

This implies that the third required boundary condition for Eq. (7.83), which hitherto has been left unspecified, depends upon the displacement effects $A_1(x_s)$ and $A_2(x_s)$ induced by perturbations of $O(\mathrm{Ne}^{-1})$ and $O(\mathrm{Ne}^{-4/3})$ respectively to the critical ramp angle β_0^*. Although these conditions are required for the unique determination of k_1 and k_2, their solution is not strictly required in the subsequent analysis.

By making use of Eqs. (5.42), (7.19) and (7.81), the asymptotic behaviour of the pressure downstream of the reattachment point can be expressed in the form:

$$p(x) = \beta_0^* + \mathrm{Ne}^{-1}\left\{p_1(x_s) + \sigma\bar{x}^{1/4}\right\} + \mathrm{Ne}^{-4/3}\,\beta_2 + \cdots \quad \text{as} \quad \bar{x} \to 0^+. \tag{7.93}$$

In addition, the corresponding asymptotic behaviours of the streamfunction and displacement thickness in region c as $\bar{x} \to 0^+$ are given respectively by:

$$\psi(x,y) = \lambda_0^{1/4}\bar{x}^{3/4}g(\zeta) + \sigma k_1(\zeta)\,\mathrm{Ne}^{-1} + \sigma\bar{x}^{-1/4}k_2(\zeta)\,\mathrm{Ne}^{-4/3} + \cdots, \tag{7.94}$$

$$A(x) = A_0(x_s) + \sigma\bar{x}^{1/4} + A_1(x_s)\bar{x}^{-1/2}\,\mathrm{Ne}^{-1} + A_2(x_s)\bar{x}^{-3/4}\,\mathrm{Ne}^{-4/3} + \cdots. \tag{7.95}$$

By expanding these solutions in terms of the inner variables defined by Eqs. (7.27) and (7.33), it can be shown that as $X \to \infty$,

$$\Psi(X,Y) = X^{3/4}g(\zeta) + \sigma\lambda_0 k_1(\zeta) + \sigma\lambda_0^{17/12}X^{-1/4}k_2(\zeta) + \cdots, \tag{7.96a}$$

$$P(X) = c_0X^{1/4} + \kappa + \cdots, \tag{7.96b}$$

$$B(X) = c_0X^{1/4} + \lambda_0^{3/2}A_1(x_s)X^{-1/2} + \lambda_0^{23/12}A_2(x_s)X^{-3/4} + \cdots, \tag{7.96c}$$

where the constant κ is defined by Eq. (7.62). The above result for the pressure $P(X)$ is also consistent with that obtained by integrating the interaction law given by Eq. (7.29).

7.6 Unsteady Numerical Algorithm

7.6.1 Formulation of the Interaction Problem

In this chapter, a novel unsteady algorithm developed by the author shall be employed in order to solve the nonlinear interaction problem discussed in Sec. 7.3. Previous experience has shown that interactive boundary layer problems involving separation can be successfully solved using the *unsteady* form of the governing equations, and by advancing the solution in time until a steady-state is reached. In order to consider small perturbations about the critical ramp angle β_0^* (cf. Eq. (7.1)), the streamwise coordinate X in the upstream asymptote given by Eq. (7.58) was replaced by $X - \Lambda$ (where Λ is a parameter), which is equivalent to a streamwise shift in the position of the ramp corner.

It is convenient to introduce the shear stress τ and velocity components U and V defined respectively by:

$$\tau = \frac{\partial U}{\partial Y}, \quad U = \frac{\partial \Psi}{\partial Y}, \quad V = -\frac{\partial \Psi}{\partial X}. \tag{7.97}$$

The nonlinear inner interaction problem given by Eqs. (7.35)–(7.38), along with the interaction law (7.29), can be expressed in the form:

$$\frac{\partial \tau}{\partial t} + U\frac{\partial \tau}{\partial X} + V\frac{\partial \tau}{\partial Y} = \frac{\partial^2 \tau}{\partial Y^2}, \tag{7.98a}$$

$$\frac{\mathrm{d}P}{\mathrm{d}X} = \frac{\mathrm{d}B}{\mathrm{d}X} - \frac{\mathrm{d}F}{\mathrm{d}X} + 1, \tag{7.98b}$$

$$\Psi = U = 0 \quad \text{at} \quad Y = 0, \tag{7.98c}$$

$$\tau = Y + B(X) + \cdots \quad \text{as} \quad Y \to \infty, \tag{7.98d}$$

$$\tau = Y + \mu(\Lambda - X)^{-1/2} + \frac{\mu}{2}(\Lambda - X)^{-5/4} s_2''(\xi) + \cdots \quad \text{as} \quad X \to -\infty, \tag{7.98e}$$

where the similarity variable ξ is defined by:

$$\xi = \frac{Y}{(\Lambda - X)^{1/4}}. \tag{7.99}$$

It should be noted that an unsteady time derivative term has also been included in Eq. (7.98a), where t denotes the time step, and that the surface geometry $F(X)$ enters into these equations only via the interaction law (7.98b). In order to avoid problems associated with the discontinuous derivative of the surface geometry $F(X)$ at $X = 0$, the ramp corner was rounded slightly by defining $F(X)$ as follows:

$$F(X) = \frac{1}{2}\left\{X + \sqrt{X^2 + R^2}\right\}, \tag{7.100}$$

where the *rounding parameter* R was taken as 0.5.

The upstream boundary condition given by Eq. (7.98e) involves the function s_2 which was derived in Sec. 7.4, and whose solution is shown in Fig. 7.2. It is also evident from Eq. (7.98e) that large positive values of Λ correspond to comparatively small ramp angle perturbations, i.e.

$$\beta_2 \to 0 \quad \text{as} \quad \Lambda \to \infty, \tag{7.101}$$

whilst negative values of Λ correspond to larger perturbations, i.e.

$$\beta_2 \to \infty \quad \text{as} \quad \Lambda \to -\infty. \tag{7.102}$$

7.6.2 Finite-difference scheme

The unsteady boundary layer equation (7.98a) was approximated using second-order accurate formulae for the spatial derivatives and first-order approximations in time as follows:

$$\frac{\tau_{i,j} - \tau^*_{i,j}}{\Delta t} + U^*_{i,j}\left(\frac{\partial \tau}{\partial X}\right)^*_{i,j} + V^*_{i,j}\left(\frac{\tau_{i,j+1} - \tau_{i,j-1}}{2\Delta Y}\right) = \frac{\tau_{i,j+1} - 2\tau_{i,j} + \tau_{i,j-1}}{(\Delta Y)^2}. \tag{7.103}$$

A uniform mesh defined by:

$$X_i = X_{\min} + (i-1)\Delta X, \quad 1 \le i \le I, \tag{7.104}$$

$$Y_j = (j-1)\Delta Y, \quad 1 \le j \le J. \tag{7.105}$$

has been employed, and an asterisk is used to denote quantities evaluated at the previous time step. It should also be noted that conventional central differences have been used in the transverse direction, whilst the streamwise convective term is represented by an upwind or downwind formula depending on the local direction of the flow, i.e.

$$\left(\frac{\partial \tau}{\partial X}\right)^*_{i,j} = \begin{cases} \frac{\tau^*_{i-2,j} - 4\tau^*_{i-1,j} + 3\tau^*_{i,j}}{2\Delta X} & \text{for} \quad U^*_{i,j} \ge 0, \\ \frac{-3\tau^*_{i,j} + 4\tau^*_{i+1,j} - \tau^*_{i+2,j}}{2\Delta X} & \text{for} \quad U^*_{i,j} < 0. \end{cases} \tag{7.106}$$

Equation (7.103) defines the following tri-diagonal problem for $\tau_{i,j}$, $3 \le i \le I$:

$$a_j \tau_{i,j-1} + b_j \tau_{i,j} + c_j \tau_{i,j+1} = r_j, \qquad 2 \le j \le J-1, \tag{7.107}$$

where

$$a_j = -\frac{2}{(\Delta Y)^2} - \frac{1}{\Delta t}, \tag{7.108a}$$

$$b_j = \frac{1}{(\Delta Y)^2} + \frac{V^*_{i,j}}{2\Delta Y}, \tag{7.108b}$$

$$c_j = \frac{2}{(\Delta Y)^2} - a_j, \tag{7.108c}$$

$$r_j = U^*_{i,j}\left(\frac{\partial \tau}{\partial X}\right)^*_{i,j} - \frac{\tau^*_{i,j}}{\Delta t}. \tag{7.108d}$$

A similar finite-difference formulation for the momentum equation was employed by Cassel *et al.* (1995, 1996) for the solution of the triple-deck equations given in Chapter 5. In order to implement the interaction law (7.98b), the following fundamental relationships (which follow from Eqs. (7.98a) and (7.98c–d) must be considered:

$$\frac{\mathrm{d}P}{\mathrm{d}X} = \left(\frac{\partial \tau}{\partial Y}\right)_{Y=0}, \qquad \frac{\mathrm{d}B}{\mathrm{d}X} = \left(\frac{\partial \tau}{\partial X}\right)_{Y\to\infty}. \tag{7.109}$$

Using these results, Eq. (7.98b) can be expressed solely in terms of the shear stress and known surface geometry $F(X)$ as follows:

$$\left(\frac{\partial\tau}{\partial Y}\right)_{Y=0} = \left(\frac{\partial\tau}{\partial X}\right)_{Y\to\infty} - \frac{\mathrm{d}F}{\mathrm{d}X} + 1. \tag{7.110}$$

This equation yields the first required boundary condition for τ and can be approximated using the following second-order accurate difference formula:

$$\frac{-3\tau_{i,1} + 4\tau_{i,2} - \tau_{i,3}}{2\Delta Y} = \frac{\tau^*_{i-2,J} - 4\tau^*_{i-1,J} + 3\tau_{i,J}}{2\Delta X} - \left(\frac{\mathrm{d}F}{\mathrm{d}X}\right)_i + 1. \tag{7.111}$$

It should be noted that a backward (upwind) quotient has been employed at the outer edge of the computational domain where $j = J$ since the interaction problem does not permit upstream influence. In addition, the shear stress is assumed unknown at the current streamwise location X_i where the solution is sought, whilst the solution at the previous two spatial steps $i-1$ and $i-2$ is assumed known from the previous time step (hence the asterisk). The foregoing equation can be rearranged in the following form:

$$\frac{-3\tau_{i,1} + 4\tau_{i,2} - \tau_{i,3}}{2\Delta Y} - \frac{3\tau_{i,J}}{2\Delta X} = \frac{\tau^*_{i-2,J} - 4\tau^*_{i-1,J}}{2\Delta X} - \left(\frac{\mathrm{d}F}{\mathrm{d}X}\right)_i + 1 = M^*. \tag{7.112}$$

It is also evident from Eq. (7.98d) that

$$\left(\frac{\partial\tau}{\partial Y}\right)_{Y\to\infty} = 1 \approx \frac{\tau_{i,J-2} - 4\tau_{i,J-1} + 3\tau_{i,J}}{2\Delta Y}, \tag{7.113}$$

which is the second required boundary condition. Equations (7.107), (7.108), (7.112) and (7.113) can be expressed in the following form:

$$\begin{pmatrix} -A & B & -C & & & & D \\ a_2 & b_2 & c_2 & & & & \\ & \cdot & \cdot & \cdot & & & \\ & & \cdot & \cdot & \cdot & & \\ & & & \cdot & \cdot & \cdot & \\ & & & & a_{J-1} & b_{J-1} & c_{J-1} \\ & & & & C & -B & A \end{pmatrix} \begin{pmatrix} T_1 \\ T_2 \\ \cdot \\ \cdot \\ \cdot \\ T_{J-1} \\ T_J \end{pmatrix} = \begin{pmatrix} M^* \\ r_2 \\ \cdot \\ \cdot \\ \cdot \\ r_{J-1} \\ 1 \end{pmatrix}, \tag{7.114}$$

where $T_j = \tau_{i,j}$ is the shear stress at the current streamwise location X_i. In addition,

$$A = \frac{3}{2\Delta Y}, \quad B = \frac{2}{\Delta Y}, \quad C = \frac{1}{2\Delta Y}, \quad D = -\frac{3}{2\Delta X}. \tag{7.115}$$

Unless otherwise specified, all the other elements in the coefficient matrix are zero.

7.6.3 Solution procedure

Starting from the upstream solution given by Eq. (7.98e) at $i = 1$ and 2, Eq. (7.114) was solved (for $3 \leq i \leq I$) to determine the solution at the current streamwise location X_i, using the computed solution from the previous location as the initial distribution. The solution was marched downstream to $X = X_{\max}$ to yield a new distribution of $\tau_{i,j}$ throughout the entire computational domain. The marching technique was then repeated in order to determine the solution at the next time step, and the procedure is repeated until a steady-state is reached.

An efficient Gaussian elimination solver for tri-diagonal systems was employed, suitably modified to take into account the extra non-diagonal elements in the coefficient matrix of Eq. (7.114). Firstly, the J-th row of the system was expressed in tri-diagonal form using the $(J-1)$-th row as follows:

$$-(BE + b_{J-1})T_{J-1} + (AE - c_{J-1})T_J = E - r_{J-1}, \quad E = \frac{a_{J-1}}{C}. \tag{7.116}$$

Next, the matrix was reduced using Gaussian elimination to upper row-echelon form using the lower-diagonal elements a_j as pivots (which are non-zero from

Eq. (7.108a)), which yields the reduced system of equations:

$$\begin{pmatrix} -A & B & -C & & & D \\ & \tilde{b}_2 & \tilde{c}_2 & & & -D \\ & & \cdot & \cdot & & \cdot \\ & & & \cdot & \cdot & (-1)^{j-1}D \\ & & & & \cdot & \cdot \\ & & & & \tilde{b}_{J-1} & \tilde{c}_{J-1} \\ & & & & & \tilde{b}_J \end{pmatrix} \begin{pmatrix} T_1 \\ T_2 \\ \cdot \\ \cdot \\ \cdot \\ T_{J-1} \\ T_J \end{pmatrix} = \begin{pmatrix} M^* \\ \tilde{r}_2 \\ \cdot \\ \cdot \\ \cdot \\ \tilde{r}_{J-1} \\ \tilde{r}_J \end{pmatrix}, \tag{7.117}$$

where the tilde ˜ indicates the computed elements after the elimination process. The use of a_j as the pivot elements enables the entries of the J-th column to be known in advance. This reduced system of equations were then solved very efficiently using backward substitution.

The streamwise velocity U and streamfunction Ψ were then determined by integrating Eqs. (7.97) using the Trapezoidal rule, subject to the no-slip conditions at the body surface $U_{i,1} = \Psi_{i,1} = 0$. The transverse velocity $V = -\partial\Psi/\partial X$ was then determined using forward or backward differences depending on the sign of $U_{i,j}$ in a manner similar to that used in Eq. (7.106). It was observed that the use of central differences render the algorithm unstable.

The computation was marched forward in time until a steady-state was reached, and this was assumed to take place when the maximum difference in the skin friction distribution between successive time steps was less than a specified tolerance level ϵ, which was taken as 10^{-7} for all of the results shown here. A linear stability analysis shows that this novel unsteady algorithm is numerically stable if the Courant-Friedrichs-Lewy criterion is satisfied (see, for example, Anderson 1995 and Guardino 1995):

$$\Delta t \leq \frac{\Delta X}{|U_{\max}|}. \tag{7.118}$$

It follows from Eq. (7.98d) that the maximum streamwise velocity

$$U_{\max} \sim \frac{1}{2} Y_{\max}^2. \tag{7.119}$$

However, due to the non-linearity of the boundary layer equations, as well as the possibility of instabilities which may arise from the implementation of the boundary conditions (7.112)–(7.113), the time step Δt was restricted to values at least one-half of that indicated by Eq. (7.118).

An important feature of this method is that the shear stress is assumed unknown at both $j = 1$ and $j = J$, and is determined from the solution of the above system of equations. This is in stark contrast to the steady-state approach used by Smith & Daniels (1981), in which the shear stress at the outer edge $T_J = \tau_{i,J}$ is assumed known from the previous iteration. It turns out that physically unrealistic converged solutions are obtained if this approach is used in the present unsteady algorithm. In fact, the generation of spurious steady-state solutions is not uncommon in unsteady CFD codes (see also the recent review of Yee & Sweby 1998). The novel algorithm described above is globally second-order accurate in space and first-order accurate in time[2] , and was found to be robust. It was also observed that the third-order term in Eq. (7.98e) is of crucial importance in order to obtain the correct upstream asymptotic behaviour given by Eq. (7.37).

Once the shear stress τ has been determined throughout the entire computational domain, the displacement function $B(X)$ is found using Eq. (7.98d), which can also be expressed in the form:

$$B(X) = \lim_{Y \to \infty} (\tau - Y). \tag{7.120}$$

The pressure $P(X)$ can then be determined at any desired time using the interaction law given by Eq. (7.98b), and it can be shown that

$$P(X) = B(X) - F(X) + X + \kappa, \tag{7.121}$$

where κ was defined by Eq. (7.62).

[2]Since steady-state solutions are sought, the first-order accuracy in time is irrelevant.

7.7 Results & Discussion

Calculations were carried out using a number of mesh sizes and the results are believed to be globally grid independent. Unless otherwise stated, all the numerical results shown here were obtained using a uniform mesh with $I = 150$, $J = 100$, $X_{\min} = -50$, $X_{\max} = 50$ and $Y_{\max} = 10$. In addition, the time step Δt was taken as 5×10^{-3}.

It is evident from Fig. 7.3 that the numerical solution for the case $\Lambda = 0$ exhibits the correct upstream asymptotic behaviour given by Eqs. (7.58) (with $Y = 0$) and (7.61), namely

$$\left.\begin{aligned} \tau_s(X) &= \mu(-X)^{-1/2} + \cdots \\ P(X) &= X + \mu(-X)^{-1/2} + \tfrac{1}{2}b_2(-X)^{-5/4} + \kappa + \cdots \end{aligned}\right\} \quad \text{as} \quad X \to -\infty, \tag{7.122}$$

where $\mu \approx -0.956$ and $b_2 \approx 1.312$. The third-order term in Eq. (7.58) can be omitted from the expression for the skin friction because $s_2''(0) = 0$. Moreover, the solution clearly tends to the downstream asymptotic solution given by Eqs. (7.96a–c), which to leading-order can be expressed in the form:

$$\tau_s(X) = g''(0)X^{1/4} + \cdots, \quad P(X) = c_0 X^{1/4} + \kappa + \cdots \quad \text{as} \quad X \to \infty, \tag{7.123}$$

where c_0 is the constant in the asymptotic expansion (7.66) of the function $g(\eta)$ for large η. The numerical solution of Eqs. (6.52)–(6.53) (with $\omega = 0$) yields $c_0 \approx 0.995$ and $g''(0) \approx 2.009$. It is interesting to observe that Eq. (7.123) also yields a reasonably accurate shear-stress distribution for small values of X, even though the formula is strictly only valid for large X.

Solutions were also obtained for various values of Λ, and the results for the surface shear stress are presented in Fig. 7.5. These results show that as Λ becomes large (i.e. as the ramp angle perturbation β_2 decreases), the size of the separated region is reduced and ultimately vanishes as $\Lambda \to \infty$. Moreover, all

the solutions exhibit virtually the same downstream behaviour, which is why the higher-order terms in Eqs. (7.96a–c) can be neglected. In addition, the reattachment point is very close to the point $X = 0$ for all values of Λ, which implies that the separated flow region is always located upstream of the ramp corner.

The separated region is shown graphically in Figs. 7.4 and 7.6, where the velocity vectors are plotted for the cases $\Lambda = 0$ and -7 respectively. It is evident from these pictures that the speed of the fluid in the reversed flow region is much smaller in comparison to the rest of the flow field. Moreover, the strength of the recirculation region increases and a vortex is generated which moves upwards into the flow for decreasing values of Λ.

The convergence histories of the numerical solutions are shown in Fig. 7.7, where Δ is the maximum difference in the skin friction distribution between successive time steps, i.e.

$$\Delta = \max\left(\tau_{i,1} - \tau_{i,1}^{*}\right), \quad 1 \leq i \leq I. \tag{7.124}$$

Clearly, the time required to obtain steady-state solutions increases as Λ decreases, and no converged solution using the current mesh size could be achieved for values of Λ less than -7.22.[3] A similar kind of numerical breakdown was observed in the steady-state calculations of Zhikharev (1993) for the marginal separation from a subcritical cold wall (see Appendix C). In fact, the impossibility of obtaining converged solutions at a finite value of the controlling parameter is typical of interactive boundary layer calculations (Smith 1988).

[3]Steady-state solutions for $\Lambda < -7.22$ could be obtained using a coarser grid, but with less resolution of the separated flow region.

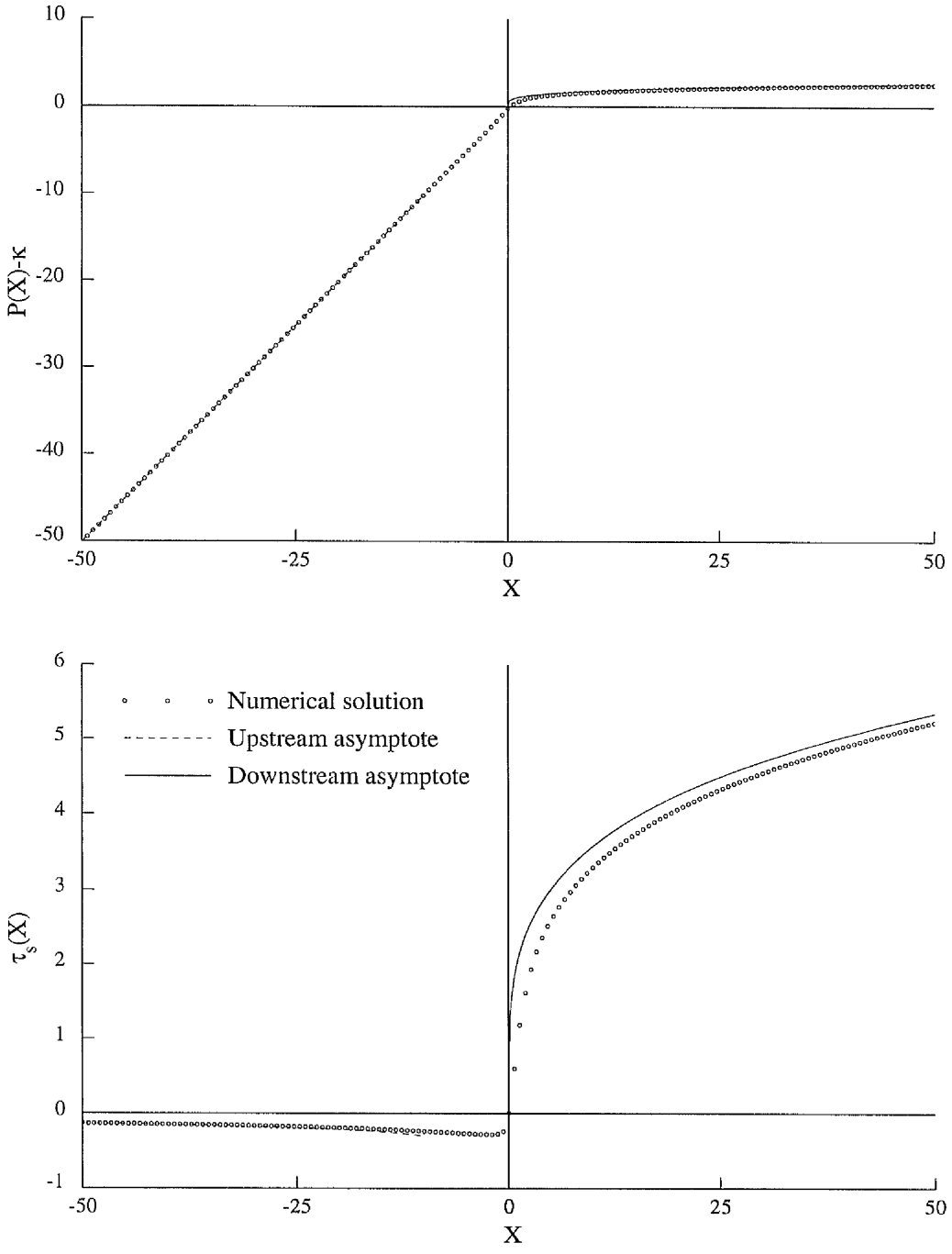

Figure 7.3: Pressure $P(X) - \kappa$ and skin friction $\tau_s(X)$ distributions for $\Lambda = 0$.

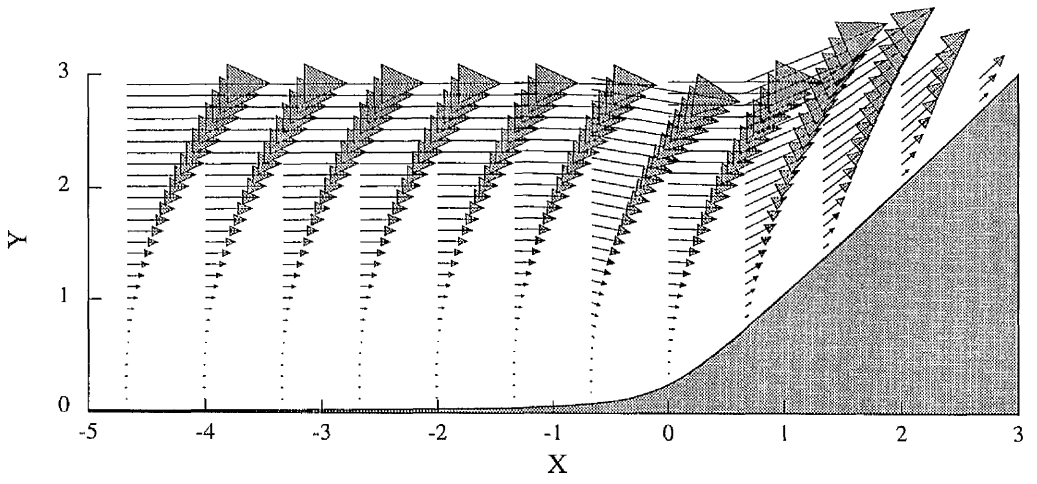

Figure 7.4: Velocity vectors for $\Lambda = 0$ in the vicinity of the ramp corner.

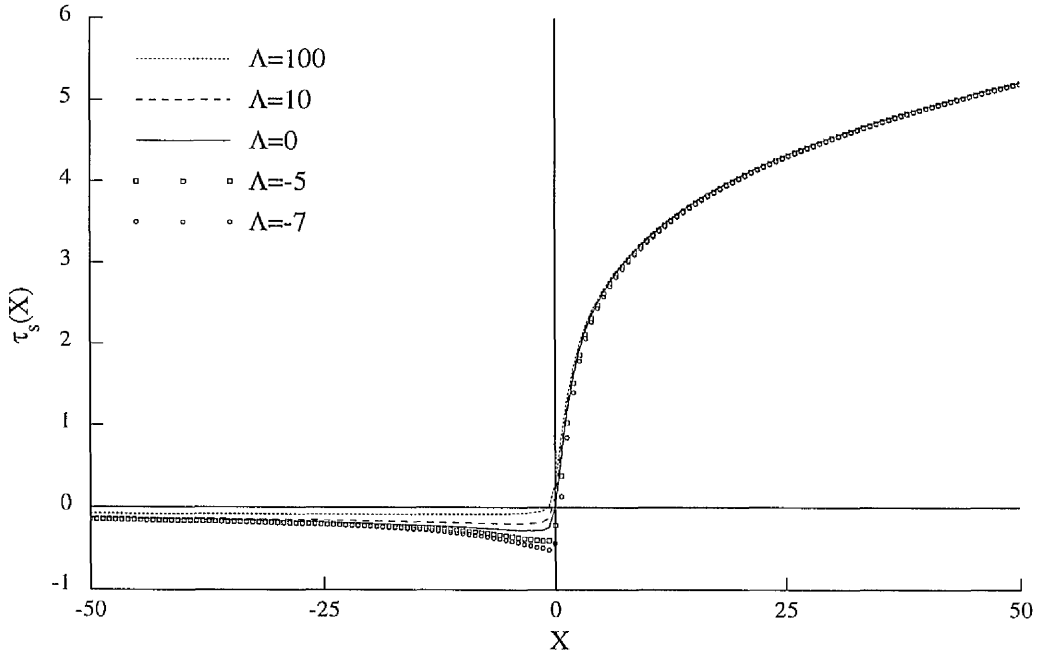

Figure 7.5: Skin friction $\tau_s(X)$ distributions for various values of Λ.

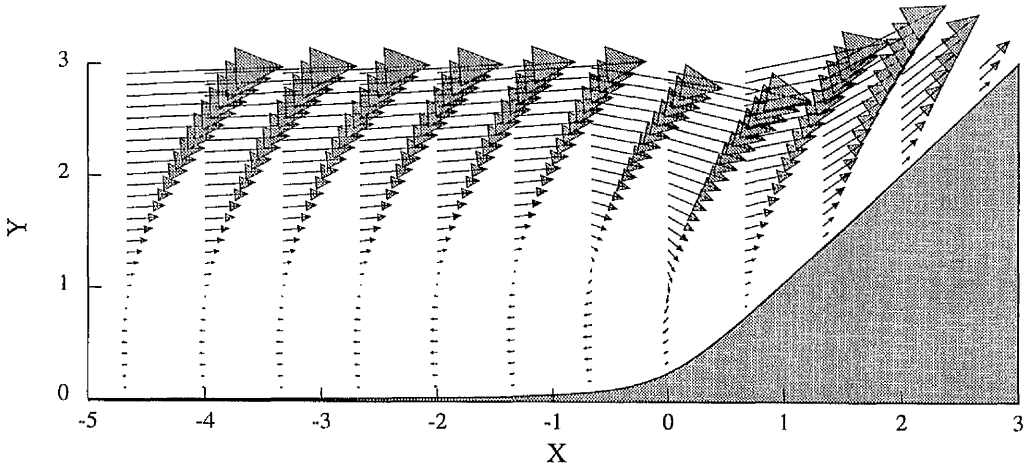

Figure 7.6: Velocity vectors for $\Lambda = -7$ in the vicinity of the ramp corner.

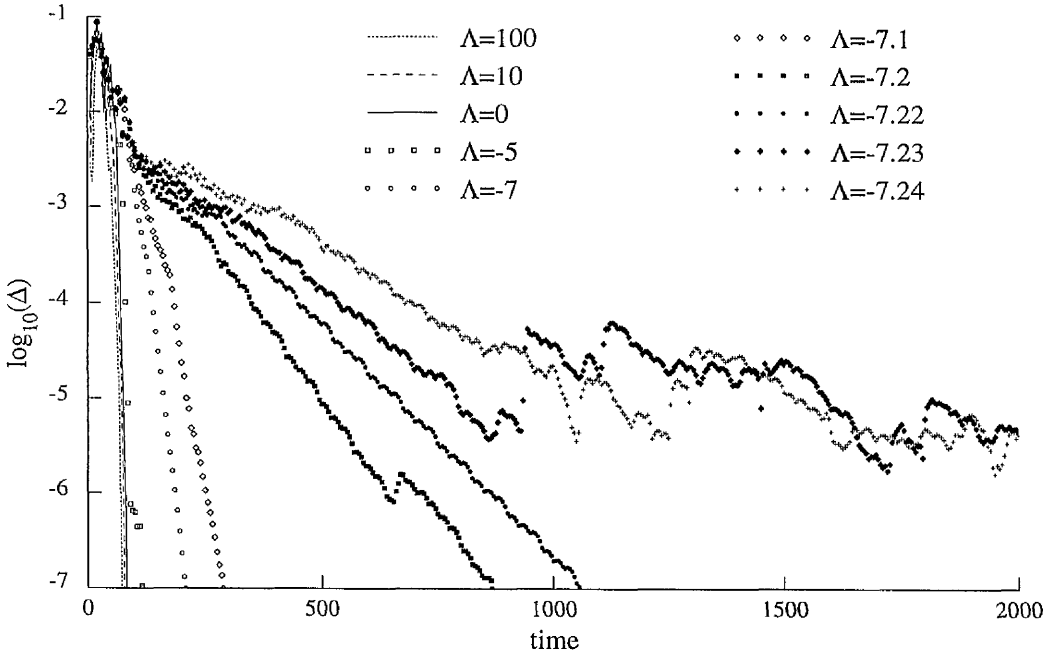

Figure 7.7: Residual histories for various values of Λ.

7.8 Extension to Axially-Symmetric Flows

For $z \sim \mathrm{Ne}^{-4/3}$, it can be inferred from Eq. (7.26a) that the pressure $q(x,z)$ in the inviscid layer above the inner interaction regions 5 and 6 can be expressed in the following form:

$$\begin{aligned} q(x,z) = q_0(z) + (\mathrm{Ne}^{-1}\ln \mathrm{Ne})q_1(z) + \mathrm{Ne}^{-1}\,q_2(z) \\ + \mathrm{Ne}^{-4/3}\,Q(X,Z) + \cdots, \end{aligned} \tag{7.125}$$

where X and Z are $O(1)$ variables defined by (cf. Eq. (7.27)):

$$x = x_s + (\mathrm{Ne}^{-1}\ln \mathrm{Ne})\tilde{X}_0 + \mathrm{Ne}^{-1}\,\bar{X}_0 + \lambda_0^{-5/3}\,\mathrm{Ne}^{-4/3}\,X, \tag{7.126a}$$

$$z = \lambda_0^{-5/3}\,\mathrm{Ne}^{-4/3}\,Z. \tag{7.126b}$$

Notice that x and z are scaled identically (with respect to terms of $O(\mathrm{Ne}^{-4/3})$) to avoid degeneration of the wave equation (5.20). Matching with the asymptotic expansion for the surface pressure given by Eq. (7.26a) requires that:

$$\left.\begin{aligned} q_0 &\to p_0(x_s), \\ q_1 &\to \lambda_0\tilde{X}_0, \\ q_2 &\to p_1(x_s) + \lambda_0\bar{X}_0, \end{aligned}\right\} \quad \text{as} \quad z \to 0. \tag{7.127}$$

Upon substitution of Eqs. (7.26b), (7.8) and (7.126) into the axially-symmetric wave equation (5.20), it follows that in the cold wall limit $\mathrm{Ne} \to \infty$:

$$q_i(z) = A_i \ln(z + r) + B_i, \qquad i = 1,\ 2,\ 3, \tag{7.128}$$

$$\frac{\partial^2 Q}{\partial X^2} - \frac{\partial^2 Q}{\partial Z^2} = 0, \tag{7.129}$$

where A_i and B_i are constants and r is the radius. It can also be inferred from the matching condition (5.29) that

$$\frac{\partial q_i}{\partial z} = 0, \qquad i = 1,\ 2,\ 3, \tag{7.130}$$

$$\frac{\mathrm{d}^2 B}{\mathrm{d}X^2} - \frac{\mathrm{d}^2 F}{\mathrm{d}X^2} - \frac{\mathrm{d}^2 P}{\mathrm{d}X^2} = 0. \tag{7.131}$$

Applying the boundary conditions given by Eqs. (7.128) and (7.130) shows that:

$$q_0 = p_0(x_s),\ q_1 = \lambda_0 \tilde{X}_0,\ q_2 = p_1(x_s) + \lambda_0 \bar{X}_0. \tag{7.132}$$

Moreover, the *inner* pressure distribution $Q(X, Z)$ for the axially-symmetric case is governed by the *two-dimensional* wave equation (7.129), which has the well-known *D'Alembert* solution (cf. Eq. (5.38)). In addition, it can be inferred from Eqs. (7.28) and (7.131) that

$$\frac{\mathrm{d}P}{\mathrm{d}X} = \frac{\mathrm{d}B}{\mathrm{d}X} - \frac{\mathrm{d}F}{\mathrm{d}X} + 1, \tag{7.133}$$

which is identical to the 2D interaction law given by Eq. (7.29). Consequently, the problem for AXI flows in the vicinity of the separation point reduces to the solution of an equivalent 2D case.

Conclusions & Suggestions for Further Work

In Part I of this thesis, the self-similar equations for the hypersonic flow over very slender 2D and AXI bodies of the form $y_s(x) = rx^{3/4}$ have been solved numerically. These solutions are of practical interest, since they yield reliable estimates for the skin friction and heat transfer rates without recourse to the solution of the full Navier-Stokes equations. The influence of the slenderness ratio r on the boundary layer thickness δ was also determined analytically, and new quadratic and cubic formulae for δ have been derived. It was also observed that there exists an optimum value of r which results in minimum drag and heat transfer on AXI bodies.

The upstream propagation of disturbances from the trailing-edge was considered by means of perturbing the boundary layer flow near the leading-edge, and analysing the resulting eigenvalue problem. Upstream influence was discovered for the AXI case for slenderness ratios and surface enthalpies greater than certain critical values. The numerical results for the 2D flat plate were found to be in good agreement with solutions obtained by previous authors. Asymptotic results have been obtained for very hot bodies, and the effects of varying the Prandtl number and ratio of specific heats have also been considered. New analytical results have also been obtained for cases in which the boundary layer thickness is

negligible in comparison to the body thickness, particularly for power-law bodies of the form $y_s(x) = rx^\alpha$ where $\alpha < 3/4$. It was discovered that the upstream influence effect decays exponentially as the leading edge is approached, and an analytic expression has been obtained for the upstream influence eigenvalue.

In Part II, the equations describing the interaction between the boundary layer (which proved to be predominantly inviscid) and external flow have been successfully solved for both 2D and AXI hypersonic flows over compression and expansion corners with strong wall cooling. In particular, the pressure distribution in the inviscid upper-deck has been computed using both the Method of Characteristics and finite-difference 'Leap-frog' method, and it was observed that the former approach yielded oscillation-free solutions. The resulting pressure gradient was subsequently employed in the solution of the boundary layer equation in the viscous sublayer using a fully-implicit downstream marching technique as far downstream as the separation point (for cases in which the flow does not separate, the solution can be continued indefinitely downstream). As expected, it was observed that the flow separates for compression ramps if the ramp angle is greater than a certain critical value. For AXI flows, it was observed that the pressure gradient becomes favourable at a certain distance downstream of the ramp corner, and that the minimum in the skin friction distribution increases as the radius is decreased *for fixed ramp angle.* It was also discovered that the flow over expansion corners separates if the radius is smaller than a certain critical value. New self-similar solutions were also found far downstream of the ramp corner for flows without separation, and also for cases exhibiting incipient separation.

Separated hypersonic flows over 2D compression ramps with strong subcritical wall cooling have been considered using an asymptotic theory based on the 'compensation' regimes originally described by Smith & Daniels (1981) for incompressible flows in order to remove the Goldstein singularity at the separation point.

The resulting fundamental inner interaction problem was successfully solved for various ramp angles close to the critical angle using a novel semi-implicit unsteady algorithm developed by the author, and the solutions are believed to be the first ever obtained for the present case. It was observed that the separated region lies entirely upstream of the ramp corner. In addition, asymptotic solutions far upstream and downstream of the interaction region were derived, and the numerical solutions were found to be in very good agreement with both of these analytical results. Finally, it was shown that the asymptotic theory considered here, as well as marginal separation theory, can both be used to describe the separation process occurring in axially-symmetric flows.

There is much further interesting work which can be carried out to extend the present study, some ideas of which are listed below.

- Analysis of the hypersonic flow over axially-symmetric compression or expansion corners for cases in which the radius of the body is of the same order of magnitude as, or even much less than, the boundary layer thickness. As discussed in Sec. 1.2, this situation corresponds to the case $\Omega \sim 1$.

- Development of a modified triple-deck theory for cases in which the ramp corner is located in a region of strong global viscous interaction. Brown *et al.* (1975b) have already considered this case for 2D flows under the assumption that γ is close to unity. The effect of wall cooling would also be of particular interest.

- Analysis of the hypersonic flow with transcritical wall cooling (i.e. where the Pearson integral $|\mathcal{L}| \ll 1$).

- Consideration of the overall body rotation, since this may provide dynamical stability to a vehicle in flight. If the axis of rotation is parallel to the oncoming freestream flow, the problem would not be as formidable as

it may first appear since the formulation would be mathematically two-dimensional. Furthermore, it is anticipated that the boundary layer would bifurcate into two layers for relatively high rotation rates.

- Consideration of non-zero angles-of-attack. This would complicate the formulation of the problem for AXI cases since the flow would be truly three-dimensional.

- Inclusion of real gas effects (including chemical reactions), and the use of a more realistic temperature-viscosity law, such as *Sutherland's Law*, since these are important for real hypersonic flows (see, for example, Anderson 1989 for further details).

Appendix A

Numerical Solution of Ordinary Differential Equations

A.1 Initial-Value Problems

Consider a general nonlinear second-order initial-value problem of the form:

$$y'' = \phi(x, y, z), \quad z = y', \quad a \leq x \leq b, \tag{A.1}$$

$$y(a) = \alpha, \quad y'(a) = \lambda, \tag{A.2}$$

This equation can be solved using the following second-order accurate Predictor-Corrector method (for $2 \leq i \leq N$):

$$y_i^* = y_{i-1} + hz_{i-1}, \tag{A.3}$$

$$z_i^* = z_{i-1} + h\phi(x_{i-1}, y_{i-1}, z_{i-1}), \tag{A.4}$$

$$y_i = y_{i-1} + h\left(\frac{z_{i-1} + z_i^*}{2}\right), \tag{A.5}$$

$$z_i = z_{i-1} + h\phi\left(\frac{x_{i-1} + x_i}{2}, \frac{y_{i-1} + y_i^*}{2}, \frac{z_{i-1} + z_i^*}{2}\right). \tag{A.6}$$

It should be noted that a uniform grid defined by:

$$x_i = a + (i-1)h, \quad 1 \leq i \leq N, \tag{A.7}$$

has been employed, where h is a constant step size and N is the number of intervals. This method has been successfully used to solve Eqs. (7.50)–(7.52).

A.2 Boundary-Value Problems

A.2.1 Second-order equations

In this appendix, a global finite-difference method shall be described for the numerical solution of a general nonlinear second-order boundary-value problem of the form:

$$y'' = \phi(x, y, z), \quad z = y', \quad a \leq x \leq b, \tag{A.8}$$

$$y(a) = \alpha, \quad y(b) = \beta. \tag{A.9}$$

This equation can be approximated using second-order accurate central differences as follows:

$$\frac{y_{i+1} - 2y_i + y_{i-1}}{h^2} = \phi\left(x_i, y_i, \frac{y_{i+1} - y_{i-1}}{2h}\right), \quad 2 \leq i \leq N-1. \tag{A.10}$$

The boundary conditions (A.9) imply that $y_1 = \alpha$ and $y_N = \beta$. This $N \times N$ system of nonlinear equations can be solved using Newton's iterative method (see Burden & Faires 1993). If y_i is an approximation to the solution everywhere, it can be shown that an improved approximation is given by $y^* = y_i + v_i$, where v_i is given by the solution of the following tri-diagonal system of linear equations:

$$\begin{pmatrix} 1 & 0 & & & & & \\ a_2 & b_2 & c_2 & & & & \\ & \cdot & \cdot & \cdot & & & \\ & & \cdot & \cdot & \cdot & & \\ & & & \cdot & \cdot & \cdot & \\ & & & & a_{N-1} & b_{N-1} & c_{N-1} \\ & & & & & 0 & 1 \end{pmatrix} \begin{pmatrix} v_1 \\ v_2 \\ \cdot \\ \cdot \\ \cdot \\ v_{N-1} \\ v_N \end{pmatrix} = \begin{pmatrix} 0 \\ r_2 \\ \cdot \\ \cdot \\ \cdot \\ r_{N-1} \\ 0 \end{pmatrix}. \tag{A.11}$$

The matrix in the foregoing equation is known as the *Jacobian* matrix and its non-zero elements are given by (for $2 \leq i \leq N-1$):

$$a_i = -1 - \frac{h}{2}\frac{\partial \phi}{\partial z}, \tag{A.12a}$$

$$b_i = 2 + h^2 \frac{\partial \phi}{\partial y}, \tag{A.12b}$$

$$c_i = -1 + \frac{h}{2}\frac{\partial \phi}{\partial z}, \tag{A.12c}$$

$$r_i = y^*_{i+1} - 2y^*_i + y^*_{i-1} - h^2\phi. \tag{A.12d}$$

This system of equations can be solved very efficiently using a tri-diagonal Gaussian elimination routine with backward substitution[1] . In order to start the solution procedure, an initial distribution for $y(x)$ satisfying the boundary conditions (A.9) is required. The solution is assumed to converge only when the maximum change between successive iterations is less than a specified tolerance level ϵ.

This method can also be extended to cope with more complicated boundary conditions. If, for example, the boundary condition $y(a) = \alpha$ is replaced by $y'(a) = \mu$, then this latter condition could be approximated by

$$\left(\frac{\mathrm{d}y}{\mathrm{d}x}\right)_{i=1} = \mu \approx \frac{-3y_1 + 4y_2 - y_3}{2h}. \tag{A.13}$$

This requires that the first row of Eq. (A.11) should be replaced by the following equation:

$$-3v_1 + 4v_2 - v_3 = r_1, \tag{A.14}$$

where $r_1 = 2h\mu + 3y^*_1 - 4y^*_2 + y^*_3$. Using the second row of Eq. (A.11), this equation can be expressed in tri-diagonal form as follows:

$$(a_2 - 3c_2)v_1 + (b_2 + 4c_2)v_2 = r_2 + c_2 r_1. \tag{A.15}$$

[1] Alternatively the Thomas algorithm (see, for example, Anderson 1995) could be employed, but the implementation of derivative boundary conditions would be less straightforward.

A.2.2 Third-order equations

The algorithm described above can be readily extended to solve third-order (or even higher-order) nonlinear equations of the form:

$$w''' = \phi(w, x, y, z), \quad z = y', \quad y = w', \quad a \leq x \leq b, \tag{A.16}$$

$$w(a) = \gamma, \quad w'(a) = \alpha, \quad w'(b) = \beta. \tag{A.17}$$

These equations can be expressed in the form:

$$y'' = \phi(w, x, y, z), \quad z = y', \quad a \leq x \leq b, \tag{A.18a}$$

$$y(a) = \alpha, \quad y(b) = \beta, \tag{A.18b}$$

$$w(x) = \gamma + \int_a^x y(\xi)\, \mathrm{d}\xi. \tag{A.18c}$$

Equation (A.18a–b) can be solved using the method discussed earlier and Eq. (A.18c) can be integrated using the Trapezoidal Rule:[2]

$$w_i = w_{i-1} + \frac{h}{2}(y_i + y_{i-1}). \tag{A.19}$$

This recurrence relation can be used to integrate Eq. (A.18c) for $2 \leq i \leq N$, starting from the initial condition $w_1 = \gamma$.

The finite-difference algorithm described in this section is globally second-order accurate and was found to be very robust. Moreover, the method works equally well for linear as well as nonlinear problems, and convergence is achieved within a relatively small number of iterations. An alternative method to solve boundary-value problems involves using a 'shooting' technique to integrate Eq. (A.8) using any marching technique (such as the Runge-Kutta or Predictor-Corrector method described earlier in this appendix), starting from the initial conditions (A.2) for an estimated value of λ. The procedure is repeated until a value of λ is found such that $y(b)$ is close to β (see, for example, Burden & Faires 1993). However, this method usually requires reasonably accurate initial approximations for $y'(a)$ in order for convergence to be achieved.

[2]Since the complete algorithm is globally second-order accurate, little or no accuracy is gained by the use of the more accurate Simpson's Rule.

Appendix B

Derivation of the Compatibility Equation

In this appendix, the compatibility equation (6.17) shall be derived with a minimum of detail (for full details see, for example, Kincaid 1991). Consider a general quasi-linear hyperbolic equation of the form:

$$a\frac{\partial^2 u}{\partial x^2} + b\frac{\partial^2 u}{\partial x \partial y} + c\frac{\partial^2 u}{\partial y^2} + e = 0. \tag{B.1}$$

The quantities a, b, c and e are assumed to be functions of x, y, u, s and t, where s and t are defined by Eq. (6.16) but such that $b^2 - 4ac$ is positive in the domain being considered. By defining a curve C in the xy-plane by $x = x(s)$ and $y = y(s)$, where s is a real number, it can be easily shown that along this curve

$$\frac{\partial^2 u}{\partial x^2} = \frac{\mathrm{d}p}{\mathrm{d}x} - \frac{\partial^2 u}{\partial x \partial y}\frac{\mathrm{d}y}{\mathrm{d}x}, \tag{B.2}$$

and similarly for $\partial^2 u/\partial y^2$. Hence it follows that Eq. (B.1) can be expressed in the form

$$-\frac{\partial^2 u}{\partial x \partial y}\left[a\left(\frac{\mathrm{d}y}{\mathrm{d}x}\right)^2 - b\frac{\mathrm{d}y}{\mathrm{d}x} + c\right] + a\frac{\mathrm{d}s}{\mathrm{d}x}\frac{\mathrm{d}y}{\mathrm{d}x} + c\frac{\mathrm{d}t}{\mathrm{d}x} + e\frac{\mathrm{d}y}{\mathrm{d}x} = 0. \tag{B.3}$$

The curve C is now chosen such that the term $\partial^2 u/\partial x \partial y$ disappears from the foregoing equation. Consequently the original hyperbolic equation reduces to an

ordinary differential equation along the two characteristic curves, which are given by the two distinct roots of the equation

$$a\left(\frac{\mathrm{d}y}{\mathrm{d}x}\right)^2 - b\frac{\mathrm{d}y}{\mathrm{d}x} + c = 0. \tag{B.4}$$

In particular,

$$a = 1,\ b = 0,\ c = -1 \quad \text{and} \quad e = -\frac{j}{(y+r)}\frac{\partial q}{\partial y} \tag{B.5}$$

for the axially-symmetric wave equation (5.20) considered in this thesis, and the characteristic curves are simply straight lines with gradient ± 1.

Appendix C

Marginal Separation Theory

C.1 Supercritical Flows

C.1.1 Two-dimensional case

Marginal separation occurs when the skin friction vanishes linearly at the separation point, and was first considered by Ruban (1981, 1982) and Stewartson *et al.* (1982) for incompressible flows. Kerimbekov *et al.* (1994) have shown that marginal separation occurs in the hypersonic flow over 2D compression ramps with supercritical wall cooling (see also the numerical results of Chapter 6). In particular, it was shown that the inner viscous sublayer (region I in Fig. 5.1) develops a multi-layer structure with streamwise extent $\Delta x \sim \mathrm{Ne}^{-2/3}$ in the vicinity of the reversed flow region, as shown in Fig. C.1. The structure of the solution in each of the regions labelled a, b, c and d was determined by Ruban (1981). It turns out that the solution in regions 'a' and 'c' (and similarly in regions 'b' and 'd') can be expressed using the same asymptotic expansion, which is in contrast to the more complicated structure considered in Fig. 7.1.

It was shown by Kerimbekov *et al.* (1994) that the appropriately scaled displacement function $B(X)$ in the inner interaction regions 1 and 2 satisfies the

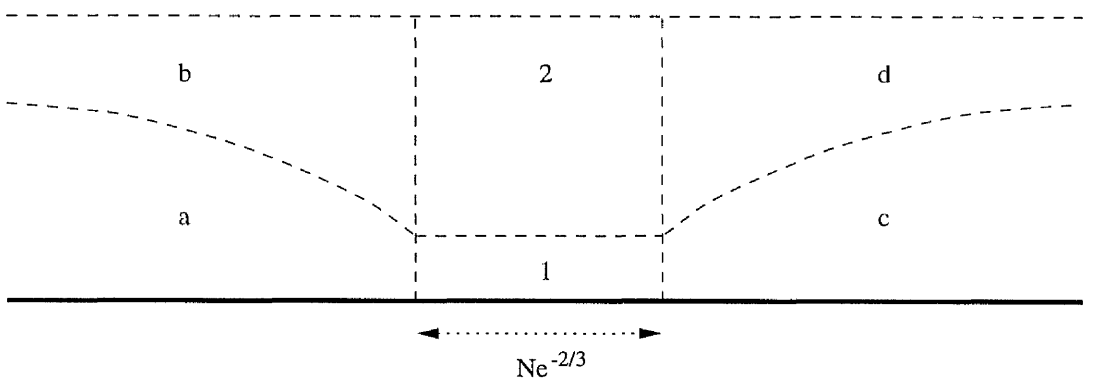

Figure C.1: Sketch of the multi-layer structure in the viscous sublayer in the vicinity of the marginal separation point (not to scale).

following integro-differential equation:

$$B^2 - X^2 + 2a = n \int_{-\infty}^{X} \frac{B'(\xi) + 1}{(X - \xi)^{1/2}} \, \mathrm{d}\xi, \qquad n = \frac{\Gamma(3/4)}{\sqrt{2}\,\Gamma(5/4)}, \tag{C.1}$$

where

$$B(X) \to -X + aX^{-1} + \cdots \quad \text{as} \quad X \to -\infty, \tag{C.2a}$$

$$B(X) \to X + \cdots \quad \text{as} \quad X \to \infty. \tag{C.2b}$$

The parameter a is proportional to the perturbation β_2 about the critical ramp angle β_0^* (cf. Eq. (5.32)). The numerical solution of the foregoing fundamental equation was obtained by Kerimbekov *et al.* (1994), and it was shown that separation occurs for values of a greater than 1.287. It was also observed that the separation point moves progressively upstream as the ramp angle is increased (i.e. for increasing a); however the reversed flow region is always located on the ramp surface.

C.1.2 Axially-symmetric case

Although marginal separation theory was originally developed for 2D flows, it will now be shown using an argument analogous to that employed in Sec. 7.8 that the theory is also applicable to AXI flows. The analysis of Kerimbekov *et al.* (1994) suggests that the pressure $q(x,z)$ and displacement function $A(x)$ in the inviscid layer above the inner interaction regions 1 and 2 can be expressed in the following asymptotic forms (for $z \sim \mathrm{Ne}^{-2/3}$):

$$q(x,z) = q_0(z) + \mathrm{Ne}^{-2/3}\, q_1(x,z) + \mathrm{Ne}^{-1}\, q_2(z) + \mathrm{Ne}^{-4/3}\, q_3(x,z) + \mathrm{Ne}^{-5/3}\, Q(X,Z) + \cdots, \tag{C.3a}$$

$$A(x) = A_0(x_0) + \mathrm{Ne}^{-2/3}\, B(X) + \cdots, \tag{C.3b}$$

where X and Z are $O(1)$ variables defined by (cf. Eq. (7.126)):

$$x = x_s + \mathrm{Ne}^{-2/3}\, X, \quad z = \mathrm{Ne}^{-2/3}\, Z. \tag{C.4}$$

Substitution of Eqs. (C.3)–(C.4) into the axially-symmetric wave equation (5.20) and matching condition (5.29), and taking the cold wall limit $\mathrm{Ne} \to \infty$, it can be shown that:

$$q_0(z) = p_0(x_s) \quad \text{and} \quad q_2(z) = p_1(x_s), \tag{C.5}$$

in order to match with the asymptotic expansion for the pressure on the body surface given by Kerimbekov *et al.* (1994). The functions q_1 and q_3 satisfy the equations:

$$\frac{\partial^2 q_i}{\partial x^2} - \frac{\partial^2 q_i}{\partial z^2} - \frac{j}{z+r}\frac{\partial q_i}{\partial z} = 0 \qquad (i = 1,\ 3), \tag{C.6a}$$

$$q_1 \to \lambda_0 X,\ q_3 \to \frac{1}{2}\lambda_1 X^2 \quad \text{as} \quad z \to 0, \tag{C.6b}$$

$$\frac{\partial q_i}{\partial z} = -\,\mathrm{sgn}(\mathcal{L})\frac{\mathrm{d}^2 p_i}{\mathrm{d}x^2} \quad \text{as} \quad z \to 0, \tag{C.6c}$$

where λ_0 and λ_1 are constants. Furthermore, it follows that $Q(X,Z)$ satisfies the *two-dimensional* wave equation (7.129). Thus the 2D marginal separation theory

described by Kerimbekov *et al.* (1994) can also be applied to AXI flows in the neighbourhood of the marginal separation point. This is particularly important for the flow over AXI expansion corners shown in Figs. 6.9 and 6.10, where it was discovered that marginal separation occurs downstream of the ramp corner if the body radius is smaller than a certain critical value.

C.2 Subcritical Flows

Zhikharev (1993) considered the case of marginal separation from a cold wall with subcritical wall cooling. It was shown that under certain circumstances, marginal separation theory can break down in the vicinity of the reattachment point x_r, and that an additional inner region with streamwise extent $\Delta x \sim \mathrm{Ne}^{-4/3}$ centered on x_r should be considered. The resulting nonlinear interaction problem took the form:

$$\frac{\partial \Psi}{\partial Y}\frac{\partial^2 \Psi}{\partial X \partial Y} - \frac{\partial \Psi}{\partial X}\frac{\partial^2 \Psi}{\partial Y^2} = -\frac{\mathrm{d}P}{\mathrm{d}X} + \frac{\partial^3 \Psi}{\partial Y^3}, \tag{C.7a}$$

$$\Psi = \frac{\partial \Psi}{\partial Y} = 0 \quad \text{at} \quad Y = 0, \tag{C.7b}$$

$$\Psi \to \frac{1}{6}Y^3 + \frac{1}{2}B(X)Y^2 + \cdots \quad \text{as} \quad Y \to \infty, \tag{C.7c}$$

$$\Psi \to \frac{1}{6}Y^3 + \frac{1}{2}cY^2 + \cdots \quad \text{as} \quad X \to -\infty, \tag{C.7d}$$

$$\frac{\mathrm{d}P}{\mathrm{d}X} = \frac{\mathrm{d}B}{\mathrm{d}X} - 1, \tag{C.7e}$$

where the parameter c is proportional to x_r. It is important to note that this system of equations differs from that considered in Sec. 7.3 in both the upstream boundary condition (C.7d) and the interaction law (C.7e), which is due to the fact that the reattachment region was assumed to take place well upstream of the ramp corner where $F(X) = 0$. Zhikharev (1993) used a line-relaxation method based on a Newton iteration procedure to obtain solutions of Eqs. (C.7a–e), and found that a reversed-flow singularity occurs for $c > 1.225$.

Bibliography

ABRAMOWITZ, M. & STEGUN, I. A. (1965): "Handbook of Mathematical Functions." *Dover Publications.*

ANDERSON, J. D. (1989): "Hypersonic and High Temperature Gas Dynamics." *McGraw-Hill.*

ANDERSON, J. D. (1995): "Computational Fluid Dynamics." *McGraw-Hill.*

ASHLEY H. & LANDAHL, M. (1965): "Aerodynamics of Wings and Bodies." *Dover Publications.*

BERTIN, J. J., GLOWINSKI, R. & PERIAUX, J. (1989): "Hypersonics (Volumes I & II)." *Birkhäuser.*

BOS, S. H. (1998): "Numerical Methods to Solve Viscous-Inviscid Interaction Problems." *Ph.D. thesis, University of Manchester.*

BROWN, S. N., CHENG, H. K. & LEE, C. J. (1990): "Inviscid-viscous interaction on triple-deck scales in a hypersonic flow with strong wall cooling." *J. Fluid Mech.*, vol. 220, pp. 309–337.

BROWN, S. N. & STEWARTSON, K. (1975a): "A non-uniqueness of the hypersonic boundary layer." *Q. J. Mech. Appl. Maths*, vol. 28, pp. 75–90.

BROWN, S. N. STEWARTSON, K. & WILLIAMS, P. G. (1975b): "Hypersonic self-induced separation." *Phys. Fluids*, vol. 18, no. 6, pp. 633–639.

BURDEN, R. L. & FAIRES, J. D. (1993): "Numerical Analysis." *PWS-KENT Publishing Company, Boston.*

BUSH, W. B. & CROSS, A. K. (1967): "A Comment on Hypersonic Viscous Interaction Theory." *AIAA Journal*, vol. 5, no. 7, pp. 1370–1372.

CASSEL, K. W., RUBAN, A. I. & WALKER, J. D. A. (1995): "An instability in supersonic boundary-layer flow over a compression ramp." *J. Fluid Mech.*, vol. 300, pp. 265–285.

CASSEL, K. W., RUBAN, A. I. & WALKER, J. D. A. (1996): "The influence of wall cooling on hypersonic boundary-layer separation and stability." *J. Fluid Mech.*, vol. 321, pp. 189–216.

CHENG, H. K. (1993): "Perspectives on Hypersonic Viscous Flow Research." *Ann. Rev. of Fluid Mech.*, vol. 25, pp. 455-484.

CHERNYI, G. G. (1961): "Introduction to Hypersonic Flow." *Academic Press.*

COX, R. N. & CRABTREE, L. F. (1965): "Elements of Hypersonic Aerodynamics." *The English Universities Press Ltd..*

DEWEY, C. F. (1963): "Use of Local Similarity Concepts in Hypersonic Viscous Interaction Problems." *AIAA Journal*, vol. 1, no. 1, pp. 20–33.

DORODNITSYN, A. A. (1942): "Laminar Boundary Layer in Compressible Fluid." *Dokl. Akad. Nauk. SSSR*, vol. 34, pp. 213–219.

DORRANCE, W. H. (1962): "Viscous Hypersonic Flow." *McGraw-Hill.*

DUDIN, G. N. (1978): "Calculation of a Boundary Layer on Triangular Plate in Strong Viscous Interaction Regime." *Uchenye Zapiski TsAGI*, vol. 9, pp. 65–70.

DUDIN, G. N. (1983): "Finite-Difference Method of Solution for Three-Dimensional Boundary-Layer Equations in Strong Viscous Interaction Regime." *Trudy TsAGI*, VYP. 2190, pp. 3–25.

ELLINWOOD, J. W. & MIRELS, H. (1968): "Axisymmetric hypersonic flow with strong viscous interaction." *J. Fluid Mech.*, vol. 34, pp. 687–703.

ELLIOTT, J. W. & SMITH, F. T. (1986): "Separated supersonic flow past a trailing edge at incidence." *Int. J. Comput. Fluids*, vol. 14, no.2, pp. 109–116.

EMANUEL, G. (1994): "Analytical Fluid Dynamics." *CRC Press.*

FERRI, A. (1939): *Att. Guidonia (Rome)*, no. 17.

GAJJAR, J. & SMITH, F. T. (1983): "On hypersonic self-induced separation: hydraulic jumps and boundary layers with algebraic growth." *Mathematika*, vol. 30, pp. 77–93.

GLAUERT, M. B. & LIGHTHILL, M. J. (1955): *Proc. R. Soc. Lond.*, vol. A230, pp. 188–203.

GOLDSTEIN, S. (1948): "On laminar boundary-layer flow near a position of separation." *Q. J. Mech. Appl. Maths*, vol. 1, pp. 43–69.

GUARDINO, C. (1995): "Computation of Hypersonic Blunt Body Flows using Flux Vector Splitting Techniques." *M.Sc. thesis, University of Manchester.*

HAYES, W. D. & PROBSTEIN, R. F. (1959): "Hypersonic Flow Theory." *Academic Press, New York.*

INGER, G. R. (1995): "New Similarity Solutions for Hypersonic Boundary Layers with Applications to Inlet Flows." *AIAA Journal*, vol. 33, no. 11, pp. 2080–2086.

KERIMBEKOV, R. M., RUBAN, A. I. & WALKER, J. D. A. (1994): "Hypersonic boundary-layer separation on a cold wall." *J. Fluid Mech.*, vol. 274, pp. 163–195.

KHORRAMI, A. F. & SMITH, F. T. (1994): "Hypersonic aerodynamics on thin bodies with interaction and upstream influence." *J. Fluid Mech.*, vol. 277, pp. 85–108.

KINCAID, D. R. (1991): "Numerical Analysis: Mathematics of Scientific Computing." *Brooks/Cole.*

KLUWICK, A., GITTLER, P. & BODONYI, R. J. (1984): "Viscous-inviscid interactions on axisymmetric bodies of revolution in supersonic flow." *J. Fluid Mech.*, vol. 140, pp. 281–301.

KOZLOVA, I. G. & MIKHAILOV, V. V. (1970): "On a Strong Viscous Interaction over Delta and Swept Wings." *Akad. Nauk. SSSR. Izv. Mekh. Zhidk Gaza*, vol. 6, pp. 94–99.

LANDAU, L. D. & LIFSCHITZ, E. M. (1944): "Mechanics of Continuous Media." *Moscow: Gostechizdat (in Russian).*

LEES, L. (1953): "On the Boundary-Layer Equations in Hypersonic Flow and Their Approximate Solutions." *Journal of the Aeronautical Sciences, Readers' Forum*, vol. 20, no. 2.

LIGHTHILL, M. J. (1953): "On boundary layers and upstream influence. II. Supersonic flows without separation." *Proc. R. Soc. Lond.*, vol. A 217, 1131, pp. 478–507.

MESSITER, A. F. (1970): "Boundary-layer flow near the trailing edge of a flat plate." *SIAM J. Appl. Maths*, vol. 18, pp. 241–257.

MIKHAILOV, V. V., NEILAND, V. YA. & SYCHEV, V. V. (1971): "The Theory of Viscous Hypersonic Flow." *Ann. Rev. of Fluid Mech.*, vol. 3, pp. 371–396.

MIRELS, H. (1962): "Hypersonic Flow Over Slender Bodies with Power Law Shocks." *Advances in Applied Mechanics VII*, vol. 34, pp. 1–54.

NEILAND, V. YA (1969): "On the Theory of Laminar Boundary-Layer Separation in Supersonic Flow." *Akad. Nauk. SSSR. Izv. Mekh. Zhidk Gaza*, vol. 4, pp. 53–57.

NEILAND, V. YA (1970): "Upstream Propagation of Disturbances in Hypersonic Boundary Layer Interactions." *Akad. Nauk. SSSR. Izv. Mekh. Zhidk Gaza*, vol. 4, pp. 40–49.

NEILAND, V. YA (1973): "Peculiarities of Boundary-Layer Separation on a Cooled Body and its Interaction with a Hypersonic Flow." *Akad. Nauk. SSSR. Izv. Mekh. Zhidk Gaza*, vol. 6, pp. 99–109.

PRANDTL, L. (1904): "Über Flüssigkeitsbewegung bei sehr Kleiner Reiburg." *Verb. III Intern. Math. Krongr., Heidelberg; Leipzig*, pp. 484–491, Teubner.

RIZZETTA, D. P., BURGGRAF, O. R. & JENSON, R. (1978): "Triple-deck solutions for viscous supersonic and hypersonic flow past corners." *J. Fluid Mech.*, vol. 89, pp. 535–552.

ROSENHEAD, L. (1963): "Laminar Boundary Layers." *Oxford University Press.*

RUBAN, A. I. & SYCHEV, V. V. (1973): "Hypersonic Viscous Gas Flow Over Small Aspect Ratio Wings." *Uch. Zap. TsAGI*, vol. 4, no. 5, pp. 18–25.

RUBAN, A. I. (1981): "Singular solution for boundary layer equations with continuous extension downstream of zero skin friction point." *Akad. Nauk. SSSR. Izv. Mekh. Zhidk Gaza*, no. 6, pp. 42–52.

RUBAN, A. I. (1982): "Asymptotic theory for short separation bubbles on the leading edge of thin airfoil." *Akad. Nauk. SSSR. Izv. Mekh. Zhidk Gaza*, no. 1, pp. 42–51.

SMITH, F. T. & DANIELS, P. G. (1981): "Removal of Goldstein's singularity at separation in flow past obstacles in wall layers." *J. Fluid Mech.*, vol. 110, pp. 1–37.

SMITH, F. T. (1988): "A reversed-flow singularity in interacting boundary layers." *Proc. R. Soc. Lond.*, vol. 420, pp. 21–52.

STEWARTSON, K. (1955a): "The asymptotic boundary layer on a circular cylinder in axial incompressible flow." *Q. Appl. Maths.*, vol. 13, no. 2, pp. 113–122.

STEWARTSON, K. (1955b): "On the Motion of a Flat Plate at High Speed in a Viscous Compressible Fluid–II. Steady Motion." *Journal of the Aeronautical Sciences*, May 1955, pp. 303–309.

STEWARTSON, K. (1964): "Viscous Hypersonic Flow Past a Slender Cone." *Physics of Fluids*, vol. 7, no. 5, pp. 668–675.

STEWARTSON, K. & WILLIAMS, P. G. (1969): "Self-induced Separation." *Proc. R. Soc. Lond.*, vol. A 312, pp. 181–206.

STEWARTSON, K. (1970): "Is the singularity at separation removable ?." *J. Fluid Mech.*, vol. 44, pp. 347–364.

STEWARTSON, K. (1974): "Multistructured Boundary Layers on Flat Plates and Related Bodies." *Advances in Applied Mechanics*, vol. 14, pp. 145–239.

STEWARTSON, K., SMITH, F. T. & KAUPS, K. (1982): "Marginal Separation." *Stud. Apll. Maths*, vol. 67, pp. 45–61.

SYCHEV, V. V. (1972): "On laminar separation." *Akad. Nauk. SSSR. Izv. Mekh. Zhidk Gaza*, no. 3, pp. 47–59.

SYCHEV, V. V., RUBAN, A. I., SYZHEV, VIK. V. & KOROLEV, G. L. (1998): "Asymptotic Theory for Separated Flows." *Cambridge University Press.*

TALBOT, L., KOGA, T. & SHERMAN, P. M. (1958): "Hypersonic Viscous Flow over Slender Cones." *NACA TN 4327.*

TOWNEND, L. H. (1991): "Research and design for hypersonic aircraft." *Phil. Trans. R. Soc. Lond.*, vol. A 335, pp. 201–224.

WALBERG, G. D. (1991): "Hypersonic flight experience." *Phil. Trans. R. Soc. Lond.*, vol. A 335, pp. 91–119.

WALKER, J. D. A., BARNETT, M. & SMITH, F. T. *editors* (1993): "Advances in Analytical Methods in Modelling of Aerodynamic Flows." *AIAA Proceedings of International Workshop, Poland, July 12–14.*

WEI, H. (1964): *AIAA Paper*, vol. 64, pp. 428.

WERLE, M. J. & DAVIS, R. T. (1972): "Incompressible laminar boundary layers on a parabola at angle of attack: a study of the separation point." *Trans. ASME E: J. Appl. Mech*, vol. 39, pp. 7–12.

WERLE, M. J., DWOYER, D. L. & HANKEY, W. L. (1973): "Initial Conditions for the Hypersonic-Shock/Boundary-Layer Interaction Problem." *AIAA Journal*, vol. 11, no. 4, pp. 525–530.

YASUHARA, M. (1962): "Axisymmetric Viscous Flow Past Very Slender Bodies of Revolution." *J. Aero. Sciences*, pp. 667- 688.

YEE, H. C. & SWEBY, P. K. (1998): "Aspects of Numerical Uncertainties in Time Marching to Steady-State Numerical Solutions." *AIAA Journal*, vol. 36, no. 5, pp. 712–724.

ZHIKHAREV, C. N. (1993): "Separation Phenomenon in Hypersonic Flow with Strong Wall Cooling: Subcritical Regime." *Theoret. Comput. Fluid Dynamics*, vol. 4, pp. 209–226.

JOHN RYLANDS
UNIVERSITY
LIBRARY OF
MANCHESTER